Paclitaxel-2'-*O*-pentadecylhemiglutarate:

A Prodrug Strategy for Albumin Based Drug Delivery

Michael Joseph Hackett

A dissertation submitted to the faculty of the University of North Carolina at Chapel Hill in partial fulfillment of the requirements for the degree of Doctor of Philosophy in the School of Pharmacy (Molecular Pharmaceutics).

Chapel Hill
2011

Approved By

Moo J. Cho, Ph.D., Advisor

Rudy L. Juliano, Ph.D., Chair

Fan Yuan, Ph.D., Reader

Michael B. Jarstfer, Ph.D., Reader

Qisheng Zhang, Ph.D., Reader

ABSTRACT

Michael Joseph Hackett: Paclitaxel-2'-*O*-pentadecylhemiglutarate: A Prodrug Strategy for Albumin Based Drug Delivery (Under the direction of Moo J. Cho, Ph.D.)

Delivery of antineoplastic agents to solid tumors remains a great challenge in formulation development. Preclinical successes often do not translate into clinical therapies due to the intrinsic imperfections of current models. The presented formulation begins with clinical observations indicating the ubiquitous protein, serum albumin, naturally accumulates selectively in spontaneously developed tumors. Albumin then provides a natural shuttle for therapeutic agents to solid tumors. To test this, a fatty diacid, 3-pentadecylglutaric acid (PDG), was synthesized. This fatty acid has the capacity to bind albumin tightly while concomitantly binding a therapeutic moiety, in this case paclitaxel. The paclitaxel-2'-*O*-pentadecylhemiglutarate conjugate binds albumin tightly but the extreme hydrophobicity led to poor loading efficiency and the formation of 120 nm albumin aggregates; a similar phenomenon observed in the clinically approved ABRAXANE. This aggregation was found to be the result of a specific interaction between paclitaxel and albumin.

Dissociation of the conjugate from albumin is exceedingly slow with less than 3% released over 48 h under sink conditions. When administered to tumor bearing mice, the formulation behaved similarly to covalently attached albumin conjugates. Rapid and uniform organ distribution was observed followed by a slow re-emergence of complex into the vasculature giving rise to a half-life of 23 h. This is comparable to the half-life of the protein itself in mice. Tumor accumulation was moderate (~1%) and biochemical stability analysis

of the conjugate suggests little conversion (<6% over 72 h) to free drug would occur. Despite decreased cytotoxicity, lower doses of the conjugate demonstrated comparable efficacy to TAXOL without the need for surfactants.

Modification of paclitaxel was accomplished in a single step using PDG anhydride presenting a cost-effective method for improving the pharmacokinetics of a drug. Conceptually, this study lays the foundation for using the PDG technology for modifying other therapeutic agents. The success of the formulation is highly dependent on the selected therapeutic modality which can be broadly limited to any therapeutic agent bearing a nucleophilic moiety. It is expected a more hydrophilic drug that does not exhibit albumin binding may lead to increased efficacy in addition to improved pharmacokinetics.

ACKNOWLEDGEMENTS

I would like to thank Boka Hadzija, Ph.D. for her dedication to the scientific discipline of pharmacy, for her tutelage as my professor when I assisted in her Basic Pharmaceutics class, for our weekly meetings where we would sit down over coffee and solve the world's problems. (somebody's got to do it) Perhaps one day this university will rightfully name a building in your honor; hopefully large enough to house all your awards. You may be gone but you're not forgotten.

I would like to thank the Pharm D's. The scraps from your weekly catered meetings provided ample sustenance for the lab.

I would like to thank Penny Neisen-Roufs, Ph.D., Phil Garner, Ph.D. and Anthony Pearson, Ph.D. for providing an opportunity to learn organic chemistry at their hands and at the cost of their sanity. I would similarly like to thank Thomas Kelley, Ph.D. for providing an opportunity to learn biochemistry in his laboratory.

I would like to thank Ricky, Robbie and the rest of the UNC custodial staff for their hard work maintaining a clean, functional environment. Thanks for the late night conversations.

I would like to thank Karl Koshlap, Ph.D. for keeping the NMR facility functional and available at all times.

I would like to thank Arlene Bridges, Ph.D. for providing mass spectral data for all intermediates and products as well as developing and running a LC/MS protocol for determining the stability of our drug.

I would like to thank Kathryn Fiscelli, Ph.D., Holly Maguire, Kim Hoenerhoff and Lee Daub for their outstanding work in ensuring all chemical orders were processed and received as expected. Their diligence was surpassed only by their affability.

I would like to thank my doctoral advisory committee for making themselves available on short notice and providing sage guidance to help me progress in a timely manner.

I would like to thank my Cho labmates; John An, Ph.D., David Gaul, Ph.D., Roland Cheung, Ph.D., Patrick Guley (soon to be Ph.D.), Shyam Joolakanti, Ph.D., Megan Hartranft, Tianxiang (Kevin) Han and Kayla Knilans. Thank you all for your support during the everyday struggles of graduate school.

I would like to thank my family; Dennis and Karen Hackett, Patrick, Melanie, Erin and Becki. Thank you for your constant support and encouragement; nobody believes in me more than all of you. I love you all.

Last but not least, I would like to thank my advisor, business partner and scientific role model, Moo J. Cho, Ph.D. Obviously none of this would have been possible without your guidance and veritably infinite patience during all our adversity. I aspire to one day be as erudite yet as humble as yourself. Best of luck to you and your wonderful wife June Cho, Ph.D. during your retirement. You have certainly earned it.

PREFACE

I was trained as a synthetic chemist by Phil Garner, Ph.D. at Case Western as an undergraduate. While I enjoyed it, I was unfulfilled and wanted a way to translate the compounds I made into medically useful products. I thus applied to the Medicinal Chemistry program at the UNC School of Pharmacy, or so I thought. During website reconstruction, the Med Chem website was down and assuming the four listed programs were all just ramifications of one program, I used the information for the only functional website; Molecular Pharmaceutics. I received a call from Dr. Cho informing me of my mistake along with an elevator pitch on behalf of the MoPh program. I had never heard of drug delivery but the idea of designing drugs to be delivered specifically within the body sounded as amazing as it did impossible. Intrigued, I recalled the best advice, courtesy of Dr. Garner, I received while looking for grad schools; “follow the science.” So I did and joined the MoPh program in the summer of 2006 to the elation of the Med Chem department I am sure.

After a rotation with Dr. Huang, I recall talking to Cho about joining his lab to work on PRINT particles. On my first day I entered the lab and the smell of aldrithiol and dichloromethane washed over me; I knew I was home. Well, first I replaced the dichloromethane smell with ether. Then I knew I was home. Cho and I worked on a few preliminary projects together while I finished classes, but the projects were unsuccessful. Cho then discussed a project of using a fatty acid for binding albumin. He mentioned it in passing as an interesting idea but having had several students take on the idea and fail in the past, he had all but given up hope. I loved the idea and immediately set to work making

the same mistakes as everyone in the past. Then, after some 30 trips back to the drawing board, I scribbled out a new molecule to make my life easier. Like Archimedes standing in the tub only to notice the water level rise, or the apple falling on Newton's head; I too had a Eureka moment. I showed the molecule to Cho who immediately shared my enthusiasm, and within a few hours I returned with a synthetic scheme to make the 3-cetylglutaric anhydride.

Several months later, having survived the LAH and KCN involved in the synthesis, I was purifying over a gram of the molecule in AcCl by filtration. Some water was aspirated into the vacuum flask which immediately reacted with the AcCl releasing a great deal of heat which exploded the suspension out the top of the filter barely missing my and Patrick Guley's faces. Rather than restart the synthesis, I decided to keep my face and design a new one. Again, within a day I had designed a brand new synthesis which shortened the number of steps and the toxicity of the involved reagents and . . . it failed . . . consistently. Eventually it was tweaked into the synthesis presented in **Chapter III** which is shorter, easier and less dangerous than the initial synthesis. Recently we've even thought of shortening it further via Michael addition of a Grignard but that's another story. The result was the 3-cetylglutaric anhydride truncated by one methylene; 3-pentadecylglutaric anhydride now affectionately named **PDG**.

Cho's idea of using a fatty acid to bind albumin was coming to fruition and our zeal prompted us to take off at breakneck speed; only to realize we had no idea where we were going. Eventually we regained our composure and focus. We had not been averse to challenges up to this point nor were we strangers to struggle. So we decided to shoot for the moon and undertook paclitaxel as our first endeavor. Edison said it best.

“If I find 10,000 ways something won't work, I haven't failed.
I am not discouraged, because every wrong attempt discarded
is another step forward.”

-Thomas Alva Edison

TABLE OF CONTENTS

Page

LIST OF TABLES

LIST OF SCHEMES

LIST OF FIGURES

LIST OF ABBREVIATIONS AND SYMBOLS

ε	molar extinction coefficient
$t_{1/2}$	serum half-life
DMAP	4-dimethylaminopyridine
ApoE/A1	apolipoprotein E/A1
AUC	area under the curve
BD	biodistribution
BOC	tert-butyloxycarbonyl
Bn	benzyl
C_0	estimated initial serum concentration
Cbz	carbobenzyloxy
CD	circular dichroism
CHAPS	3-[(3-Cholamidopropyl)dimethylammonio]-1-propanesulfonate
cmc	critical micellar concentration
Ci	curie
Cl	systemic clearance
CrEL	cremophor EL
D5W/D1W	5%, 1% (w/v) dextrose in water
DCC	dicyclohexylcarbodiimide
DCM	dichloromethane
dFdC	difluorodeoxycytidine or gemcitabine
DHA	docosahexaenoic acid

DLS	dynamic light scattering
DMSO	dimethyl sulfoxide
dpm	disintegrations per minute
ER	endoplasmic reticulum
EtOAc	ethyl acetate
EtOH	ethanol
FA	folic acid
FITC	fluoresceinisothiocyanate
GI50	50% growth inhibitory concentration
GIPET	gastrointestinal permeation enhancement technology
HBSS	Hank's balanced salt solution
HDL	high-density lipoprotein
HSA/BSA	human/bovine serum albumin
IDL	intermediate-density lipoprotein
K_d, K_A	dissociation constant, association constant
kDa	kilodalton
LC50	50% lethal concentration
LDA	lithium diisopropylamide
LDL	low-density lipoprotein
LSC	liquid scintillation counting
Me_2CO	acetone
MeCN	acetonitrile
MeOH	methanol
MMP	matrix metalloprotease
MRT	mean residence time
MWCO	molecular weight cut-off

OGP	octylglucopyranoside
w/(o/w)	water-in-(oil-in-water)
P-gp	P-glycoprotein
PABC	p-aminobenzyloxycarbonyl
PAMAM	polyamidoamine
PBS	phosphate buffered saline
PCC	pyridiniumchlorochromate
PDG	3-pentadecylglutaric
PDI	polydispersity index
PEG	polyethylenglycol
PD	pharmacodynamic
PK	pharmacokinetic
PLG	poly-L-glutamic acid
PLGA	poly(lactic-co-glycolic acid)
PP	paclitaxel-2'-*O*-pentadecylglutarate
PSA	prostate specific antigen
PTX	paclitaxel
PVDF	polyvinylidene fluoride
REAL	reversible aqueous lipidization
RES	reticuloendothelial system
RGD	Arg-Gly-Asp
rHDL	recombinant high-density lipoprotein
siRNA	small interfering ribonucleic acid
sq	squalenoyl
T20/80	Tween 20/80
t-BuOH	tert-butanol

TAT	translation transactivator
TFAA	trifluoroacetic anhydride
TGI	total growth inhibitory concentration
TLC	thin layer chromatography
TMS	tetramethylsilane
TMSO	trimethylsiloxy
TOC	Tyr^3-octreotide
TPGS	α-tocopherolpolyethyleneglycolsuccinate
Tris	tris(hydroxymethylaminomethane)
V_d	volume of distribution
VLDL	very low-density lipoprotein
$Z \pm \sigma$	mean particle size ± standard deviation

CHAPTER I

FORMULATIONS OF PACLITAXEL: REVIEW

1. Introduction

Paclitaxel (PTX) is a water-insoluble taxane primarily indicated for the treatment of breast, non-small cell lung and ovarian cancers. As a small molecule, PTX can move swiftly by diffusion dictated only by a concentration gradient. Peripheral delivery of PTX can then be effective locally as well as distributing throughout the tumor core. PTX molecules can easily partition into tumor cell membranes followed by slower release into the cytosol for microtubule bundling. For PTX to be effective in eradicating a solid tumor, it must accrue a minimum required concentration sustained for a desired period of time. Accumulation of a large fraction of the total dose at the target site warrants a safer, more effective treatment; a corollary being shortened and/or fewer doses. Most of the recent developmental efforts have incorporated mechanisms to achieve the pharmaceutical requirements presented above. Chemical efforts for identifying other taxane analogs have met the same fate of rapid clearance (*1*, *2*). Likewise, approaches with PTX derivatives including chemical delivery systems (i.e., prodrugs) have also been far from achieving delivery targeted to solid tumor (*3*, *4*). This dilemma in developing a parenteral formulation for lipophilic antineoplastic agents for targeted delivery to a solid tumor is not a unique problem with PTX. This general problem is indeed one of the most challenging issues contemporary research scientists are facing.

2. The Problems Associated with TAXOL

Like any other water-insoluble drug molecules, PTX will not be present in the circulation as a molecular dispersion (i.e., true solution). At a therapeutically meaningful concentration (~ 1 μM), over 95% of PTX exists as bound to serum albumin and orosomucoid and a smaller amount bound to LDL/HDL (*5*, *6*). Since the concentration of albumin (~40-50 mg/ml) is much greater than the other proteins, the majority of PTX in the circulation should be bound to albumin. Its 1:1 specific binding to albumin is with an

association constant close to 10^6 M^{-1} while multiple non-specific bindings are estimated by molecular docking to be approximately 10^5 M^{-1} (*7*). Observed values tend to suggest weaker binding (*8*). The compound has a lower affinity for erythrocytes and platelets but a very high affinity for the major surfactant in Cremophor EL (CrEL), polyethyleneglycol glyceroltriricinoleate. In the presence of CrEL, very little protein binding occurs and an entirely different pharmacokinetic profile emerges (*9*). Due to the complex nature of the various interactions, the pharmacokinetics observed subsequent to IV injection of CrEL-based PTX formulation (i.e., TAXOL) can lie anywhere between the kinetics of albumin bound PTX and CrEL encapsulated PTX.

The result is a rapid elimination of PTX from the circulation; 90% of PTX disappears within 3.5 hrs after 3-hr infusion in cancer patients (*10*). This is patently not due to metabolic degradation since the sum of major metabolites at a given time is less than 1% of the total (*11*). If one considers the long plasma half-life of albumin, ~ 19 days in humans (*12*), the above finding agrees with the facile transfer of PTX from its albumin complex to CrEL. PTX tends to accumulate in the liver where metabolism and biliary excretion occur (*13*). The rapid clearance has detrimental implications in delivery of PTX to the solid tumor. In this context, a more suitable vehicle must be employed for effective tumor delivery to see substantial improvements over TAXOL.

TAXOL is a 1.2 mg/mL emulsion in 10% EtOH, 10% Cremophor EL and 80% normal saline which is commonly infused over 3 hours every 2-3 weeks. The large quantity of CrEL is not well tolerated with most patients causing grade IV neutropenia and grade III hypersensitivity thus requiring a prophylactic regimen of dexamethasone (*14*). Being so abundant, the surfactant is believed to saturate the liver thus retarding the extravasation and consequential metabolism and elimination of PTX (*9*). This gives rise to non-linear or dose-dependent pharmacokinetics showing disproportionately slower elimination of the drug at

higher doses. Coupled with multiple cytochrome P450 dependent metabolism, this leads to significant inter-individual pharmacokinetics and difficult dosing of TAXOL (*15*). Constrained within the linear kinetic range, TAXOL is cleared rapidly from the body with a terminal half-life of 4 h when administered as a 6 h infusion (*16*). Outside the linear kinetic range at higher dosing or shorter infusions, for example 3 h, the half-life increases to 7-8 h (*10*). The accumulation of TAXOL in solid tumors is minimal leading to non-specific tissue uptake and toxicity. Despite this undesirable phenomenon, TAXOL is highly prescribed and moderately effective speaking volumes to the potency of the drug. A targeted formulation containing PTX should prove much more effective and tolerable for patients.

3. Desired Features of PTX Formulations

Drug delivery is an emerging field defined by a desire to formulate drugs for increased accumulation in a specific target tissue while minimizing non-specific accumulation and accompanying toxicity. This can be accomplished in several ways such as a benign prodrug only activated under specific tissue conditions, targeting to a specific feature of a tissue by way of a targeting ligand, affiliation with a carrier or any combination therein. For development of a new formulation, there are many attributes to consider (*17-19*). This review will focus on the desirable characteristics as they pertain to PTX.

Solubility. Paclitaxel is poorly soluble at 10 ug/mL in water at room temperature (*20*). The ideal formulation should be able to solubilize PTX *ad infinitum* such that it can be sterilized in a conventional manner and administered parenterally without further manipulations such as reconstitution or mixing with other solutions. The drug concentration in the formulation should be high so bolus injection is possible. Given the physicochemical properties of PTX, these may be impossible requirements to satisfy.

In Vivo Stability. When administered intravenously as TAXOL, PTX binds albumin, orosomucoid, endothelial cells, erythrocytes, platelets, while presumably residing inside the CrEL micelles for a significant period of time. Ideally a delivery vehicle should preclude non-specific association of the drug such as this while in the serum. The formulation should be biochemically stable and resist hepatic, renal and reticuloendothelial clearance. Then the drug will be available for tumor-targeted delivery. All organs are characterized by having leaky vasculature depending on the structure of endothelium. A normal continuous endothelium has pores sizes between 1.8-2.0 nm which prevents extravasation of most macromolecules (*21*). As an example, albumin of molecular weight 66.5 kDa has an assumed diameter of approximately 4 nm with the longest dimension extending 9.5 nm (*22*). In rapidly growing tumors, the vasculature can be quite leaky with large gaps in the vicinal endothelium. Observed pores in the tumor endothelia can be much larger ranging from 200 - 2000 nm (*23*). Compare this to the kidney which is defined by having fenestrated endothelia of approximately 12-30 nm (*21*). The endothelium here tends to be anionic making it resistant to most serum proteins carrying net negative charges while facilitating extravasation of cationic carriers. The liver and spleen are defined by having sinusoidal or discontinuous endothelia with pores up to 150 nm (*21*). These endothelia are also anionic thus having a higher extraction of cationic carriers.

The liver and spleen are lined with highly phagocytic cells attributed to the filtration of particles from the vasculature. Collectively they are called the reticuloendothelial system (RES). These cells can be avoided in several ways including steric hindrance via the addition of polyetheyleneglycol (PEG), minimizing opsonization and the inability to extravasate effectively through the sinusoidal endothelia (*24*). Considering the large difference in vascular pores between the tumor and the liver, a large carrier can facilitate RES aversion but still effectively extravasate into the tumor. Smaller particles, typically 20

nm or less, appear able to avoid RES uptake as well (*25*). Lastly, if the carrier is or appears natural, it may have an inherent resistance. Macrophages, for instance, have been shown to express FcRn, the albumin/IgG protection receptor (*26*). The measure of a successful formulation will be a protracted serum half-life. This is desirable as the crowded tumor can only slowly filter the blood thus a prolonged retention in the circulation will promote a sustainable infusion of drug into the tumor.

Targeting. Targeting can occur passively or actively. Passive targeting to tumors is typically attributed to the leaky vasculature associated with the vicinal endothelium (*27*). Rapidly expanding tumors compromise lymphatic drainage while concomitantly inundating the endothelium with a deluge of growth factors. Macromolecules in the circulation are then filtered into the tumor, similar to the spleen and liver. Once in the tumor periphery, active targeting can be accomplished by presentation of a tumor-specific targeting ligand. This ligand can be directly attached to the carrier, often with a linker, minimizing steric hindrance for specific receptors overexpressed on tumor cells. This provides a greater chance of tumor cell encounter and subsequent endocytosis. Examples include nutrients such as tetrahydrofolate (*28*), hormones such as tamoxifen (*29*) or peptides such as the tripeptide Arg-Gly-Asp (RGD) which targets integrin proteins on the endothelium (*30*).

Release. With the highly convective force of blood pushing macromolecules out of the vasculature into the tumor periphery but with no mode of drainage, convective forces within the tumor weaken and diffusion predominates (*31*). Small molecules then are unrestricted as they are driven by diffusion, but macromolecular carrier or therapeutic motility will be greatly impeded. Ideally, PTX should be released at this time in the tumor periphery. This can occur by manipulating specific elements of the tissue such as acidity, enzyme expression or internalization into cells. The tumor microenvironment is moderately acidic compared with normal tissue with a pH around 6-7 (*32*). A very highly acid sensitive

compound such as carboxylated dimethyl maleic acid could facilitate release (*33*). Enzyme overexpression tends to be tumor dependent. Some general examples of targeted enzymes include the cathepsins (*34*) and matrix metalloproteases (MMPs) (*35*), both of which are involved in cleavage of the extracellular matrix to allow rapid growth (*36*).

If the carrier is endocytosed by tumor cells, it will be processed into a mature endosome and subsequent lysosome. The mature endosome provides a checkpoint for release of chemically attached PTX from the carrier as well as endosomal transfer of the carrier to the cytosol. One method for endosomal release requires a weak base. During endosomal maturation, V-class proton pumps decrease the pH inside endosomes to approximately 5. This proton flux can be buffered by a weak base triggering more protons to be pumped. As protons enter the endosome, chloride counter-ions follow. This creates an osmotic gradient prompting the diffusion of water into the endosome with subsequent swelling and potential rupture or leakage from endosome to cytosol. This mechanism is referred to as the proton sponge hypothesis (*37*). Other methods include membrane disruption (*38*) or the use of highly cationic cell penetrating peptides such as the transactivator of transcription (TAT) peptide from human immunodeficiency virus (*39*). The result should be the complete release of PTX from the carrier and the released vehicle should be non-toxic and non-immunogenic.

Development. From a manufacturing perspective, a vehicle should be simple. It should be highly scalable, economical and easy to manufacture. From a practitioner's perspective, the commercial formulation should be stable, easy to formulate for administration and be administered quickly, infrequently and innocuously.

Many alternative formulations to TAXOL have been proposed. These run the gamut from clinically approved through preclinical proof of concept. There is no known magic

bullet formulation for PTX and these ideal characteristics are meant only as a basis of comparison. The great number and variation in the methods of PTX delivery are nevertheless encouraging.

4. Natural Drug Carriers

There are several options available for natural carriers but the most commonly used is also the most abundant, serum albumin. Albumin is maintained at ~40-50 mg/mL concentrations in the vasculature and 25 mg/mL in the interstice; twice as great as the penultimately abundant, IgG (*40*). Both albumin and IgG are naturally protected from degradation throughout the body by the Brambell receptor, FcRn (*12*). While expressed on all endothelia, FcRn has now been discovered in the kidney (*41*), hepatocytes (*42*) and on monocytes (*26*). This protection is manifest in 19 and 21 day half-lives for albumin and IgG respectively, in humans. This perfectly satisfies the pharmacokinetic requirements for formulation development (*12*). In addition to natural protection, albumin both passively and actively deposits in solid tumors where it is rapidly degraded; putatively because the most abundant protein provides the most abundant sustenance (*43*). Passive accumulation of albumin is believed to occur due to the leaky vasculature of the tumor endothelium (*27*). Active accumulation is believed to occur via an overexpression of albondin (gp60) and secreted protein acidic and rich in cysteines, SPARC, at the tumor endothelium (*44*). These proteins are responsible for albumin flux into the interstice; gp60 transcellularly and SPARC paracellularly. Despite this accumulation, albumin is still degraded extensively throughout the body; 15% in the liver (*45*), 10% in the kidneys (*46*) and 40-60% in the muscle and skin (*47*, *48*). Other potential natural carriers include IgG, LDL/HDL and transferrin which all demonstrate similar passive tumor accumulation as albumin (*49*, *50*). The half-lives of LDL and transferrin can drop to 1/3 of their intrinsic half-life due to catabolism by a growing tumor. Consequently, these particles are naturally programmed carriers for tumoral delivery

although little has been done with these particles for PTX delivery. Synthetic LDL has been formulated and administered (*51*, *52*) while transferrin has been used primarily as a targeting ligand (*53*, *54*).

The only clinically approved alternative to TAXOL is Abi-007 (ABRAXANE). ABRAXANE is formulated by suspending PTX with albumin followed by nebulization under high pressure. This consequently entraps the hydrophobic PTX molecules inside the albumin core resulting in 130 nm particles. This greatly narrows the technology to apply only to hydrophobic drugs with moderately high affinity for albumin. The particles are believed to break down in serum but the albumin may or may not retain the native form. If the albumin is unable to refold properly, it could reduce or relinquish its affinity for all major receptors. This does not appear to be the case for gp60 or SPARC (*44*), but at the time of this writing there has been no mention associating ABRAXANE with FcRn. ABRAXANE is much better tolerated than TAXOL and docetaxel allowing greater doses of PTX and shorter 30 minute infusions on the same schedule as TAXOL; every 3 weeks (*44*, *55*, *56*). A dose of ABRAXANE contains 100 mg of PTX for every 900 mg albumin or about 8.5 eq of PTX per albumin for a 10% loading capacity. The complexity of formulation requires recombinant albumin instead of native albumin extant in the patient.

Another technology utilizing albumin involves a PTX prodrug attached to a tumor-specific cleavable peptide and a free maleimide (**Fig. I-1**) (*57*). Albumin is known to have 35 cysteines with 17 locked in disulfides leaving only Cys_{34} with a free thiol. This thiol is known to react quickly via Michael addition across maleimides. Unlike ABRAXANE, this approach does use the native albumin of the patient with efficient binding complete within 30 minutes. It then has a tumor specific release mechanism for prostate cancer due to the overexpression of prostate-specific antigen (PSA). This allows flexibility to generate tumor-specific release mechanisms for various malignancies as well as a more generalized

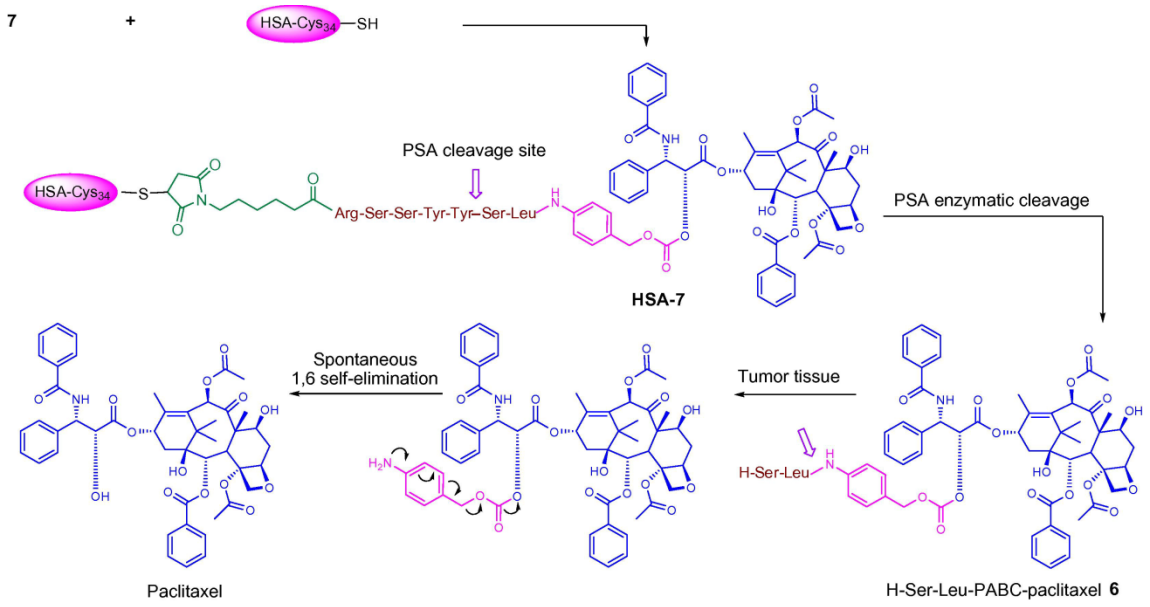

Figure I-1. Synthesis and theoretical *in vivo* decomposition of the sequentially labile Michael adduct of PTX. When albumin begins to accumulate in a solid tumor, specific cleavage by the often prostate-specific antigen (PSA) facilitates spontaneous decomposition of the p-aminobenzyloxycarbonyl (PABC) carbonate at the 2'-OH of PTX releasing the free drug. The free drug is then able to diffuse throughout the tumor tissue. Figure reproduced with permission from *Eur J Cancer* (*57*).

approach for a commonly overexpressed enzyme such as cathepsins or matrix metalloproteases (MMPs). Scalability can be expensive requiring the synthesis of a hexapeptide-maleimide conjugate and subsequent condensation with a Leu-p-aminobenzyloxycarbonyl-PTX conjugate. As demonstrated, this only allows a 1:1 albumin:PTX construct which constitutes about 1% loading capacity. Adding more PTX molecules is synthetically feasible but they will be conjugated further from the carrier which could subsequently destabilize the construct. This technology is not cargo specific, and has been demonstrated with a variety of drugs including doxorubicin (ε-maleimidocaproyl)hydrazone (Doxo-EMCH) which is in clinical trials (*58*). With minor chemical modifications this technology could potentially allow the simultaneous injection of multiple classes of drugs for combination therapy (*59*).

When administered intravenously, maleimide-based albumin conjugates dilute about 90% during the distribution phase as albumin permeates the body extensively. After equilibration, the conjugates will slowly eliminate with half-lives approaching that of the native protein. This is demonstrated in **Fig. I-2** where a maleimide derivative of an anti-HIV peptide is chemically conjugated to albumin *in vivo* (*60*). The observed half-lives of 25.8 h for rats and 102.4 h for rhesus monkeys correlate well with the half-lives of intact albumin; 1 and 5 days respectively. Extrapolation of these data suggests the half-life of albumin conjugates in humans could approach 19 days.

Albumin is intrinsically a useful carrier for antineoplastics. It also has many useful features for drug loading. Albumin is a fatty acid carrier having 6-7 binding sites in the nanomolar dissociation range (*61*). This could be exploited by the use of acylated prodrugs. This technique would not require recombinant albumin, provided the prodrug is soluble as micelles, and would not be constrained to any specific drug molecule. An example of this is the long-circulating insulin detemir (LEVEMIR) (*62*). This technique allows a moderate

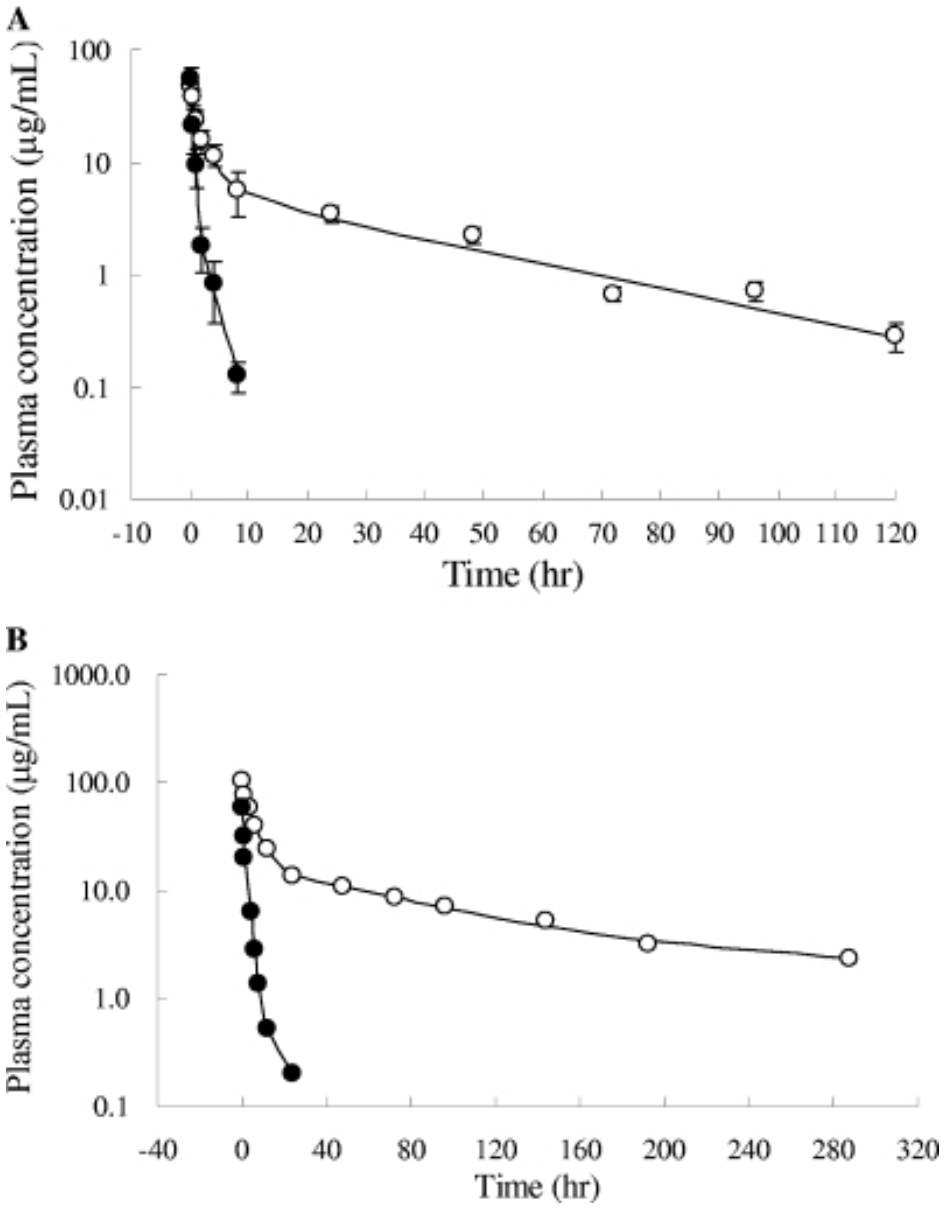

Figure I-2. Serum pharmacokinetics of an anti-HIV peptide conjugated to Cys_{34} of albumin. Both panels show a ten-fold decrease in concentration prior to the protracted half-life. This is not clearance from the system but distribution throughout the body. At equilibrium, the re-emergence of extravascular conjugate into the circulation is what gives rise to the long terminal half-life. Results in rats (**A**) and rhesus monkeys (**B**) show half-lives of 1 and 4.3 days which corresponds well with the half-lives of native albumin in the respective species. Figure reproduced with permission from *Antimicrob Agents Chemother* (*60*).

drug:carrier ratio, although not as high as ABRAXANE. While albumin does accumulate in tumors, it also extensively permeates the tissues, particularly muscle, giving the prodrugs ample time for dissociation (*63*). Binding of fatty acids does cause a natural transition in the structure of albumin (*64*) which may or may not affect the affinity for intrinsic receptors. Albumin has many nucleophlic lysines and electrophilic glutaric/aspartic anhydrides which can be used for direct conjugation of a large quantity of drugs. This is not cargo specific and could allow a large proportion of drug loading but would be difficult to accomplish *in vivo* thus requiring recombinant albumin. Additionally, it has been shown the more lysine residues that are modified, the affinity for the gp60 receptor drops while the affinity for scavenger receptors such as gp18 and gp30 increase (*65*, *66*). This could greatly reduce the circulation life of the complex.

5. Synthetic Macromolecular Drug Carriers

Synthetic carriers offer another opportunity for drug delivery. Because they are entirely synthetic, they can be constructed to specific dimensions and functionality providing meticulous control over the final product. This can allow the generation of very high capacity carriers with mechanisms for triggered drug release. Once built to the desired size, the carrier can be derivatized with cargo, targeting moieties, steric protection, release mechanisms; all the important components necessary for a successful delivery vehicle. This is necessary as these carriers, despite often being made of natural products, are biologically foreign and treated as such. Overcoming this resistance can lead to the addition of many amenities which can be synthetically taxing and expensive.

An example of a polymer made of natural components is the amino acid based scaffold of poly-(L)-glutamic acid (PLG). PLG-PTX completed phase III clinical trials but was not sufficient to file a new drug application (*67*, *68*). PLG-PTX begins with a 36-kDa polymer of repeating glutamic acid residues which are coupled with the 2'-OH on PTX attaining 20%

loading capacity (*69*). This prodrug should be quite labile due to large quantities of esterases and peptidases with non-specific hydrolytic activity. Being amino acid based, degradation of the particles occurs readily, however, release of PTX from the polymer is slow (*70*). PTX is released as a monoglutamyl ester at the 2'-OH. Comparable doses of PTX versus PLG-PTX show PLG-PTX is less potent. This is most likely due to the inability of the glutamyl-PTX monomer to bind tubulin as is seen with succinic acid derivatives at the 2'-OH of PTX (*71-73*). PLG-PTX shows mostly accumulation in the spleen and liver, followed closely by the kidneys and lungs. The accumulation in the tumor is about a quarter of the liver and spleen accumulation per gram of tissue. All these organs have persistent concentrations of drug, even after 6 days (*74*). Since PLG-PTX is completely chemistry based, it has the potential for further modification with a release mechanism similar to the aforementioned p-aminobenzyloxycarbonyl (PABC). This could facilitate PTX release without greatly affecting the synthetic load, the solubility or the drug loading. The addition of another equivalent of glutamic acid residues prior to PTX allows an increase in the loading capacity of the polymer and resulted in the spontaneous formation of ~20 nm particles which could greatly alter the pharmacokinetics of the formulation (*75*).

Similar to PLG, other benign polymers can be formulated such as polylactic-co-glycolic acid (PLGA) polymers. These lipophilic polymers are water insoluble and thus dissolved in a solvent such as chloroform. As opposed to chemical conjugation, these polymers form coacervates around the hydrophobic molecules. Dissolution of PTX and PLGA as well as polyethyleneglycol-biotin modified polylactic acid are added to a 2.5% o/w emulsion (*76*). The 40 kDa PLGA polymers can adsorb at the interface with PTX in the core. Replacing the oil phase with water stabilizes the 220 nm coacervate due to van der Waals interactions with PTX. This method allowed up to 18% drug loading of a biotin targeted formulation. Pharmacokinetic (PK) analysis was not performed but the formulation

showed only 20-30% drug leakage over 3 days in PBS at 37℃. This led to only a very moderate increase in efficacy (*76*). Other PLGA formulations have been derivatized with various targeting ligands such as the RGD peptide (*77*), wheat germ agglutinin (*78*) and transferrin (*79*). The half-life of the transferrin-modified PLGA particles is about 5.5 h and biodistribution shows primarily uptake in the liver, spleen and kidneys indicative of filtration and reticuloendothelial system (RES) sequestration (*79*). This is surprising although not uncommon as the particles of about 200 nm diameter should be too large for the various fenestrations aside from the tumor. This distribution is most likely a result of a high degree of shear flexibility promoting extravasation.

Another class of synthetic polymers is dendrimers which have been used extensively and are some of the more highly functionalized of the synthetic carriers. Traditional polyamidoamine (PAMAM) dendrimers are symmetrical polymers built by alternating ethylenediamine and methyl acrylate moieties (*80*). Initially ethylenediamine is reacted with 4 equivalents of methyl acrylate via Michael addition resulting in 4 methyl esters. This is called generation 0.5 (G0.5). Next, all the esters are condensed with a large excess of ethylenediamine. This keeps the net number of functional groups constant but converts the surface to cationic amines and the generation is incremented by a half-step; G1.0. Cationic dendrimers are known to be toxic so the final condensation can be done with ethanolamine allowing which coats the surface with primary alcohols. This removes the charge from the surface of the dendrimer whil still providing a nucleophilic moiety for functionalization (*81*). Alternatively, the amines can be capped, most commonly with acetyl groups.

One such formulation began with a G5 dendrimer with 82 out of 110 primary amines acetylated. To the remaining amines were grafted 2'-O-paclitaxelhemisuccinate, fluoresceinisothiocyanate (FITC) and tetrahydrofolate as a drug, tracer and targeting ligand respectively (**Fig. I-3**) (*80*). The final product contained an average 5 FITC fluorescent

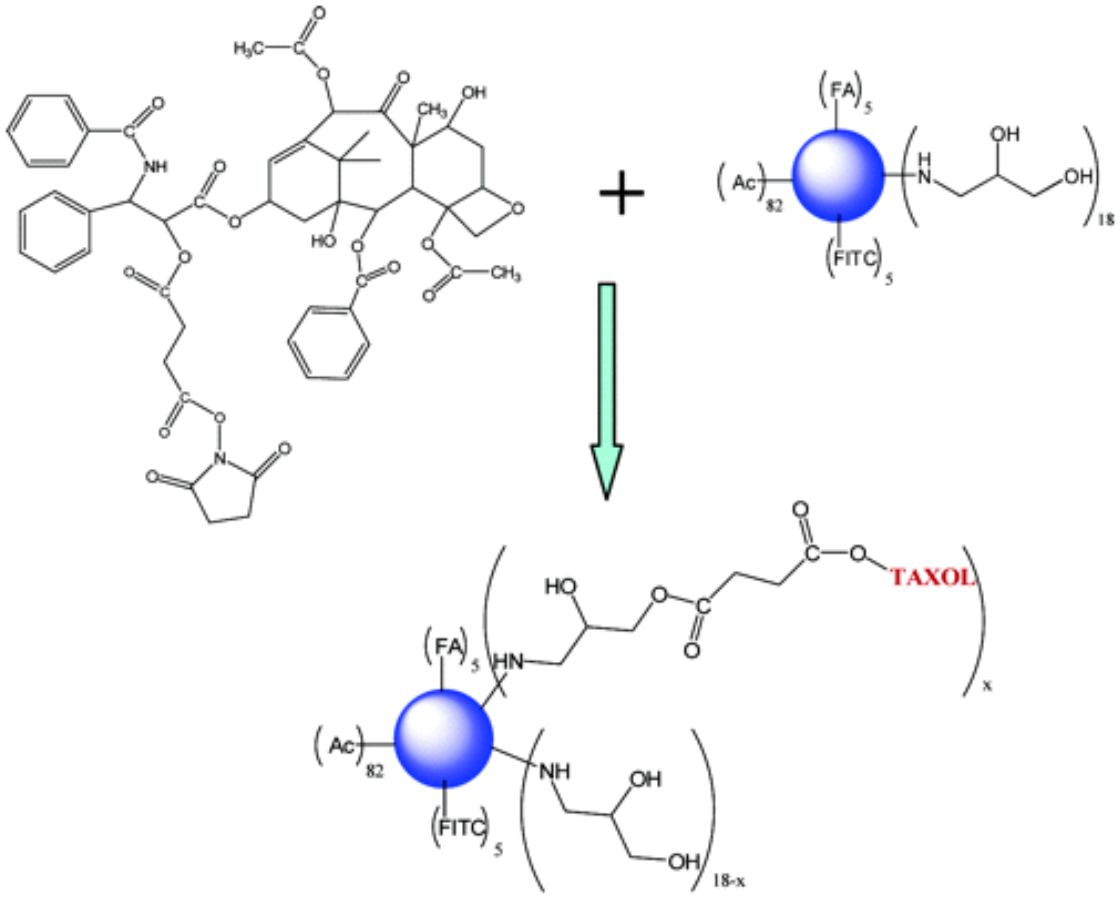

Figure I-3. Structure of G5 dendrimer derivatized with paclitaxel (PTX), folic acid (FA) and fluoresceinisothiocyanate (FITC). This construct is designed to target tumor cells which commonly overexpress the folate receptor. The PTX is used for cytotoxicity and FITC as a fluorescent tracer. At 20 nm, diffusion of the dendrimer in the tumor environment will be minimal, so uptake will most likely occur peripherally. Figure reproduced with permission from *Biomacromolecules* (*80*).

tracers, 4.8 folates and 3 PTX succinate molecules per dendrimer. The loading capacity in this formulation is low (~6%) but can be improved via the addition of triazine moieties allowing triple the cargo loading without a large increase in size (*82*). These dendrimers allowed 18-30% PTX loading by mass with ~18% by weight dendrimer and the rest polyethyleneglycol (PEG). Each dendrimer is approximately 26 kDa which is roughly 1/3 of an albumin molecule so the loading capacity is comparable to ABRAXANE. Being comparable to albumin in final molecular weight, it will utilize mostly convection for movement, redering diffusion within the tumor a slow processs. Due to their size, dendrimers should be essentially invisible to phagocytic systems. The dendrimers will however be subject to extravasation through the sinusoids of the liver and the smaller fenestrations in the kidneys, particularly if the dendrimer is cationic.

While the folate receptor is ubiquitous, it is highly overexpressed in several tumor cell lines which would promote receptor mediated endocytosis in the tumor microenvironment (*83*). The large number of unused amines and capped amines allows the potential for conjugating more drug or more targeting ligand. This could improve toxicity and avidity and could be titrated to find an optimal ratio. Grafted on the dendrimer surface, the folate may not be readily accessible to the folate receptors, however this could be remedied by conjugating PEG moieties with folate on the distal end. Due to diffusion constraints, the dendrimers will most likely only encounter folate receptors on peripheral tumor cells. Once internalized the dendrimer has a built-in endosomal escape mechanism with the internal tertiary amines providing a weak base to act as a proton sponge.

Drug release does not have to be induced by peptidases or esterases alone. Alternative release mechanisms include the PABC self-immolative release mechanism (*84*) mentioned earlier as well as disulfides (*85*) which can release in the cytosol and possibly the endosome. Thermally-sensitive dendrimers have also been developed which can promote

drug release due to specific heating of the tumor environment (*86*). This has been accomplished in the past for thermally-sensitive liposomes (*87*) by use of near-infrared lasers (*88*). Recently it has been proposed dendrimers be rendered entirely self-immolative (*89*). This technique, if the trigger can be highly tumor specific, would allow complete and instantaneous release of the drug at the active site along with the benign building blocks of the dendrimer. An acid-sensitive cap or enzyme-specific cap could be a very useful triggering mechanism, particularly for endosomal release. If a single dendrimer coated with a targeting ligand and PTX were endoctyosed, it would have the osmotic pressure of a single molecule. If upon acidification, the entire dendrimer immolated into 1000 non or monoionized membrane impermeable fragments, the osmotic pressure should theoretically increase 1000 fold. This alone may potentially be a useful tool for endosomal escape for larger membrane impermeable therapies.

6. Lipid-Based Formulations

One technology undergoing phase III clinical trials is a stabilized nanoemulsion containing PTX. The α-tocopherolpolyethyleneglycolsuccinate (TPGS), nanodroplets of about 40-80 nm contain a derivative of vitamin E, and 10 mg/mL PTX. This is higher than TAXOL (1.2 mg/mL) but the loading capacity is comparatively low at about 8% (*90*). The concentrations attained with this formulation are much greater thus expediting infusion times to 15 minutes. The simplicity of the formulation and familiarity of administration are beneficial but despite the better solubility and infusion rate, this formulation still suffers from neutropenia related toxicities (*91*). At 40-80 nm, these particles could be subject to both renal and hepatic filtration in addition to tumor extravasation (*92*). The addition of vitamin E could be advantageous for a variety of reasons. One shortcoming of PTX is several tumors are PTX resistant due to overexpression of P-glycoprotein (P-gp) (*93*). The surfactant TPGS has been shown to act as an inhibitor for P-gp which could allow PTX to be more

effiective in these tumors (*94*). Additionally, TPGS has been shown to have adjuvant toxicity with PTX, putatively by inducing caspase-8 (*95*). If synergistic, this could require lower dosing of PTX compared to TAXOL thus decreasing the chance of neutropenia. The use of intact drug in this formulation could make it more potent than typical prodrugs. There is, however, an issue of stability as the particles may be prone to flocculation (*96*).

Another formulation in phase III clinical trials is docosahexaenoic acid PTX (DHA-PTX). This formulation uses an ω-3 fatty acylated PTX at the 2'-OH to improve solubility in the TAXOL vehicle. Formulation only requires 20% of the CrEL of TAXOL but still only yields 3% drug loading (*97*). As with other 2'-OH derivatives, this derivative does not bind microtubules and will require hydrolysis for full toxicity (*98*). After hydrolysis, the released DHA has been extensively shown to sensitize tumors to apoptosis (*99-101*). While more tolerable than TAXOL, this formulation still suffers from neutropenia (*102*) due to the CrEL which demonstrates toxicity even at 20% of the dose. An increase in half-life of the formulation is observed in humans despite the decrease in CrEL; 112 h as compared to 85 h for TAXOL (*103*). LDL is known to efficiently bind unsaturated fatty acids, much better than albumin, and could provide a good vehicle for this molecule (*104*). Partial binding of LDL could explain the slightly protracted half-life observed for DHA-PTX.

Last is a technology involving a squalenoic acid derivative of PTX (sqPTX). Initially this technology was developed by directly conjugating squalenoic acid to the hydrophilic nucleoside antagonist gemcitabine (difluorodeoxycytidine, dFdC) (*105*). The resultant amphiphile showed self assembly into particles when diluted into water from a water miscible co-solvent. This technology has now also been applied to the notoriously hydrophobic PTX (*106*). Despite having no apparent hydrophilic headgroup, this monomer spontaneously aggregates into nanoassemblies of ~100 nm. The addition of a triethyleneglycol or undecaethyleneglycol linker between the PTX and squalenoic acid

resulted in an increase in particle size up to ~300 nm. Both were able to solubilize PTX to a concentration of 5 mg/mL. The 100 nm sqPTX nanoassemblies were highly resistant to hydrolysis from pH 4-9 and were resistant to enzymatic hydrolysis in serum. As with other 2'-OH prodrugs, it is unable to bind microtubules thus requiring hydrolysis for activation, particularly as the conjugate experiences greatly reduced cytotoxicity compared to PTX. The PEGylated conjugates appear more cytotoxic and prone to hydrolysis in serum thus the cytotoxicity is most likely derived from higher PTX concentrations. The 100 nm size may result in an increased liver and spleen accumulation due to RES uptake.

The tumor localized sqPTX may not readily release PTX so a tumor specific cleavage of the sqPTX could be added to render a more potent formulation. Considering this technology contains only two molecules of similar molecular weight, the drug loading is high at 70% and the manufacture inexpensive. The sqPTX or one of the pegylated prodrugs could be built into a carrier such as a liposome as was done with sqdFdC (*107*), although the amphiphilic nature of sqdFdC may make it more amenable than sqPTX for this process. Derivatization of the liposomes with PEG could help shield the particles from detection by the RES (*108*). Derivatization with targeting ligands on the distal end of PEG at tunable concentrations for increased avidity and receptor mediated endocytosis could facilitate intratumoral delivery. Liposomes tend to offer a poor drug loading for PTX (~3%) and sqPTX would not see much improvement (*109*).

7. Summary

There are many different vehicles to formulate PTX for a more targeted and effective delivery and no single formulation exemplifies all the ideal characteristics of a delivery vehicle. Natural carriers offer an interesting concept of using millions of years of biological evolution to design drug carriers that can be utilized in a myriad of ways. There is very little control over the vehicle though as small changes can disrupt the natural tendencies of the

carrier. These formulations tend to result in lower loading capacities and non-specific tissue destinations. However, this approach is relatively inexpensive and effective provided the formulation can piggyback on the natural abundance of the carrier as opposed to requiring a recombinant carrier.

Synthetic carriers offer the most control as they are limited only by synthetic potential. This can allow higher loading capacity, endosomal escape mechanisms and more controlled and well-defined vehicles with the ability to titrate the level of drug and targeting ligand. These macromolecules can be tailored to specific tumors based on easily exchangeable targeting ligands but may experience greater biological resistance due to the unnatural composition of the vehicles requiring the addition of a steric enhancer such as PEG. This high degree of tunability comes at a cost. The more functionalized the vehicle, the more taxing and expensive the synthesis.

Lastly the lipid based technologies appear the most flexible having the ability to use natural carriers such as albumin or LDL, self-associate into vesicles or micelles or be integrated into synthetic carriers such as liposomes. These formulations are perhaps the least expensive and easiest to manufacture but may experience issues with solubility. There is no express vehicle for targeted delivery or inherent release mechanisms. As a result, these formulations may be more susceptible to non-specific sequestration or immunogenicity. As all these ideas coalesce and develop, it will be interesting to see how the formulations adapt. As the old adage says: the early bird gets the worm, but the second mouse gets the cheese.

8. References

1. Terwogt, J. M., Nuijen, B., Huinink, W. W., and Beijnen, J. H. (1997) Alternative formulations of paclitaxel, *Cancer Treat. Rev. 23*, 87-95.

2. Crown, J., O'Leary, M., and Ooi, W. (2004) Docetaxel and paclitaxel in the treatment of breast cancer: a review of clinical experience, *Oncologist 9 Suppl 2*, 24-32.

3. Ueda, Y., Mikkilineni, A. B., Knipe, J. O., Rose, W. C., Casazza, A. M., and Vyas, D. M. (1993) Novel water soluble phosphate prodrugs of taxol® possessing in vivo antitumor activity, *Bioorg. Medicinal Chem. Lett. 3*, 1761-1766.

4. Magri, N. F., and Kingston, D. G. (1988) Modified taxols, 4. Synthesis and biological activity of taxols modified in the side chain, *J. Nat. Prod. 51*, 298-306.

5. Kumar, G. N., Walle, U. K., Bhalla, K. N., and Walle, T. (1993) Binding of taxol to human plasma, albumin and alpha 1-acid glycoprotein, *Res. Commun. Chem. Pathol. Pharmacol*. *80*, 337-344.

6. Sykes, E., Woodburn, K., Decker, D., and Kessel, D. (1994) Effects of Cremophor EL on distribution of Taxol to serum lipoproteins., *Br. J. Cancer 70*, 401-404.

7. Paal, K., Shkarupin, A., and Beckford, L. (2007) Paclitaxel binding to human serum albumin--automated docking studies, *Bioorg. Med. Chem. 15*, 1323-1329.

8. Bertucci, C., Cimitan, S., Riva, A., and Morazzoni, P. (2006) Binding studies of taxanes to human serum albumin by bioaffinity chromatography and circular dichroism, *J Pharm. Biomed. Anal. 42*, 81-87.

9. Sparreboom, A., van Zuylen, L., Brouwer, E., Loos, W. J., de Bruijn, P., Gelderblom, H., Pillay, M., Nooter, K., Stoter, G., and Verweij, J. (1999) Cremophor EL-mediated alteration of paclitaxel distribution in human blood: clinical pharmacokinetic implications, *Cancer Res. 59*, 1454-1457.

10. van Zuylen, L., Karlsson, M. O., Verweij, J., Brouwer, E., de Bruijn, P., Nooter, K., Stoter, G., and Sparreboom, A. (2001) Pharmacokinetic modeling of paclitaxel encapsulation in Cremophor EL micelles, *Cancer Chemother. Pharmacol. 47*, 309-318.

11. Huizing, M. T., Sparreboom, A., Rosing, H., van Tellingen, O., Pinedo, H. M., and Beijnen, J. H. (1995) Quantification of paclitaxel metabolites in human plasma by high-performance liquid chromatography, *J. Chromatogr. B, Biomed. Appl. 674*, 261-268.

12. Andersen, J. T., and Sandlie, I. (2009) The versatile MHC class I-related FcRn protects IgG and albumin from degradation: implications for development of new diagnostics and therapeutics, *Drug Metab. Pharmacokinet. 24*, 318-332.

13. Eiseman, J. L., Eddington, N. D., Leslie, J., MacAuley, C., Sentz, D. L., Zuhowski, M., Kujawa, J. M., Young, D., and Egorin, M. J. (1994) Plasma pharmacokinetics and tissue distribution of paclitaxel in CD2F1 mice, *Cancer Chemother. Pharmacol. 34*, 465-471.

14. Sparreboom, A., Scripture, C. D., Trieu, V., Williams, P. J., De, T., Yang, A., Beals, B., Figg, W. D., Hawkins, M., and Desai, N. (2005) Comparative preclinical and clinical pharmacokinetics of a cremophor-free, nanoparticle albumin-bound paclitaxel (ABI-007) and paclitaxel formulated in Cremophor (Taxol), *Clin. Cancer Res. 11*, 4136-4143.

15. Fransson, M. N., Green, H., Litton, J., and Friberg, L. E. (2011) Influence of Cremophor EL and Genetic Polymorphisms on the Pharmacokinetics of Paclitaxel and its Metabolites using a Mechanism-Based Model, *Drug Metab. Dispos. 39,* 247-255.

16. Brown, T., Havlin, K., Weiss, G., Cagnola, J., Koeller, J., Kuhn, J., Rizzo, J., Craig, J., Phillips, J., and Von Hoff, D. (1991) A phase I trial of taxol given by a 6-hour intravenous infusion, *J. Clin. Oncol. 9*, 1261 -1267.

17. Lockman, P. R., Mumper, R. J., Khan, M. A., and Allen, D. D. (2002) Nanoparticle technology for drug delivery across the blood-brain barrier, *Drug Dev. Ind. Pharm. 28*, 1-13.

18. Dosio, F., Stella, B., Arpicco, S., and Cattel, L. (2011) Macromolecules as taxane delivery systems, *Expert Opin. Drug Deliv. 8*, 33-55.

19. Petros, R. A., and DeSimone, J. M. (2010) Strategies in the design of nanoparticles for therapeutic applications, *Nat. Rev. Drug Discov. 9*, 615-627.

20. Trissel, L. A. (1997) Pharmaceutical properties of paclitaxel and their effects on preparation and administration, *Pharmacotherapy 17*, 133S-139S.

21. Takakura, Mahato, and Hashida. (1998) Extravasation of macromolecules, *Adv. Drug Deliv. Rev. 34*, 93-108.

22. Jachimska, B., Wasilewska, M., and Adamczyk, Z. (2008) Characterization of Globular Protein Solutions by Dynamic Light Scattering, Electrophoretic Mobility, and Viscosity Measurements, *Langmuir 24*, 6866-6872.

23. Hashizume, H., Baluk, P., Morikawa, S., McLean, J. W., Thurston, G., Roberge, S., Jain, R. K., and McDonald, D. M. (2000) Openings between Defective Endothelial Cells Explain Tumor Vessel Leakiness, *Am. J. Pathol. 156*, 1363-1380.

24. Moghimi, S. M., Hunter, A. C., and Murray, J. C. (2001) Long-circulating and target-specific nanoparticles: theory to practice, *Pharmacol. Rev. 53*, 283-318.

25. Sarlo, K., Blackburn, K. L., Clark, E. D., Grothaus, J., Chaney, J., Neu, S., Flood, J., Abbott, D., Bohne, C., Casey, K., Fryer, C., and Kuhn, M. (2009) Tissue distribution of 20 nm, 100 nm and 1000 nm fluorescent polystyrene latex nanospheres following acute systemic or acute and repeat airway exposure in the rat, *Toxicology 263*, 117-126.

26. Zhu, X., Meng, G., Dickinson, B. L., Li, X., Mizoguchi, E., Miao, L., Wang, Y., Robert, C., Wu, B., Smith, P. D., Lencer, W. I., and Blumberg, R. S. (2001) MHC class I-related neonatal Fc receptor for IgG is functionally expressed in monocytes, intestinal macrophages, and dendritic cells, *J. Immunol. 166*, 3266-3276.

27. Maeda, H. (2010) Tumor-selective delivery of macromolecular drugs via the EPR effect: background and future prospects, *Bioconjug. Chem. 21*, 797-802.

28. Kularatne, S. A., and Low, P. S. (2010) Targeting of nanoparticles: folate receptor, *Methods Mol. Biol. 624*, 249-265.

29. Shanle, E. K., and Xu, W. (2010) Selectively targeting estrogen receptors for cancer treatment, *Adv. Drug Deliv. Rev. 62*, 1265-1276.

30. Garanger, E., Boturyn, D., and Dumy, P. (2007) Tumor targeting with RGD peptide ligands-design of new molecular conjugates for imaging and therapy of cancers, *Anticancer Agents Med. Chem. 7*, 552-558.

31. Zhang, X., Luck, J., Dewhirst, M. W., and Yuan, F. (2000) Interstitial hydraulic conductivity in a fibrosarcoma, *AM J. PHYSIOL-HEART C. 279*, H2726 -H2734.

32. Tannock, I. F., and Rotin, D. (1989) Acid pH in tumors and its potential for therapeutic exploitation, *Cancer Res. 49*, 4373-4384.

33. Rozema, D. B., Ekena, K., Lewis, D. L., Loomis, A. G., and Wolff, J. A. (2003) Endosomolysis by Masking of a Membrane-Active Agent (EMMA) for Cytoplasmic Release of Macromolecules, *Bioconjug. Chem. 14*, 51-57.

34. Mohamed, M. M., and Sloane, B. F. (2006) Cysteine cathepsins: multifunctional enzymes in cancer, *Nat. Rev. Cancer 6*, 764-775.

35. Gialeli, C., Theocharis, A. D., and Karamanos, N. K. (2011) Roles of matrix metalloproteinases in cancer progression and their pharmacological targeting, *FEBS J. 278*, 16-27.

36. Affara, N. I., Andreu, P., and Coussens, L. M. (2009) Delineating protease functions during cancer development, *Methods Mol. Biol. 539*, 1-32.

37. Sonawane, N. D., Szoka, F. C., and Verkman, A. S. (2003) Chloride Accumulation and Swelling in Endosomes Enhances DNA Transfer by Polyamine-DNA Polyplexes, *J. Biol. Chem. 278*, 44826 -44831.

38. Chen, H., Zhang, H., McCallum, C. M., Szoka, F. C., and Guo, X. (2007) Unsaturated cationic ortho esters for endosome permeation in gene delivery, *J. Med. Chem. 50*, 4269-4278.

39. Yang, S., Zaitseva, E., Chernomordik, L. V., and Melikov, K. (2010) Cell-penetrating peptide induces leaky fusion of liposomes containing late endosome-specific anionic lipid, *Biophys. J 99*, 2525-2533.

40. Peters, T. (1985) Serum albumin, *Adv. Protein Chem. 37*, 161-245.

41. Kobayashi, N., Suzuki, Y., Tsuge, T., Okumura, K., Ra, C., and Tomino, Y. (2002) FcRn-mediated transcytosis of immunoglobulin G in human renal proximal tubular epithelial cells, *Am. J. Physiol. Renal Physiol. 282*, F358-365.

42. Telleman, P., and Junghans, R. P. (2000) The role of the Brambell receptor (FcRB) in liver: protection of endocytosed immunoglobulin G (IgG) from catabolism in hepatocytes rather than transport of IgG to bile, *Immunology 100*, 245-251.

43. Stehle, G., Sinn, H., Wunder, A., Schrenk, H. H., Stewart, J. C., Hartung, G., Maier-Borst, W., and Heene, D. L. (1997) Plasma protein (albumin) catabolism by the tumor itself--implications for tumor metabolism and the genesis of cachexia, *Crit. Rev. Oncol. Hematol. 26*, 77-100.

44. Desai, N. P., Trieu, V., Hwang, L. Y., Wu, R., Soon-Shiong, P., and Gradishar, W. J. (2008) Improved effectiveness of nanoparticle albumin-bound (nab) paclitaxel versus polysorbate-based docetaxel in multiple xenografts as a function of HER2 and SPARC status, *Anti-Cancer Drugs 19*, 899-909.

45. KATZ, J., ROSENFELD, S., and SELLERS, A. L. (1961) Sites of plasma albumin catabolism in the rat, *Am. J. Physiol. 200*, 1301-1306.

46. Bent-Hansen, L. (1991) Initial plasma disappearance and tissue uptake of 131I-albumin in normal rabbits, *Microvasc. Res. 41*, 345-356.

47. Yedgar, S., Carew, T. E., Pittman, R. C., Beltz, W. F., and Steinberg, D. (1983) Tissue sites of catabolism of albumin in rabbits, *Am. J. Physiol. 244*, E101-107.

48. Baynes, J. W., and Thorpe, S. R. (1981) Identification of the sites of albumin catabolism in the rat, *Archives of Biochemistry and Biophysics 206*, 372-379.

49. Kratz, F., and Beyer, U. (1998) Serum proteins as drug carriers of anticancer agents: a review, *Drug Deliv. 5*, 281-299.

50. Masquelier, M., Vitols, S., Pålsson, M., Mårs, U., Larsson, B. S., and Peterson, C. O. (2000) Low density lipoprotein as a carrier of cytostatics in cancer chemotherapy: study of stability of drug-carrier complexes in blood, *J. Drug Target. 8*, 155-164.

51. Rodrigues, D. G., Maria, D. A., Fernandes, D. C., Valduga, C. J., Couto, R. D., Ibañez, O. C. M., and Maranhão, R. C. (2005) Improvement of paclitaxel therapeutic index by derivatization and association to a cholesterol-rich microemulsion: in vitro and in vivo studies, *Cancer Chemother. Pharmacol. 55*, 565-576.

52. Nikanjam, M., Gibbs, A. R., Hunt, C. A., Budinger, T. F., and Forte, T. M. (2007) Synthetic nano-LDL with paclitaxel oleate as a targeted drug delivery vehicle for glioblastoma multiforme, *J. Cont. Rel. 124*, 163-171.

53. Sahoo, S. K., and Labhasetwar, V. (2005) Enhanced antiproliferative activity of transferrin-conjugated paclitaxel-loaded nanoparticles is mediated via sustained intracellular drug retention, *Mol. Pharm. 2*, 373-383.

54. Bicamumpaka, C., and Pagé, M. (1998) In vitro cytotoxicity of paclitaxel-transferrin conjugate on H69 cells, *Oncol. Rep. 5*, 1381-1383.

55. Desai, N., Trieu, V., Yao, Z., Louie, L., Ci, S., Yang, A., Tao, C., De, T., Beals, B., Dykes, D., Noker, P., Yao, R., Labao, E., Hawkins, M., and Soon-Shiong, P. (2006)

Increased antitumor activity, intratumor paclitaxel concentrations, and endothelial cell transport of cremophor-free, albumin-bound paclitaxel, ABI-007, compared with cremophor-based paclitaxel., *Clin. Cancer Res. 12*, 1317 -1324.

56. Rizvi, N. A., Riely, G. J., Azzoli, C. G., Miller, V. A., Ng, K. K., Fiore, J., Chia, G., Brower, M., Heelan, R., Hawkins, M. J., and Kris, M. G. (2008) Phase I/II trial of weekly intravenous 130-nm albumin-bound paclitaxel as initial chemotherapy in patients with stage IV non-small-cell lung cancer, *J. Clin. Oncol. 26*, 639-643.

57. Elsadek, B., Graeser, R., Esser, N., Schäfer-Obodozie, C., Ajaj, K. A., Unger, C., Warnecke, A., Saleem, T., El-Melegy, N., Madkor, H., and Kratz, F. (2010) Development of a novel prodrug of paclitaxel that is cleaved by prostate-specific antigen: an in vitro and in vivo evaluation study, *Eur. J. Cancer 46*, 3434-3444.

58. Unger, C., Häring, B., Medinger, M., Drevs, J., Steinbild, S., Kratz, F., and Mross, K. (2007) Phase I and pharmacokinetic study of the (6-maleimidocaproyl)hydrazone derivative of doxorubicin, *Clin. Cancer Res. 13*, 4858-4866.

59. Ajaj, K. A., Biniossek, M. L., and Kratz, F. (2009) Development of Protein-Binding Bifunctional Linkers for a New Generation of Dual-Acting Prodrugs, *Bioconjug. Chem. 20*, 390-396.

60. Xie, D., Yao, C., Wang, L., Min, W., Xu, J., Xiao, J., Huang, M., Chen, B., Liu, B., Li, X., and Jiang, H. (2010) An Albumin-Conjugated Peptide Exhibits Potent Anti-HIV Activity and Long In Vivo Half-Life, *Antimicrob. Agents Chemother. 54*, 191-196.

61. Spector, A. A. (1975) Fatty acid binding to plasma albumin, *J. Lipid Res. 16*, 165-179.

62. Kurtzhals, P., Havelund, S., Jonassen, I., Kiehr, B., Larsen, U. D., Ribel, U., and Markussen, J. (1995) Albumin binding of insulins acylated with fatty acids: characterization of the ligand-protein interaction and correlation between binding affinity and timing of the insulin effect in vivo, *Biochem. J. 312 (Pt 3)*, 725-731.

63. van der Vusse, G. J. (2009) Albumin as fatty acid transporter, *Drug Metab. Pharmacokinet. 24*, 300-307.

64. Fang, Y., Tong, G. C., and Means, G. E. (2006) Structural changes accompanying human serum albumin's binding of fatty acids are concerted, *Biochimica et Biophysica Acta (BBA) - Proteins & Proteomics 1764*, 285-291.

65. Haberland, M. E., and Fogelman, A. M. (1985) Scavenger receptor-mediated recognition of maleyl bovine plasma albumin and the demaleylated protein in human monocyte macrophages, *Proc. Natl. Acad. Sci. U.S.A. 82*, 2693-2697.

66. Schnitzer, J. E., Sung, A., Horvat, R., and Bravo, J. (1992) Preferential interaction of albumin-binding proteins, gp30 and gp18, with conformationally modified albumins. Presence in many cells and tissues with a possible role in catabolism, *J. Biol. Chem. 267*, 24544-24553.

67. Langer, C. J., O'Byrne, K. J., Socinski, M. A., Mikhailov, S. M., Leśniewski-Kmak, K., Smakal, M., Ciuleanu, T. E., Orlov, S. V., Dediu, M., Heigener, D., Eisenfeld, A. J.,

Sandalic, L., Oldham, F. B., Singer, J. W., and Ross, H. J. (2008) Phase III trial comparing paclitaxel poliglumex (CT-2103, PPX) in combination with carboplatin versus standard paclitaxel and carboplatin in the treatment of PS 2 patients with chemotherapy-naïve advanced non-small cell lung cancer, *J. Thorac. Oncol. 3*, 623-630.

68. Paz-Ares, L., Ross, H., O'Brien, M., Riviere, A., Gatzemeier, U., Von Pawel, J., Kaukel, E., Freitag, L., Digel, W., Bischoff, H., García-Campelo, R., Iannotti, N., Reiterer, P., Bover, I., Prendiville, J., Eisenfeld, A. J., Oldham, F. B., Bandstra, B., Singer, J. W., and Bonomi, P. (2008) Phase III trial comparing paclitaxel poliglumex vs docetaxel in the second-line treatment of non-small-cell lung cancer, *Br. J. Cancer 98*, 1608-1613.

69. Li, C., Yu, D. F., Newman, R. A., Cabral, F., Stephens, L. C., Hunter, N., Milas, L., and Wallace, S. (1998) Complete regression of well-established tumors using a novel water-soluble poly(L-glutamic acid)-paclitaxel conjugate, *Cancer Res. 58*, 2404-2409.

70. Shaffer, S. A., Baker-Lee, C., Kennedy, J., Lai, M. S., de Vries, P., Buhler, K., and Singer, J. W. (2007) In vitro and in vivo metabolism of paclitaxel poliglumex: identification of metabolites and active proteases, *Cancer Chemother. Pharmacol. 59*, 537-548.

71. Bradley, M. O., Webb, N. L., Anthony, F. H., Devanesan, P., Witman, P. A., Hemamalini, S., Chander, M. C., Baker, S. D., He, L., Horwitz, S. B., and Swindell, C. S. (2001) Tumor targeting by covalent conjugation of a natural fatty acid to paclitaxel, *Clin. Cancer Res. 7*, 3229-3238.

72. Deutsch, H. M., Glinski, J. A., Hernandez, M., Haugwitz, R. D., Narayanan, V. L., Suffness, M., and Zalkow, L. H. (1989) Synthesis of congeners and prodrugs. 3. Water-soluble prodrugs of taxol with potent antitumor activity, *J. Med. Chem. 32*, 788-792.

73. Dosio, F., Reddy, L. H., Ferrero, A., Stella, B., Cattel, L., and Couvreur, P. (2010) Novel nanoassemblies composed of squalenoyl-paclitaxel derivatives: synthesis, characterization, and biological evaluation, *Bioconjug. Chem. 21*, 1349-1361.

74. Li, C., Newman, R. A., Wu, Q. P., Ke, S., Chen, W., Hutto, T., Kan, Z., Brannan, M. D., Charnsangavej, C., and Wallace, S. (2000) Biodistribution of paclitaxel and poly(L-glutamic acid)-paclitaxel conjugate in mice with ovarian OCa-1 tumor, *Cancer Chemother. Pharmacol. 46*, 416-422.

75. Feng, Z., Zhao, G., Yu, L., Gough, D., and Howell, S. B. (2010) Preclinical efficacy studies of a novel nanoparticle-based formulation of paclitaxel that out-performs Abraxane, *Cancer Chemother. Pharmacol. 65*, 923-930.

76. Patil, Y., Sadhukha, T., Ma, L., and Panyam, J. (2009) Nanoparticle-mediated simultaneous and targeted delivery of paclitaxel and tariquidar overcomes tumor drug resistance, *J. Cont. Rel. 136*, 21-29.

77. Danhier, F., Vroman, B., Lecouturier, N., Crokart, N., Pourcelle, V., Freichels, H., Jérôme, C., Marchand-Brynaert, J., Feron, O., and Préat, V. (2009) Targeting of tumor endothelium by RGD-grafted PLGA-nanoparticles loaded with Paclitaxel, *J. Cont. Rel. 140*, 166-173.

78. Wang, C., Ho, P. C., and Lim, L. Y. (2010) Wheat germ agglutinin-conjugated PLGA nanoparticles for enhanced intracellular delivery of paclitaxel to colon cancer cells, *Int. J. Pharm. 400*, 201-210.

79. Neha Shah, Kiran Chaudhari, Prudhviraju Dantuluri, R. S. R. Murthy, and Susobhan Das. (2009) Paclitaxel-loaded PLGA nanoparticles surface modified with transferrin and Pluronic®P85, an in vitro cell line and in vivo biodistribution studies on rat model, *J. Drug Target. 17,* 533-542.

80. Majoros, I. J., Myc, A., Thomas, T., Mehta, C. B., and Baker, J. R. (2006) PAMAM Dendrimer-Based Multifunctional Conjugate for Cancer Therapy: Synthesis, Characterization, and Functionality, *Biomacromolecules 7*, 572-579.

81. Mishra, V., Gupta, U., and Jain, N. K. (2009) Surface-engineered dendrimers: a solution for toxicity issues, *J. Biomater. Sci. Polym. Ed. 20*, 141-166.

82. Lim, J., and Simanek, E. E. (2008) Synthesis of water-soluble dendrimers based on melamine bearing 16 paclitaxel groups, *Org. Lett. 10*, 201-204.

83. Kelemen, L. E. (2006) The role of folate receptor alpha in cancer development, progression and treatment: cause, consequence or innocent bystander?, *Int. J. Cancer 119*, 243-250.

84. Erez, R., Segal, E., Miller, K., Satchi-Fainaro, R., and Shabat, D. (2009) Enhanced cytotoxicity of a polymer-drug conjugate with triple payload of paclitaxel, *Bioorg. Med. Chem. 17*, 4327-4335.

85. Lim, J., Chouai, A., Lo, S., Liu, W., Sun, X., and Simanek, E. E. (2009) Design, Synthesis, Characterization, and Biological Evaluation of Triazine Dendrimers Bearing Paclitaxel Using Ester and Ester/Disulfide Linkages, *Bioconjug. Chem. 20*, 2154-2161.

86. Haba, Y., Harada, A., Takagishi, T., and Kono, K. (2004) Rendering poly(amidoamine) or poly(propylenimine) dendrimers temperature sensitive, *J. Am. Chem. Soc. 126*, 12760-12761.

87. Yarmolenko, P. S., Zhao, Y., Landon, C., Spasojevic, I., Yuan, F., Needham, D., Viglianti, B. L., and Dewhirst, M. W. (2010) Comparative effects of thermosensitive doxorubicin-containing liposomes and hyperthermia in human and murine tumours, *Int. J. Hyperthermia 26*, 485-498.

88. Wu, G., Mikhailovsky, A., Khant, H. A., and Zasadzinski, J. A. (2009) Chapter 14 - Synthesis, characterization, and optical response of gold nanoshells used to trigger release from liposomes, *Meth. Enzymol. 464*, 279-307.

89. Meijer, E. W., and van Genderen, M. H. P. (2003) Chemistry: Dendrimers set to self-destruct, *Nature 426*, 128-129.

90. Dhillon, T., Stebbing, J., and Bower, M. (2005) Paclitaxel for AIDS-associated Kaposi's sarcoma, *Expert Rev. Anticancer Ther. 5*, 215-219.

91. Bulitta, J. B., Zhao, P., Arnold, R. D., Kessler, D. R., Daifuku, R., Pratt, J., Luciano, G., Hanauske, A., Gelderblom, H., Awada, A., and Jusko, W. J. (2009) Multiple-pool cell lifespan models for neutropenia to assess the population pharmacodynamics of unbound paclitaxel from two formulations in cancer patients, *Cancer Chemother. Pharmacol. 63*, 1035-1048.

92. Bulitta, J. B., Zhao, P., Arnold, R. D., Kessler, D. R., Daifuku, R., Pratt, J., Luciano, G., Hanauske, A., Gelderblom, H., Awada, A., and Jusko, W. J. (2009) Mechanistic population pharmacokinetics of total and unbound paclitaxel for a new nanodroplet formulation versus Taxol in cancer patients, *Cancer Chemother. Pharmacol. 63*, 1049-1063.

93. Takano, M., Otani, Y., Tanda, M., Kawami, M., Nagai, J., and Yumoto, R. (2009) Paclitaxel-resistance conferred by altered expression of efflux and influx transporters for paclitaxel in the human hepatoma cell line, HepG2, *Drug Metab. Pharmacokinet. 24*, 418-427.

94. Liu, Y., Huang, L., and Liu, F. (2010) Paclitaxel nanocrystals for overcoming multidrug resistance in cancer, *Mol. Pharm. 7*, 863-869.

95. Lim, S., Choi, M. K., Kim, M. J., and Kim, J. K. (2009) Alpha-tocopheryl succinate potentiates the paclitaxel-induced apoptosis through enforced caspase 8 activation in human H460 lung cancer cells, *Exp. Mol. Med. 41*, 737-745.

96. Constantinides, P. P., Chaubal, M. V., and Shorr, R. (2008) Advances in lipid nanodispersions for parenteral drug delivery and targeting, *Adv. Drug Deliv. Rev. 60*, 757-767.

97. Sparreboom, A., Wolff, A. C., Verweij, J., Zabelina, Y., van Zomeren, D. M., McIntire, G. L., Swindell, C. S., Donehower, R. C., and Baker, S. D. (2003) Disposition of docosahexaenoic acid-paclitaxel, a novel taxane, in blood: in vitro and clinical pharmacokinetic studies, *Clin. Cancer Res. 9*, 151-159.

98. Bradley, M. O., Swindell, C. S., Anthony, F. H., Witman, P. A., Devanesan, P., Webb, N. L., Baker, S. D., Wolff, A. C., and Donehower, R. C. (2001) Tumor targeting by conjugation of DHA to paclitaxel, *J. Cont. Rel. 74*, 233-236.

99. Blanckaert, V., Ulmann, L., Mimouni, V., Antol, J., Brancquart, L., and Chénais, B. (2010) Docosahexaenoic acid intake decreases proliferation, increases apoptosis and decreases the invasive potential of the human breast carcinoma cell line MDA-MB-231, *Int. J. Oncol. 36*, 737-742.

100. Lee, C. Y., Sit, W., Fan, S., Man, K., Jor, I. W., Wong, L. L., Wan, M. L., Tan-Un, K. C., and Wan, J. M. (2010) The cell cycle effects of docosahexaenoic acid on human metastatic hepatocellular carcinoma proliferation, *Int. J. Oncol. 36*, 991-998.

101. Habermann, N., Christian, B., Luckas, B., Pool-Zobel, B. L., Lund, E. K., and Glei, M. (2009) Effects of fatty acids on metabolism and cell growth of human colon cell lines of different transformation state, *Biofactors 35*, 460-467.

102. Fracasso, P. M., Picus, J., Wildi, J. D., Goodner, S. A., Creekmore, A. N., Gao, F., Govindan, R., Ellis, M. J., Tan, B. R., Linette, G. P., Fu, C. J., Pentikis, H. S., Zumbrun, S. C., Egorin, M. J., and Bellet, R. E. (2009) Phase 1 and pharmacokinetic study of weekly docosahexaenoic acid-paclitaxel, Taxoprexin, in resistant solid tumor malignancies, *Cancer Chemother. Pharmacol. 63*, 451-458.

103. Wolff, A. C., Donehower, R. C., Carducci, M. K., Carducci, M. A., Brahmer, J. R., Zabelina, Y., Bradley, M. O., Anthony, F. H., Swindell, C. S., Witman, P. A., Webb, N. L., and Baker, S. D. (2003) Phase I study of docosahexaenoic acid-paclitaxel: a taxane-fatty acid conjugate with a unique pharmacology and toxicity profile, *Clin. Cancer Res. 9*, 3589-3597.

104. Wolfrum, C., Shi, S., Jayaprakash, K. N., Jayaraman, M., Wang, G., Pandey, R. K., Rajeev, K. G., Nakayama, T., Charrise, K., Ndungo, E. M., Zimmermann, T., Koteliansky, V., Manoharan, M., and Stoffel, M. (2007) Mechanisms and optimization of in vivo delivery of lipophilic siRNAs, *Nat. Biotech. 25*, 1149-1157.

105. Couvreur, P., Stella, B., Reddy, L. H., Hillaireau, H., Dubernet, C., Desmaële, D., Lepêtre-Mouelhi, S., Rocco, F., Dereuddre-Bosquet, N., Clayette, P., Rosilio, V., Marsaud, V., Renoir, J., and Cattel, L. (2006) Squalenoyl nanomedicines as potential therapeutics, *Nano Lett. 6*, 2544-2548.

106. Dosio, F., Reddy, L. H., Ferrero, A., Stella, B., Cattel, L., and Couvreur, P. (2010) Novel nanoassemblies composed of squalenoyl-paclitaxel derivatives: synthesis, characterization, and biological evaluation, *Bioconjug. Chem. 21*, 1349-1361.

107. Pili, B., Reddy, L. H., Bourgaux, C., Lepêtre-Mouelhi, S., Desmaële, D., and Couvreur, P. (2010) Liposomal squalenoyl-gemcitabine: formulation, characterization and anticancer activity evaluation, *Nanoscale 2*, 1521-1526.

108. Li, S., and Huang, L. (2009) Nanoparticles evading the reticuloendothelial system: role of the supported bilayer, *Biochim. Biophys. Acta 1788*, 2259-2266.

109. Sharma, A., and Straubinger, R. M. (1994) Novel taxol formulations: preparation and characterization of taxol-containing liposomes, *Pharm. Res. 11*, 889-896.

CHAPTER II

FATTY ACIDS AS THERAPEUTIC AUXILIARIES: REVIEW

This chapter is being submitted for publication as a review to the *Journal of Lipid Research* and is formatted in the style of this journal.

1. Introduction

When a drug is administered parenterally to a patient with a systemic disorder, it is immediately diluted throughout 6 liters of blood and potentially 18 L of interstitial volume. The site of action for the drug will typically encompass only a very small fraction of total body volume so concentrations of drug at the target will be minimal. This dissipative nature of distribution poses a major problem for drug formulation leading to poor efficacy and high toxicity. The nascent discipline of drug delivery endeavors to selectively alter the distribution of a drug for accumulation at the target site with diminution at non-specific sites. This can be accomplished by utilizing a targeting mechanism that takes advantage of the specific milieu associated with the site of action. Arguably the simplest method of targeting is to ascertain extant mechanisms by which the body naturally engages the tissue of interest and piggyback on them; for example, endemic hepatic expression of the asialoglycoprotein receptor (1) or the accumulation and consumption of serum albumin in arthritic joints (2). There are a myriad of delivery mechanisms, far too many to recount in a single review. This review will focus on a subset of technologies utilizing fatty acids and triglycerides to improve the drug profiles for oral and intravenous administration.

2. Formulations to Improve Oral Absorption

Ingested lipids are highly insoluble and thus aggregate as micelles or submicron emulsions depending on composition. The presence of these lipids in the intestines triggers the release of lipases, phosphoplipases and bile salts designed to hydrolyze triglycerides to diacylglycerides and monoacylglycerides releasing free fatty acids. Glycerides and long-chain fatty acids bind apical fatty acid binding proteins which deliver them to the endoplasmic reticulum (ER) of the enterocyte (3). Shorter-chain fatty acids which exhibit higher solubility can bind monocarboxylic acid transporters (4). Fatty acids can be transported to the portal vein for first-pass transfer to the liver, presumably via albumin

binding. Alternatively, fatty acids can be reacylated into triglycerides and incorporated in chylomicrons which are delivered to the lamina propria and eventually the systemic circulation via the thoracic duct (3). These particles eventually mature into very low-density lipoprotein (VLDL) then low-density lipoprotein (LDL) or high-density lipoprotein (HDL) if they contain a large quantity of phospholipids. Lymphatic absorption is a potentially useful mechanism for oral drug delivery to the systemic circulation as it bypasses the first-pass clearance of the liver altogether.

2.1. Caprates

One method to promote absorption of high solubility, low permeability molecules such as peptides is co-formulation with medium-chain fatty acids. Caprates (C10:0) are believed to induce the transient opening of tight junctions facilitating paracellular absorption (5). This process has been thoroughly demonstrated in Caco-2 cell culture (6), rat ilea (7), human ilea (8) and human colon biopsies (9). While mechanistically complex, caprates and caprylates (C8:0) are believed to modulate tight junctions through phospholipase C induced release of Ca^{2+} and subsequent protein kinase C activation (6; 10). This phenomenon is not observed for lauric acid (C12:0), although lauric acid too is believed to facilitate paracellular permeability (11). These fatty acids are non-toxic and have been used successfully in many formulations (12). High doses of sodium caprate alone have shown success for the absorption of 2'-*O*-methoxyethyl phosphorothioate antisense oligonucleotide gapmers against tumor necrosis factor-α achieving up to 13% bioavailability in humans (13). After absorption by the paracellular route, these molecules will be directed to the liver where a substantial portion may be extracted and degraded (14). This is the most likely reason bioavailabilities remain low. This idea has been streamlined through the Gastrointestinal Permeation Enhancement Technology (GIPET) (15). The technology involves formulating a drug along with caprate and caprylate salts in an enteric soft gel. Hydrophilic molecules like

peptides can quickly dissolve and diffuse through the intestinal lumen. Conversely, fatty acid salts will dissolve slower as they need to form micelles and possibly partition into bile salt emulsions before binding monocarboxylic acid transporters. This process may be significantly slower, leaving the peptide in a hazardous environment with the highly proteolytic brush border enzymes (16; 17). Application of the technology to low molecular weight heparin resulted in a doubling of the bioavailability, however this number is still quite low at approximately 8%. The relative bioavailability of oral acyline, a gonadotropin hormone releasing antagonist, increased up to 16-fold in beagles (12) and showed activity in human volunteers (18) despite a very modest total bioavailability.

2.2. Triglyceride Formulations

Alternatively fatty acids can be used to elude first-pass metabolism by disguising a drug as a triglyceride. Valproic acid was esterified at the *sn*-2 position on the glycerol backbone of lysophosphatidylcholine (19). This molecule showed an ability to absorb across the gut lumen of rats and get packaged into chylomicrons for distribution to the lymphatics. The technology was only able to achieve 9% bioavailability, 60% of which was due to lymphatic uptake. The prodrug showed great resistance to lipases *in vitro* suggesting the issue may not be premature release of valproic acid for portal absorption. The bioavailability appears dependent on several factors including the vehicle and the pre/postprandial state; in both cases, the presence of other lipids. Formulation in peanut oil containing mostly palmitic (C16:0), stearic (C18:0), oleic (C18:1), and linoleic (C18:2) ester triglycerides promoted an increase in bioavailability. This is consistent with several other reports on long-chain triglycerides (20-22). Alternatively, formulation with medium-chain triglycerides containing caprate and caprylate esters provided lower bioavailabilities. The postprandial state also increased bioavailability compared with the starved state. Standard rat chow is approximately 3% lipid, a vast majority of which are long-chain ω-fatty acids (23).

Common to both successful scenarios is the presence of long-chain triglyceride. This observation has been noted in several other reports on lymphatically absorbed drugs as well (24-26). Long-chain fatty acids have been associated with an increase in chylomicron formation in the Golgi apparatus of enterocytes (26) which should promote increased lymphatic delivery. This methodology is amenable to both hydrophobic and hydrophilic small molecules. It may be difficult, however, to apply to large hydrophilic molecules such as oligonucleotides or peptides due to the requisite membrane partitioning.

2.3. Submicron Lipid Particles

Submicron particles have been the subject of oral delivery recently due to their ability to carry a multitude of cargoes as well as their stability and targetability. Being too large for significant paracellular absorption and lack of membrane permeability, these formulations require a different approach. The gastrointestinal tract is lined with a plethora of cells. M cells are associated with a great deal of lymphatic innervations due to their function of sampling antigen from the intestines and passing it to the various antigen presenting cells within the lymph (27). M cells have a thin glycocalyx and undergo frequent macropinocytosis. Most commonly, particle absorption from the intestines is believed to occur through M cells and enterocytes, however, the endocytosis via enterocytes tends to be more destructive as M cells are devoid of lysosomes (28). Targeting to Peyer's Patches therefore presents an opportunity for higher lymphatic absorption of particles, particularly for inducing mucosal immunity. The common mucosal immune system is an autonomous system of immunity protecting various mucosal organs, most notably the airway, gut, eye and genitals (29). It is estimated about 80% of immunocytes are involved in the common mucosal immune system which is designed to protect the vast area of mucosal organs thus preventing systemic infection. Commonly lipid particles are used for vaccine delivery due to the nature of lymphatic absorption of lipids (28). Formulation of antigens in w/o/w multiple

emulsions containing squalene solubilized in saline with nonionic poloxamer surfactants allowed successful stabilization and delivery of a recombinant fusion protein from *E. coli* to Peyer's Patches (30). The fusion protein was unable to induce mucosal immunity subsequent to parenteral administration. An orally viable tuberculosis vaccine was also developed for mucosal immunization (31). When formulated with vegetable oil, this strain of the mycobacterium was stabilized in the gastrointestinal tract for absorption by M cells. The lipid did not affect the efficacy of the vaccine even leading to greater protection when compared to the standard subcutaneous vaccine.

3. Acylation of Therapeutic Molecules

3.1. Albumin Binding

Another approach to improve the therapeutic potential of peptides or proteins is by chemical modification with lipid moieties, either through a non-reversible or a reversible linkage. The lipids do not greatly affect the solubility of proteins, as they tend to be less than 10% of the weight of the conjugate. The lipids will most likely confer binding to serum proteins, specifically albumin. The merits for binding albumin as a drug carrier are well established (32; 33). Albumin is a highly soluble protein which can confer solubility to hydrophobic drugs (34). It has a 19-day half-life in humans (35) and it is extremely abundant at 40-50 mg/mL in the vasculature. It can thus greatly retard elimination from the system. While the primary function of albumin is plasma expansion, it is also a carrier for fatty acids (36). Albumin has 6-7 fatty acid binding sites for long-chain fatty acids (37) with dissociation constants in the nanomolar range (38). The high affinity for the fatty acid binding sites is due to hydrophobic channels in the protein which cradle the aliphatic tail and cationic lysine or arginine residues at the apex of the channel which anchor the anionic carboxylate electrostatically (39; 40). While it may be appealing to make a fatty acid conjugate of a drug

to utilize these pockets, the process can disrupt the electrostatic interaction at the surface of albumin.

This high affinity is believed to be derived from two sources; hydrophobic interactions within the binding pocket which is primarily an entropy-driven process and the primarily enthalpy-driven electrostatic interactions with the anionic carboxylate of fatty acids. To test this hypothesis, in an unpublished study, fluoresceinamine (FLA) was used as a drug surrogate and derivatized with a short diethyleneglycol linker. The surrogate was subsequently attached to stearic acid (SA) and 3-pentadecylglutaric (PDG) acid via an amide as shown in **Fig. II-1**. The only difference between the two molecules is the carboxymethyl group on the PDG acid which is hypothesized to anchor the conjugate to the protein as shown in **Fig. II-2**. Both conjugates were subjected to isothermal titration calorimetry analysis at 30℃ so the physicochemical parameters could be extracted. The results show a 3.5 fold increase in affinity of PDG-FLA for delipidated human serum albumin. This is derived from greater than twofold increase in enthalpy for the PDG conjugate compared to the SA conjugate. However, the SA-FLA conjugate does show 1.5-fold higher entropy compared to the PDG conjugate. This could be a result of the carboxymethyl group on PDG preventing the proper seating of the conjugate in the binding pocket which could be remedied by increasing the tail length. If true, the two conjugates should bind with comparable changes in entropy. In this case, the calculated K_A for the PDG-FLA conjugate would be approximately 125 fold higher than the FLA-SA conjugate due solely to retention of the carboxylate.

3.2. Non-Reversible Lipidization

In non-reversible methods of lipidization, peptide or proteins are typically modified with reactive fatty acid derivatives (e.g., fatty acid chloride or anhydride) at the α-amino or

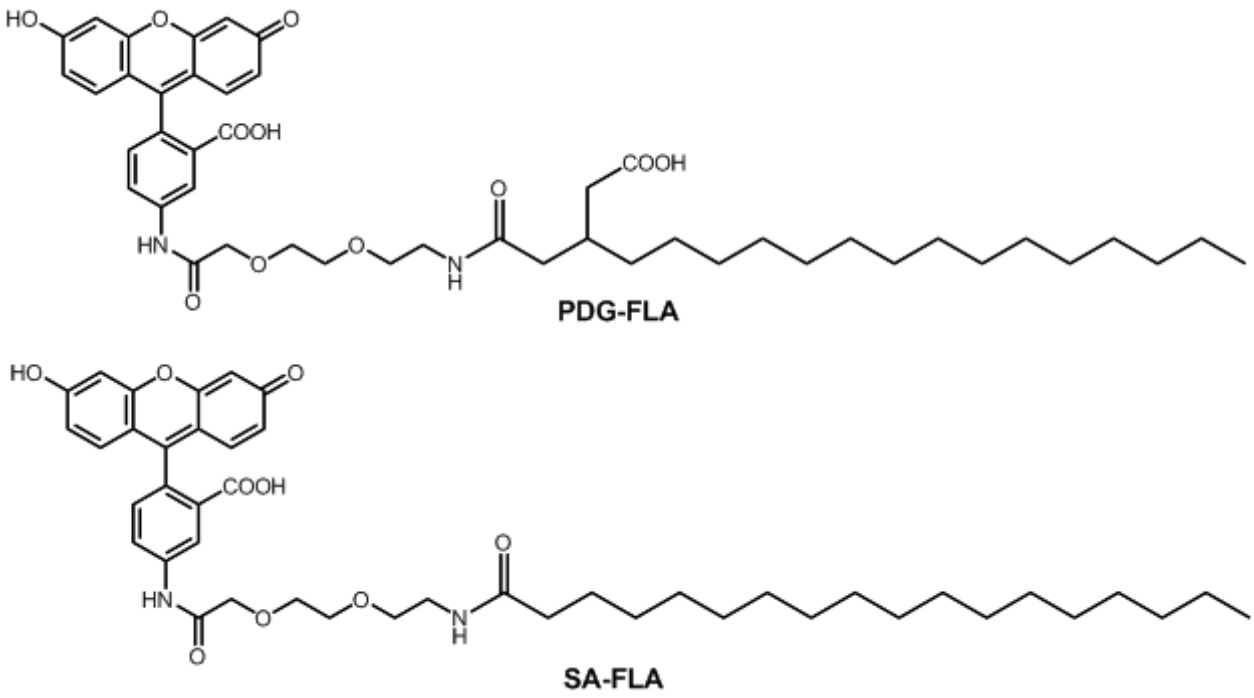

Figure II-1. FLA conjugates for isothermal titration calorimetry analysis. These water-soluble lipid conjugates were synthesized to determine the physicochemical parameters involved in albumin binding. It is expected the fatty acid tail and anionic carboxylate contribute to positive entropy and the negative enthalpy, respectively. SA, stearic acid. FLA, fluoresceinamine; PDG, 3-pentadecylglutaric acid.

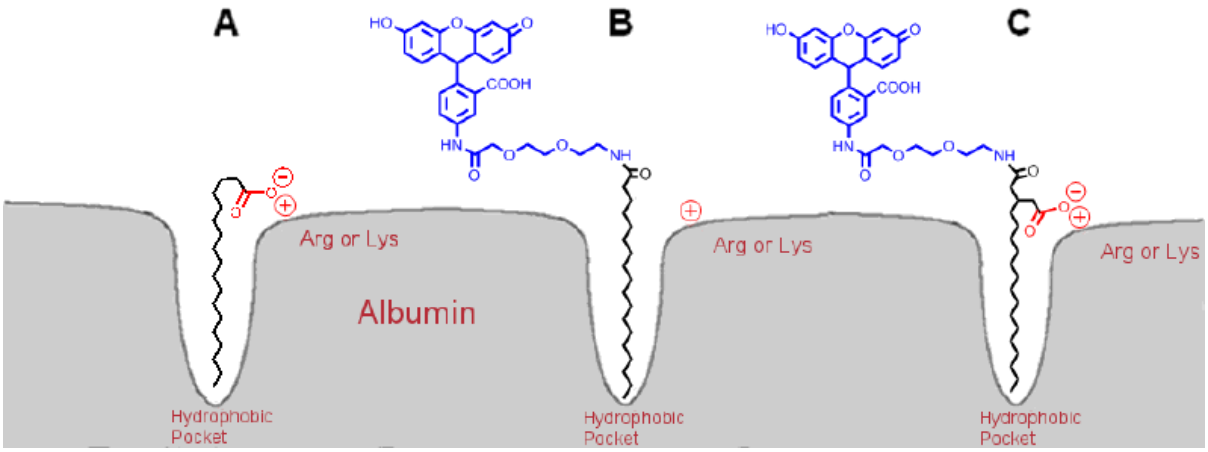

Figure II-2. A schematic representation of the hydrophobic and electrostatic interactions involved in fatty acid-albumin binding (**A**). The addition of a cargo such as fluoresceinamine may utilize only the hydrophobic interaction (**B**) or both hydrophobic and electrostatic interactions (**C**) depending on the modification chemistry.

the ε-lysyl amino groups, resulting in a stable amide bond (41-44). One example is the non-reversible lipidization of cystatin, a 13 kDa protein isolated from chicken albumen that is a known inhibitor of cathepsin-B. Palmitoylation of the amino groups in this protein increased the membrane adsorptive proclivity of the protein for endocytic internalization and subsequent inhibition of lysosomal cathepsin-B (45). This adsorption was determined to be dependent on the tail length of the fatty acid; increasing inhibition with increased tail length through stearic acid (C18:0) (46). The maturation of the late endosome to lysosome would promote binding of the internalized cystatin molecules to cathepsins that are commonly found in these vesicles, assuming the palmitoylated protein survives the conditions of the lysosome. While successful *in vitro*, membrane adsorption is non-specific, so systemic administration would conceivably benefit from the use of a carrier such as a liposome or lipoprotein for targeted accumulation and release.

The seminal use of fatty acids for this purpose was myristoylated insulin detemir (LEVEMIR, Novo Nordisk, Denmark), which was approved by the FDA in 2005. Insulin is a 5.8 kDa polypeptide consisting of two chains linked by three disulfides. In LEVEMIR, the polypeptide is myristoylated at the penultimate lysine residue (B29) (47). Intact insulin polypeptide is terminated with threonine (B30), however in LEVEMIR the terminal threonine is removed. It was found removal of the terminal threonine increased the affinity of LEVEMIR for albumin by approximately 3.5-fold (48). The reason for this change in affinity is most likely due to how the molecule fits in the albumin binding pocket. It is presumed the myristoyl amide as well as the whole lysine side chain fit in the pocket (48). If true, the binding pocket could accommodate 20 atoms from the ω-position of the myristic acid to the α-carbon branching point of lysine. Assuming the amide does not perturb binding in the pocket, this distance would be comparable to arachadic acid (C20:0) which is known to bind albumin (49). Therefore, in LEVEMIR the *C*-terminus of the B chain sits at atop of the

pocket for electrostatic interactions with lysine or arginine. If threonine is left at the *C*-terminus, as with native insulin, the *C*-terminal carboxyl group would shift three atoms away from the binding pocket making formation of the salt-bridge less likely. The result of this high affinity albumin conjugate is an increase in the half-life of insulin from 2.8 h to 8.8 h and no loss of activity when administered subcutaneously (47; 50).

More recently, a second lipidized protein drug, liraglutide (VICTOZA, Novo Nordisk), was also approved by the FDA in 2010 (51). VICTOZA is an analog of glucagon-like peptide (GLP-1), a 37-amino acid native peptide hormone that has a short pharmacological half-life of about 1 h. VICTOZA differs from GLP-1 in the substitution of Lys34 to Arg34, and in the palmitoylation at Lys26 via a γ-glutamic acid spacer. This modification results an improved pharmacokinetic profile, which is attributed to albumin-binding of liraglutide following administration. Due to the long half-life of 11-15 h following subcutaneous injection, this lipidized analog is suitable for once-daily injection. Another insulin analog, insulin degludec, is also in development by Novo Nordisk. Similar to VICTOZA, insulin degludec is palmitoylated at an ε-lysyl amino group (B29) via a γ-glutamic acid spacer, and also has the terminal threonine removed. Promising results from phase 2 clinical trials of insulin degludec have shown that subcutaneous administration three times a week produced glycemic control comparable to insulin glargine, an FDA approved long-acting basal insulin analogue in patients with type I (52) and type II diabetes (53).

3.3. Reversible Lipidization

The non-reversible lipidization of protein or peptide drugs has some limitations including the incompatibility between lipidization reagents and proteins/peptides in solution, and the loss of biological activity of the protein or peptide drug following modification. One technology to promote the half-life of the protein as well as maintain activity is reversible aqueous lipidization (REAL technology) (54). This methodology involves the use of water-

soluble acylation reagents thus circumventing the requirement of organic solvents used in non-reversible lipidization. Additionally, *in vivo* reversible bonds (i.e. disulfide or pH-sensitive bonds) are utilized to link the lipid moiety to the protein or peptide allowing regeneration of free protein or peptide following administration. In this prodrug approach the disulfide bonds between cysteine residues in the protein are reduced, and the resultant free thiols are reacted with an activated disulfide of palmitoylated cysteine (55). The weak reducing conditions of the serum can then slowly delipidate the modified protein allowing refolding and providing a controlled release of intact, bioactive protein. Reversible lipidization using a pH-sensitive linkage involves the modification of free amino groups on the protein using an amine-reactive lipidization reagent. The free protein is then slowly regenerated *in vivo* by hydrolysis at physiological pH (56).

REAL technology has been applied to both peptides and proteins demonstrating increases in half-life. When applied to Tyr^3-octreotide (TOC), a ~1 kDa somatostatin analog for controlled delivery to the liver (57; 58), the half-life of ^{125}I-labeled TOC and REAL-TOC increased from 4.2 h to 6.6 h (57). When REAL was applied to the diuretic desmopressin (~1 kDa) (59), an increase in stability, potency and half-life was observed (60). Similar improvements in pharmacokinetics, stability, and bioactivity have been observed for other proteins and peptides, including enkephalin (~0.5 kDa) (56), calcitonin (~3.4 kDa) (61) and interferon alpha (~20 kDa) (62). These benefits are most likely the result of binding to serum albumin. Similar to insulin detemir, where palmitoylation is occurring through an amide of a terminal amino acid, the carboxylate on cysteine should be readily available for fulfilling the electrostatic interaction involved in albumin binding. In support of this hypothesis, changing the REAL technology's cysteine to cysteamine by decarboxylation or masking the charge with a methyl ester caused drastic decreases in the efficacy of the drug (63). Both

modifications would eliminate the electrostatic interaction thus disrupting the high-affinity nature of albumin binding.

In addition to the improved pharmacokinetic profile, lipidization has also been utilized as an approach to facilitate the oral delivery of protein and peptide drugs. Two examples are the oral administration of calcitonin (61), and enkephalin (56). The studies have shown that, compared to unmodified protein, the lipidized peptide drugs show improvements in the pharmacological activity as well as an increased maximal plasma concentration and AUC. Although the mechanism of enhanced oral absorption is unclear, lipidization is a viable approach in oral protein or peptide delivery.

4. Lipoproteins as Carriers

Aside from albumin, the other major family of natural lipid carriers is the lipoproteins. Lipoproteins are particles formed by the aggregation of triglycerides with less than 5% each of phospholipids, cholesterol and esterified cholesterol. The whole complex is stabilized by a massive apolipoprotein (64). The particles differ by composition, size and stabilizing protein yielding several classes; chylomicrons, VLDL, intermediate density lipoprotein (IDL), LDL and HDL (65; 66). Primarily, VLDL/LDL/HDL are used as drug carriers. VLDL receptors are commonly expressed in the capillary endothelium of muscle, heart and adipose tissues while LDL receptors tend to be expressed highly in the liver as well as many tumor tissues (65; 67). HDL is also cleared primarily by the liver using the scavenger receptor SRB1 but is also heavily consumed by various cancerous cells (68). The particles are stable with biological half-lives of several days, as well as an assumed protection from reticuloendothelial clearance (65; 69). These particles provide competition for the binding of fatty acid substrates with albumin yielding comparable delivery potentials (70), although how long the complex remains intact *in vivo* is not clearly understood.

4.1. Lipoproteins in Gene Delivery

In an exemplarily thorough study using various acylated siRNAs, it was found cholesterol and long-chain fatty acid, including stearic and behenic (C22:0) acids, conjugated siRNA show preferential binding to lipoproteins. Conversely, myristoylated, palmitoylated and oleoylated siRNA bind exclusively to albumin (71). The behenic and stearic derivatives bound HDL/LDL with "dissociation constants" of 100 µM and 300 µM, respectively. The affinity was estimated by the ratio of bound/unbound cholesterol siRNA at given concentrations of lipoprotein. Rather than a dissociation constant, this is better described as a partition coefficient as there is no specific binding site provided by the lipid aggregates but rather a propensity to partition into the particle. This affinity is further confounded by the significant variability in composition of natural lipoprotein particles as opposed to the known and well characterized structure of albumin. The behenic and stearic derivatives bound albumin with dissociation constants of approximately 200 µM and saturated the protein at 3.6 molar equivalents. These values are in stark contrast to the free fatty acids which bind in the low nanomolar dissociation range with ~6 binding sites for stearic acid and 4 for behenic acid (38; 49). Here again, the acylation chemistry eliminates the carboxylate moiety of all fatty acids so albumin binding affinity is expected to decrease. In this instance the loss of affinity is several orders of magnitude.

A major concern for these complexes is *in vivo* stability. The higher the "affinity", the more the kinetics will mimic the kinetics of the carriers themselves. These proteins are all catabolized throughout the body hence the respective ratio of catabolism in various systems is also important in terms of both efficacy and toxicity. To answer these questions, the pharmacokinetics of a cholesterol conjugate of siRNA (**Fig. II-3**) was analyzed in mice using a dual label; ^{125}I on the carrier (LDL, HDL, or albumin) and ^{32}P on the cholesterol siRNA. All three carriers demonstrated protracted half-lives whereas the conjugated siRNAs were

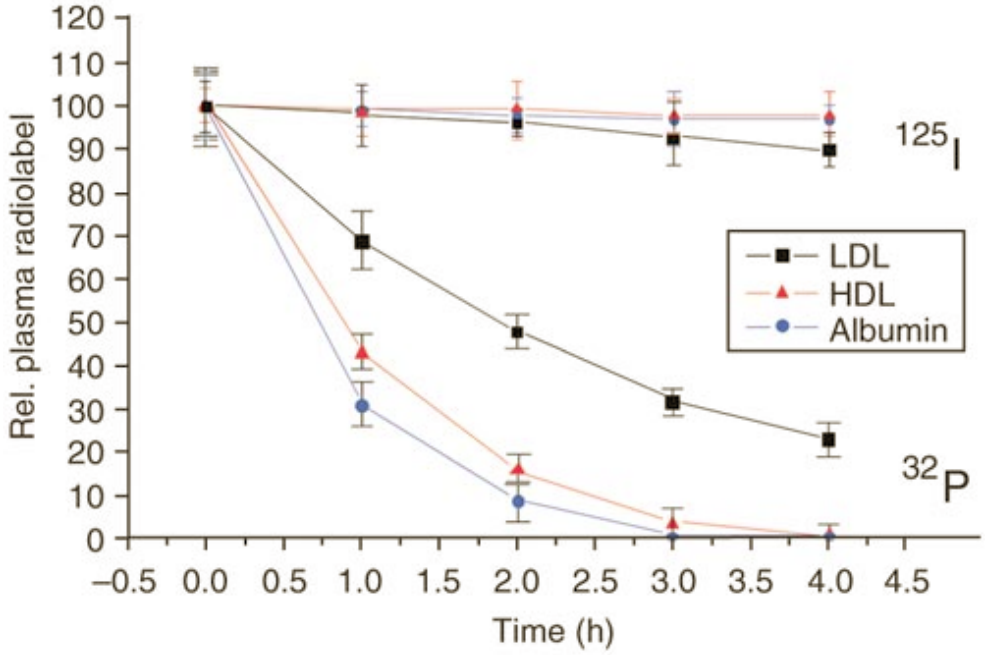

Figure II-3. The serum pharmacokinetics of a cholesterol derivative of ^{32}P-labeled siRNA and various ^{125}I-labeled serum components known to bind cholesterol. Notice the relatively weak binding of the cholesterol-esterified siRNA to the serum components resulted in a significantly different profile compared to the carriers alone. Figure reproduced with permission from *Nat Biotech* (*71*).

completely cleared from the vasculature within 5 hours clearly reflecting the relatively low affinity of the conjugates for the carriers. The biodistribution of cholesterol siRNA associated with the various carriers (**Fig. II-4**) shows a relatively uniform distribution throughout the body with a slight preference for the liver when bound to albumin or HDL. The LDL-bound cholesterol conjugate of siRNA by contrast shows minimal uptake in any tissue aside from the liver.

4.2. Use of Lipoproteins in Targeting Specific Disease-State Cells

Delivery via HDL has recently focused on cancerous cells. The carriers used are recombinant, formed by suspending triglycerides with bacterially expressed Apolipoprotein A1 (Apo-A1) followed by heating and sonication (72). The advent of Apo-A1 fusion proteins delineated two possibilities; the fusion protein could be therapeutic or, since the Apo-A1 sits at the interface, the fusion protein could include a targeting peptide (73). In one instance, interleukin-11α was selected as a targeting peptide as the receptor is highly expressed in various cancer cell lines (74; 75). These technologies showed selective targeting to osteosarcoma masses and the addition of a cytotoxic peptide demonstrated efficacy *in vitro*. Efficacy was also demonstrated *in vivo* by fusing the cell penetrating TAT peptide from the human immunodeficiency virus to Apo-A1 carrying unmodified doxorubicin in the particle (73). The particles release about 40% of the encapsulated doxorubicin within 5 h in normal saline containing 1% BSA. Intratumoral injection of the rHDL showed efficacy of about 30% reduced tumor volume compared to the untreated control. The results were comparable regardless of the presence of the TAT peptide or the rHDL itself, as free doxorubicin had comparable efficacy. Considering the release rate, most of the doxorubicin is probably released quickly into the tumor. To prevent this leakage or dissociation, the doxorubicin could be acylated, which would greatly increase the permeability into rHDL. Commonly, ω-3 fatty acids such as docosahexaeoic acid and linolenic acid are used as these not only

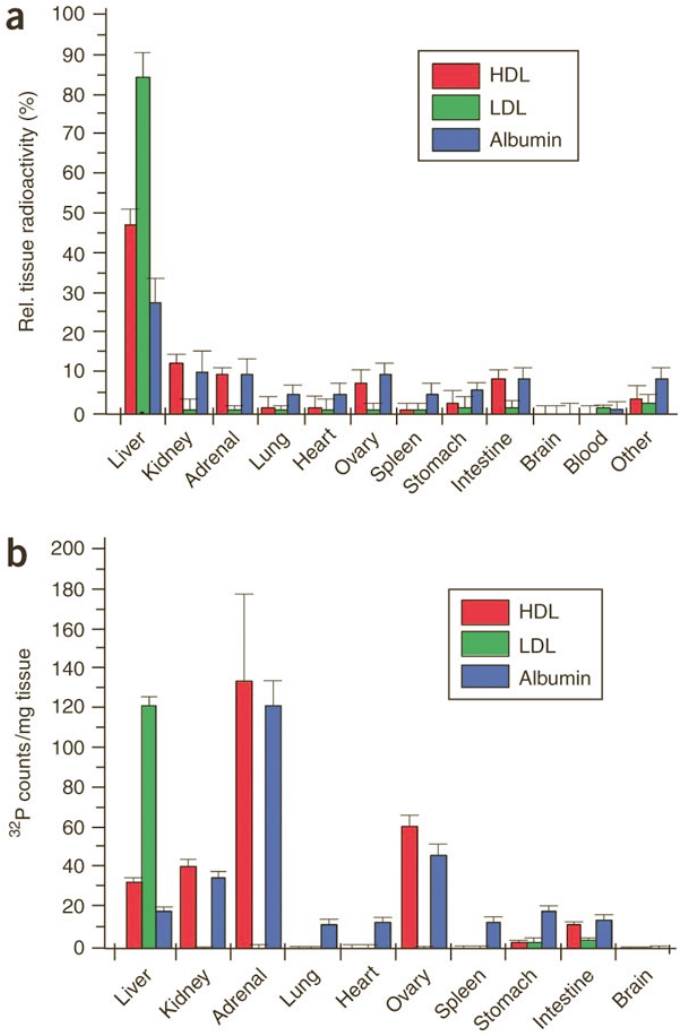

Figure II-4. Biodistribution analysis of albumin, LDL and HDL bound cholesterol-esterified [^{32}P]-siRNA 4 h post tail-vein injection to mice. Primarily the liver promotes the greatest release of the cholesterol conjugate from the lipoprotein carriers. Whereas albumin and HDL distribute the conjugate uniformly, LDL shows accumulation solely in the liver. Figure reproduced with permission from *Nat Biotech* (*71*).

promote membrane permeability, but the ω-3 fatty acids show increased sensitization and even moderate toxicity to a variety of tumor cells (76-78). A similar approach involved using recombinant Apo-$A1_{Milano}$, a mutant with higher affinity for the HDL receptor (79). These particles were loaded with 10-hydroxycamptothecin at up to 80% efficiency and showed a controlled release of 25% of the dose over 24 h when dialyzed in buffer. Biodistribution in naïve mice shows primarily uptake in the kidneys and to a lesser extent the liver and spleen. Biodistribution was not yet performed on tumor bearing mice at the time of this writing.

As with HDL, small synthetic LDL particles have been developed. Coined “nano-LDL”, the lipoprotein is a synthetic LDL receptor-binding domain coupled with a lipid-binding motif for the purpose of targeting cancerous cells; as an example glioblastoma multiforme (80). The particle was formed with phospholipids and triglycerides as well as an oleic acid derivative of paclitaxel (PTX) (81). The nano-LDL was able to solubilize the paclitaxel prodrug at 0.33 mg/mL and was shown to be very toxic to multiple glioblastoma multiforme cell lines expressing variable amounts of the LDL receptor. It is suggested most neurons do not express high levels of the LDL receptor, which could make this vehicle very selective for glioblastoma multiforme cells in the brain. The difficulty for LDL to cross the blood-brain barrier coupled with the ubiquitous expression of the LDL receptor systemically will preclude the use of this approach for parenteral administration. Considering the apolipoprotein used is synthetic, this may simply require a change in the targeting motif for systemic cancers. Brain accumulation has been demonstrated using particles coated in serum ApoE or solid lipid nanoparticles coated with Tween 80 either of which may be incorporated into nano-LDL as well (82).

Aside from cancer, LDL is often associated with atherosclerosis. An excess of oxidized LDL, due to high concentrations of bloodborne lipid and cholesterol, leads to consumption in aortic vasculature by macrophages transforming them into foam cells (83).

Over time, more macrophages are attracted and the vasculature becomes congested and the excess cholesterol forms plaques. Oxidized LDL may bind these plaques more tightly than native LDL facilitating undesirable accumulation of the lipoprotein (84) although this appears to decrease with progression of the disease. This spontaneous accumulation of LDL at the target site makes it an ideal carrier for a therapeutic (85). The steroid, dexamethasone, has been shown to prevent the transformation to foam cells. Palmitoyl dexamethasone was then easily packaged into human LDL collected by ultracentrifugation from serum. Biodistribution in atherosclerotic mice showed a decrease in distribution to the liver and increase to the target site, the aorta. This persisted for 7 days and successfully protected early atherosclerotic lesions from worsening but it did not affect the underlying dyslipidemia. Due to the difficulty in isolating large quantities of human LDL, the potential for transferring bloodborne pathogens and variability in particles, native LDL may be a difficult vehicle to use systemically (86). Synthetic LDL-like emulsions, as in the case nano-LDL, may prove more efficient for development (81; 87). The lipid composition of the emulsion can be more properly controlled preventing off site targeting. Monounsaturated fatty acids for instance tend to promote uptake and cholesteryl ester hydrolysis in macrophages (88).

5. Concluding Remarks

Employing fatty acids in delivering both large and small therapeutic agents has the potential to increase oral bioavailability as well as provide increased half-life, stability and permeability. Large hydrophilic compounds may benefit from paracellular absorption using tight junction modifiers such as medium-chain fatty acids. As this does not avoid hepatic first pass, in many instances, it does not greatly increase oral bioavailability but may be useful for macromolecules which would otherwise not be absorbed intact. Targeting to the lymphatics via chylomicron partitioning in the ER of enterocytes can increase bioavailability

by circumventing hepatic first pass clearance although the process appears slow. This may be the result of the slow formation of chylomicrons, a step that includes difficulty for fatty acid drug conjugate to become triglyceride. Nonetheless, the formulation of a lymphatically absorbed drug with long-chain triglycerides, which are known to induce the formation of chylomicrons, increases the bioavailability of drug. The oral route also provides a useful method for mucosal vaccination. Targeted delivery of antigens to M-cells in the Peyer's Patches allows uptake of the antigen by antigen presenting cells of the common mucosal immune system. All these methods are designed to improve the profile of poorly bioavailable drugs and the results in most cases are very moderate. The drugs then should be metabolically stable and highly potent to be successful.

Parenterally administered drugs can be improved via acylation with various fatty acids. Lipidized therapeutics exhibit greater half-lives allowing less frequent dosing. The addition of fatty acids can disrupt the structure of larger therapeutics such as peptides or proteins rendering them less effective. The increase in hydrophobicity can also lead to non-specific adsorptive endocytosis. Reversible lipidization can rectify these issues by slowly releasing intact peptides or proteins into the system. This has been successfully applied to peptides and proteins of various sizes for both parenteral and oral administration. Lipidized therapeutics can also be used to target albumin or serum lipoproteins. This provides an alternative to the ubiquitous concept of pegylation for prolonging circulatory life. Acylation is highly reversible due to copious amounts of esterases and lipases found throughout the body. The chemistry is cost-effective, straightforward and the myriad of potential fatty acids allows tailoring of prodrugs for a specific purpose.

A major concern for using protein complexation is the stability of the complex *in vivo*. In the case of albumin, the complex is concentration driven. At the time of injection, complexation would be highly favorable. After distribution, dissociation may become more

favorable. Albumin deposits fatty acids throughout the body (36), most notably the parenchymal cells of the liver, heart and muscle. This process can be highly efficient; cardiomyocytes extract 30-60% of the serum fatty acid content each pass although the mechanism of uptake is poorly understood. The fatty acylated prodrugs that bind albumin behave differently than the natural substrates; certainly the drastic fluctuations in affinity are partly responsible. Possibly the complexes do not stay intact during FcRn, also known as Brambell receptor, recycling. The prodrug may be ejected upon conformational change or the complex itself may not bind leading to degradation in the lysosome.

Serum proteins are now the subject of investigation for tumoral delivery due to their passive accumulation via leaky endothelium. These particles are large and driven mostly by convection which does not readily occur in the tumor; that is, they are not expected to penetrate tumor tissues effectively (89). This may preclude binding to specific receptors expressed on tumor cells in the inner tissue, however decomposition in the periphery with subsequent drug release and diffusion may still be effective. This process is believed to occur for albumin but may be slow compared to the catabolism of albumin throughout the rest of the body. LDL and HDL have shorter half-lives than albumin and expression of their respective receptors are common. This can have a significant impact on toxicity. It is clear the complexes do not behave similar to the carriers. The proteins have half-lives of multiple days whereas complexes are cleared much more rapidly. Whether this is purely an issue of “affinity” or lack of protection by natural process such as FcRn recycling is not well understood. Because these issues exist for synthetic drug delivery vehicles as well, the use of natural carriers may prove to be simpler, less-expensive and evolutionarily advantageous.

6. References

1. Fiume, L., Di Stefano, G. 2010. Lactosaminated human albumin, a hepatotropic carrier of drugs. *Eur. J. Pharm. Sci*. **40**: 253-262.

2. Ballantyne, F.C., Fleck, A., Dick, W.C. 1971. Albumin metabolism in rheumatoid arthritis. *Ann. Rheum. Dis.* **30**: 265-270.

3. Mansbach, C.M., Siddiqi, S.A. 2010. The biogenesis of chylomicrons. *Annu. Rev. Physiol*. **72**: 315-333.

4. Thwaites, D.T., Anderson, C.M.H. 2007. H+-coupled nutrient, micronutrient and drug transporters in the mammalian small intestine. *Exp. Physiol.* **92**: 603-619.

5. Lindmark, T., Nikkilä, T., Artursson, P. 1995. Mechanisms of absorption enhancement by medium chain fatty acids in intestinal epithelial Caco-2 cell monolayers. *J. Pharmacol. Exp. Ther*. **275**: 958-964.

6. Lindmark, T., Kimura, Y., Artursson, P. 1998. Absorption enhancement through intracellular regulation of tight junction permeability by medium chain fatty acids in Caco-2 cells. *J. Pharmacol. Exp. Ther*. **284**: 362-369.

7. Söderholm, J.D., Oman, H., Blomquist, L., Veen, J., Lindmark, T., Olaison, G. 1998. Reversible increase in tight junction permeability to macromolecules in rat ileal mucosa in vitro by sodium caprate, a constituent of milk fat. *Dig. Dis. Sci*. **43**: 1547-1552.

8. Söderholm, J.D., Olaison, G., Peterson, K.H., Franzén, L.E., Lindmark, T., Wirén, M., Tagesson, C., Sjödahl, R. 2002. Augmented increase in tight junction permeability by luminal stimuli in the non-inflamed ileum of Crohn's disease. *Gut* **50**: 307-313.

9. Wallon, C., Braaf, Y., Wolving, M., Olaison, G., Söderholm, J.D. 2005. Endoscopic biopsies in Ussing chambers evaluated for studies of macromolecular permeability in the human colon. *Scand. J. Gastroenterol*. **40**: 586-595.

10. Soboll, S., Gründel, S., Schwabe, U., Scholz, R. 1984. Influence of fatty acids on energy metabolism. 2. Kinetics of changes in metabolic rates and changes in subcellular adenine nucleotide contents and pH gradients following addition of octanoate and oleate in perfused rat liver. *Eur. J. Biochem*. **141**: 231-236.

11. Tomita, M., Hayashi, M., Awazu, S. 1995. Absorption-enhancing mechanism of sodium caprate and decanoylcarnitine in Caco-2 cells. *J. Pharmacol. Exp. Ther.* **272**: 739 -743.

12. Maher, S., Leonard, T.W., Jacobsen, J., Brayden, D.J. 2009. Safety and efficacy of sodium caprate in promoting oral drug absorption: from in vitro to the clinic. *Adv. Drug Deliv. Rev*. **61**: 1427-1449.

13. Tillman, L.G., Geary, R.S., Hardee, G.E. 2008. Oral delivery of antisense oligonucleotides in man. *J. Pharm. Sci.* **97**: 225-236.

14. Taki, Y., Sakane, T., Nadai, T., Sezaki, H., Amidon, G.L., Langguth, P., Yamashita, S. 1998. First-pass metabolism of peptide drugs in rat perfused liver. *J. Pharm. Pharmacol.* **50**: 1013-1018.

15. Leonard, T.W., Lynch, J., McKenna, M.J., Brayden, D.J. 2006. Promoting absorption of drugs in humans using medium-chain fatty acid-based solid dosage forms: GIPET. *Expert Opin. Drug Deliv.* **3**: 685-692.

16. Bai, J.P. 1994. Subcellular distribution of proteolytic activities degrading bioactive peptides and analogues in the rat small intestinal and colonic enterocytes. *J. Pharm. Pharmacol*. **46**: 671-675.

17. Bai, J.P., Amidon, G.L. 1992. Structural specificity of mucosal-cell transport and metabolism of peptide drugs: implication for oral peptide drug delivery. *Pharm. Res.* **9**: 969-978.

18. Amory, J.K., Leonard, T.W., Page, S.T., O'Toole, E., McKenna, M.J., Bremner, W.J. 2009. Oral administration of the GnRH antagonist acyline, in a GIPET®-enhanced tablet form, acutely suppresses serum testosterone in normal men: single-dose pharmacokinetics and pharmacodynamics. *Cancer Chemother. Pharmacol*. **64**: 641-645.

19. Dahan, A., Duvdevani, R., Shapiro, I., Elmann, A., Finkelstein, E., Hoffman, A. 2008. The oral absorption of phospholipid prodrugs: in vivo and in vitro mechanistic investigation of trafficking of a lecithin-valproic acid conjugate following oral administration. *J. Cont. Rel.* **126**: 1-9.

20. Faisal, W., O'Driscoll, C.M., Griffin, B.T. 2010. Bioavailability of lycopene in the rat: the role of intestinal lymphatic transport. *J. Pharm. Pharmacol*. **62**: 323-331.

21. Han, S., Yao, T., Zhang, X., Gan, L., Zhu, C., Yu, H., Gan, Y. 2009. Lipid-based formulations to enhance oral bioavailability of the poorly water-soluble drug anethol trithione: effects of lipid composition and formulation. *Int. J. Pharm.* **379**: 18-24.

22. Porter, C.J.H., Kaukonen, A.M., Taillardat-Bertschinger, A., Boyd, B.J., O'Connor, J.M., Edwards, G.A., Charman, W.N. 2004. Use of in vitro lipid digestion data to explain the in vivo performance of triglyceride-based oral lipid formulations of poorly water-soluble drugs: studies with halofantrine. *J. Pharm. Sci.* **93**: 1110-1121.

23. Langley-Evans, S.C., Clamp, A.G., Grimble, R.F., Jackson, A.A. 1996. Influence of dietary fats upon systolic blood pressure in the rat. *Int. J. Food Sci. Nutr.* **47**: 417-425.

24. Caliph, S.M., Faassen, W.A.F., Vogel, G.M., Porter, C.J.H. 2009. Oral bioavailability assessment and intestinal lymphatic transport of Org 45697 and Org 46035, two highly lipophilic novel immunomodulator analogues. *Curr. Drug Deliv.* **6**: 359-366.

25. Trevaskis, N.L., McEvoy, C.L., McIntosh, M.P., Edwards, G.A., Shanker, R.M., Charman, W.N., Porter, C.J.H. 2010. The role of the intestinal lymphatics in the absorption of two highly lipophilic cholesterol ester transfer protein inhibitors (CP524,515 and CP532,623). *Pharm. Res*. **27**: 878-893.

26. Ghoshal, S., Witta, J., Zhong, J., de Villiers, W., Eckhardt, E. 2009. Chylomicrons promote intestinal absorption of lipopolysaccharides. *J. Lipid Res.* 2009 **50**: 90 -97.

27. Clark MA, Jepson MA, Hirst BH. Exploiting M cells for drug and vaccine delivery. Advanced Drug Delivery Reviews 2001 Aug;50(1-2):81-106.

28. Hussain, N., Jaitley, V., Florence, A.T. 2001. Recent advances in the understanding of uptake of microparticulates across the gastrointestinal lymphatics. *Adv. Drug Deliv. Rev.* **50**: 107-142.

29. Holmgren, J., Czerkinsky, C. 2005. Mucosal immunity and vaccines. *Nat. Med.* **11**: 545-553.

30. Tomasi, M., Dertzbaugh, M.T., Hearn, T., Hunter, R.L., Elson, C.O. 1997. Strong mucosal adjuvanticity of cholera toxin within lipid particles of a new multiple emulsion delivery system for oral immunization. *Eur. J. Immunol.* **27**: 2720-2725.

31. Clark, S.O., Kelly, D.L., Badell, E., Castello-Branco, L.R., Aldwell, F., Winter, N., Lewis, D.J., Marsh, P.D. 2010. Oral delivery of BCG Moreau Rio de Janeiro gives equivalent protection against tuberculosis but with reduced pathology compared to parenteral BCG Danish vaccination. *Vaccine* **28**: 7109-7116.

32. Kratz, F. 2008. Albumin as a drug carrier: design of prodrugs, drug conjugates and nanoparticles. *J. Cont. Rel.* **132**: 171-183.

33. Varshney, A., Sen, P., Ahmad, E., Rehan, M., Subbarao, N., Khan, R.H. 2010. Ligand binding strategies of human serum albumin: how can the cargo be utilized? *Chirality* **22**: 77-87.

34. Hussain, R., Siligardi, G. 2010. Novel drug delivery system for lipophilic therapeutics of small molecule, peptide-based and protein drugs. *Chirality* **22 Suppl 1**: E44-46.

35. Andersen, J.T., Sandlie, I. 2009. The versatile MHC class I-related FcRn protects IgG and albumin from degradation: implications for development of new diagnostics and therapeutics. *Drug Metab. Pharmacokinet.* **24**: 318-332.

36. van der Vusse, G.J. 2009. Albumin as fatty acid transporter. *Drug Metab. Pharmacokinet*. **24**: 300-307.

37. Bhattacharya, A.A., Grüne, T., Curry, S. 2000. Crystallographic analysis reveals common modes of binding of medium and long-chain fatty acids to human serum albumin. *J. Mol. Biol.* **303**: 721-732.

38. Spector, A.A. 1975. Fatty acid binding to plasma albumin. *J. Lipid Res*. **16**: 165-179.

39. Curry, S., Mandelkow, H., Brick, P., Franks, N. 1998. Crystal structure of human serum albumin complexed with fatty acid reveals an asymmetric distribution of binding sites. *Nat. Struct. Mol. Biol* **5**: 827-835.

40. Simard, J.R., Zunszain, P.A., Ha, C., Yang, J.S., Bhagavan, N.V., Petitpas, I., Curry, S., Hamilton, J.A. 2005. Locating high-affinity fatty acid-binding sites on albumin by x-ray crystallography and NMR spectroscopy. *Proc. Natl. Acad. Sci. U.S.A*. **102**: 17958-17963.

41. Hashimoto, M., Takada, K., Kiso, Y., Muranishi, S. 1989. Synthesis of palmitoyl derivatives of insulin and their biological activities. *Pharm. Res*. **6**: 171-176.

42. Cheng, W., Satyanarayanajois, S., Lim, L. 2006. Aqueous-Soluble, Non-Reversible Lipid Conjugate of Salmon Calcitonin: Synthesis, Characterization and In Vivo Activity. *Pharm Res.* **24**: 99-110.

43. Cheng, W., Lim, L. 2009. Synthesis, characterization and in vivo activity of salmon calcitonin coconjugated with lipid and polyethylene glycol. *J. Pharm. Sci.* **98**: 1438-1451.

44. al-Obeidi, F., Hruby, V.J., Yaghoubi, N., Marwan, M.M., Hadley, M.E. 1992. Synthesis and biological activities of fatty acid conjugates of a cyclic lactam alpha-melanotropin. *J. Med. Chem*. **35**: 118-123.

45. Kocevar, N., Obermajer, N., Strukelj, B., Kos, J., Kreft, S. 2007. Improved acylation method enables efficient delivery of functional palmitoylated cystatin into epithelial cells. *Chem. Biol. Drug Des.* **69**: 124-131.

46. Kocevar, N., Obermajer, N., Kreft, S. 2008. Membrane permeability of acylated cystatin depends on the fatty acyl chain length. *Chem. Biol. Drug Des.* **72**: 217-224.

47. Kurtzhals, P. 2007. Pharmacology of insulin detemir. *Endocrinol. Metab. Clin. North Am.* **36 Suppl 1**: 14-20.

48. Kurtzhals, P., Havelund, S., Jonassen, I., Kiehr, B., Larsen, U.D., Ribel, U., Markussen, J. 1995. Albumin binding of insulins acylated with fatty acids: characterization of the ligand-protein interaction and correlation between binding affinity and timing of the insulin effect in vivo. *Biochem. J.* **312 (Pt 3)**: 725-731.

49. Choi, J., Ho, J., Curry, S., Qin, D., Bittman, R., Hamilton, J.A. 2002. Interactions of very long-chain saturated fatty acids with serum albumin. *J. Lipid Res*. **43**: 1000-1010.

50. Sørensen, A.R., Stidsen, C.E., Ribel, U., Nishimura, E., Sturis, J., Jonassen, I., Bouman, S.D., Kurtzhals, P., Brand, C.L. 2010. Insulin detemir is a fully efficacious, low affinity agonist at the insulin receptor. *Diabetes Obes. Metab.* **12**: 665-673.

51. Elbrønd, B., Jakobsen, G., Larsen, S., Agersø, H., Jensen, L.B., Rolan, P., Sturis, J., Hatorp, V., Zdravkovic, M. 2002. Pharmacokinetics, Pharmacodynamics, Safety, and Tolerability of a Single-Dose of NN2211, a Long-Acting Glucagon-Like Peptide 1 Derivative, in Healthy Male Subjects. *Diabetes Care* **25**: 1398 -1404.

52. Birkeland, K.I., Home, P.D., Wendisch, U., Ratner, R.E., Johansen, T., Endahl, L.A., Lyby, K., Jendle, J.H., Roberts, A.P., Devries, J.H., Meneghini, L.F. 2011. Insulin Degludec in Type 1 Diabetes: A randomized controlled trial of a new-generation ultra-long-acting insulin compared with insulin glargine. *Diabetes Care* **34**: 661-665.

53. Heise, T., Tack, C.J., Cuddihy, R., Davidson, J., Gouet, D., Liebl, A., Romero, E., Mersebach, H., Dykiel, P., Jorde, R. 2011. A New-Generation Ultra-Long-Acting Basal Insulin With a Bolus Boost Compared With Insulin Glargine in Insulin-Naive People With Type 2 Diabetes: A randomized, controlled trial. *Diabetes Care* **34**: 669-674.

54. Mariko, M., Park, K. 2009. Biodrug Delivery Systems: Fundamentals, Applications and Clinical Development. 1st ed. Informa Healthcare, New York, NY.

55. Ekrami, H.M., Kennedy, A.R., Shen, W. 1995. Water-soluble fatty acid derivatives as acylating agents for reversible lipidization of polypeptides. *FEBS Lett.* **371**: 283-286.

56. Wang, J., Hogenkamp, D.J., Tran, M., Li, W., Yoshimura, R.F., Johnstone, T.B.C., Shen, W., Gee, K.W. 2006. Reversible lipidization for the oral delivery of leu-enkephalin. *J. Drug Target.* **14**: 127-136.

57. Yuan, L., Wang, J., Shen, W. 2005. Reversible Lipidization Prolongs the Pharmacological Effect, Plasma Duration, and Liver Retention of Octreotide. *Pharm. Res.* **22**: 220-227.

58. Yuan, L., Wang, J., Shen, W. 2005. Reversible Lipidization Prolongs the Pharmacological Effect, Plasma Duration, and Liver Retention of Octreotide. *Pharm. Res.* **22**: 220-227.

59. Tsay, W., Shen, M.C. 1992. Experience of desmopressin (DDAVP) administration in patients with congenital and acquired bleeding disorders. *J. Formos. Med. Assoc*. **91**: 962-969.

60. Wang, J., Shen, D., Shen, W.C. 1999. Preparation, purification, and characterization of a reversibly lipidized desmopressin with potentiated anti-diuretic activity. *Pharm. Res.* **16**: 1674-1679.

61. Wang, J., Chow, D., Heiati, H., Shen, W. 2003. Reversible lipidization for the oral delivery of salmon calcitonin. *J. Cont. Rel.* **88**: 369-380.

62. Yuan, L., Wang, J., Shen, W. 2008. Lipidization of human interferon-alpha: a new approach toward improving the delivery of protein drugs. *J. Cont. Rel.* **129**: 11-17.

63. Wang, J., Wu, D., Shen, W. 2002. Structure-activity relationship of reversibly lipidized peptides: studies of fatty acid-desmopressin conjugates. *Pharm. Res*. **19**: 609-614.

64. Lambert, D.M. 2000. Rationale and applications of lipids as prodrug carriers. *Eur. J. Pharm. Sci.* **11 Suppl 2**: S15-27.

65. Kratz, F., Beyer, U. 1998. Serum proteins as drug carriers of anticancer agents: a review. *Drug Deliv.* **5**: 281-299.

66. Alaupovic, P. 1996. Significance of apolipoproteins for structure, function, and classification of plasma lipoproteins. *Meth. Enzymol*. **263**: 32-60.

67. Goudriaan, J.R., Espirito Santo, S.M.S., Voshol, P.J., Teusink, B., van Dijk, K.W., van Vlijmen, B.J.M., Romijn, J.A., Havekes, L.M., Rensen, P.C.N. 2004. The VLDL receptor

plays a major role in chylomicron metabolism by enhancing LPL-mediated triglyceride hydrolysis. *J. Lipid Res.* **45**: 1475-1481.

68. Wasan, K.M., Brocks, D.R., Lee, S.D., Sachs-Barrable, K., Thornton, S.J. 2008. Impact of lipoproteins on the biological activity and disposition of hydrophobic drugs: implications for drug discovery. *Nat. Rev. Drug Discov.* **7**: 84-99.

69. Hamidi, M., Foroozesh, M., Zarrin, A. 2006. Lipoproteins: from physiological roles to drug delivery potentials. Crit. Rev. Ther. Drug Carrier Syst. **23**: 497-523.

70. Edwards, I.J., Berquin, I.M., Sun, H., O'Flaherty, J.T., Daniel, L.W., Thomas, M.J., Rudel, L.L., Wykle, R.L., Chen, Y.Q. 2004. Differential Effects of Delivery of Omega-3 Fatty Acids to Human Cancer Cells by Low-Density Lipoproteins versus Albumin. *Clin. Cancer Res.* **10**: 8275 -8283.

71. Wolfrum, C., Shi, S., Jayaprakash, K.N., Jayaraman, M., Wang, G., Pandey, R.K., Rajeev, K.G., Nakayama, T., Charrise, K., Ndungo, E.M., Zimmermann, T., Koteliansky, V., Manoharan, M., Stoffel, M. 2007. Mechanisms and optimization of in vivo delivery of lipophilic siRNAs. *Nat. Biotech.* **25**: 1149-1157.

72. Atkinson, D., Small, D.M. 1986. Recombinant lipoproteins: implications for structure and assembly of native lipoproteins. *Annu. Rev. Biophys. Biophys. Chem.* **15**: 403-456.

73. Murakami, T., Wijagkanalan, W., Hashida, M., Tsuchida, K. 2010. Intracellular drug delivery by genetically engineered high-density lipoprotein nanoparticles. *Nanomedicine (Lond)* **5**: 867-879.

74. Zurita, A.J., Troncoso, P., Cardó-Vila, M., Logothetis, C.J., Pasqualini, R., Arap, W. 2004. Combinatorial screenings in patients: the interleukin-11 receptor alpha as a candidate target in the progression of human prostate cancer. *Cancer Res.* **64**: 435-439.

75. Lewis, V.O., Ozawa, M.G., Deavers, M.T., Wang, G., Shintani, T., Arap, W., Pasqualini, R. 2009. The interleukin-11 receptor alpha as a candidate ligand-directed target in osteosarcoma: consistent data from cell lines, orthotopic models, and human tumor samples. *Cancer Res.* **69**: 1995-1999.

76. Blanckaert, V., Ulmann, L., Mimouni, V., Antol, J., Brancquart, L., Chénais, B. 2010. Docosahexaenoic acid intake decreases proliferation, increases apoptosis and decreases the invasive potential of the human breast carcinoma cell line MDA-MB-231. *Int. J. Oncol*. **36**: 737-742.

77. Lee, C.Y., Sit, W., Fan, S., Man, K., Jor, I.W., Wong, L.L., Wan, M.L., Tan-Un, K.C., Wan, J.M. 2010. The cell cycle effects of docosahexaenoic acid on human metastatic hepatocellular carcinoma proliferation. *Int. J. Oncol*. **36**: 991-998.

78. Habermann, N., Christian, B., Luckas, B., Pool-Zobel, B.L., Lund, E.K., Glei, M. 2009. Effects of fatty acids on metabolism and cell growth of human colon cell lines of different transformation state. *Biofactors* **35**: 460-467.

79. Zhang, X., Chen, B. 2010. Recombinant high density lipoprotein reconstituted with apolipoprotein AI cysteine mutants as delivery vehicles for 10-hydroxycamptothecin.

Cancer Lett. **298**: 26-33.

80. Nikanjam, M., Blakely, E.A., Bjornstad, K.A., Shu, X., Budinger, T.F., Forte, T.M. 2007. Synthetic nano-low density lipoprotein as targeted drug delivery vehicle for glioblastoma multiforme. *Int. J. Pharm.* **328**: 86-94.

81. Nikanjam, M., Gibbs, A.R., Hunt, C.A., Budinger, T.F., Forte, T.M. 2007. Synthetic nano-LDL with paclitaxel oleate as a targeted drug delivery vehicle for glioblastoma multiforme. *J. Cont. Rel.***124**: 163-171.

82. Olbrich, C., Gessner, A., Schröder, W., Kayser, O., Müller, R.H. 2004. Lipid-drug conjugate nanoparticles of the hydrophilic drug diminazene--cytotoxicity testing and mouse serum adsorption. *J. Cont. Rel.* **96**: 425-435.

83. Ross, R. 1993. The pathogenesis of atherosclerosis: a perspective for the 1990s. *Nature* **362**: 801-809.

84. Wang, X., Greilberger, J., Ratschek, M., Jürgens, G. 2001. Oxidative modifications of LDL increase its binding to extracellular matrix from human aortic intima: influence of lesion development, lipoprotein lipase and calcium. *J. Pathol*. **195**: 244-250.

85. Tauchi, Y., Zushida, L., Yokota, M., Chono, S., Sato, J., Ito, K., Morimoto, K. 2000. Inhibitory effect of dexamethasone palmitate-low density lipoprotein complex on low density lipoprotein-induced macrophage foam cell formation. *Biol. Pharm. Bull*. **23**: 466-471.

86. Nikanjam, M., Gibbs, A.R., Hunt, C.A., Budinger, T.F., Forte, T.M. 2007. Synthetic nano-LDL with paclitaxel oleate as a targeted drug delivery vehicle for glioblastoma multiforme. *J. Cont. Rel.* **124**: 163-171.

87. Rodrigues, D.G., Maria, D.A., Fernandes, D.C., Valduga, C.J., Couto, R.D., Ibañez, O.C.M., Maranhão, R.C. 2005. Improvement of paclitaxel therapeutic index by derivatization and association to a cholesterol-rich microemulsion: in vitro and in vivo studies. *Cancer Chemother. Pharmacol*. **55**: 565-576.

88. Lada, A.T., Rudel, L.L., Clair, R.W.S. 2003. Effects of LDL enriched with different dietary fatty acids on cholesteryl ester accumulation and turnover in THP-1 macrophages. *J. Lipid Res.* **44**: 770 -779.

89. Zhang, X.Y., Luck, J., Dewhirst, M.W., Yuan, F. 2000. Interstitial hydraulic conductivity in a fibrosarcoma. *Am. J. Physiol. Heart Circ. Physiol.* **279**: H2726-2734.

CHAPTER III

A DICARBOXYLIC FATTY ACID DERIVATIVE OF PACLITAXEL

This chapter is being submitted for publication to *Bioconjugate Chemistry* and is formatted in the style of this journal.

1. Abstract

TAXOL remains a potent chemotherapy for breast, lung and ovarian cancers, however the resultant hypersensitivity and neutropenia from the Cremophor EL in the formulation undermines the health of already debilitated patients. To combat the poor solubility of the active ingredient, paclitaxel, a fatty diacid was synthesized for chemical ligation to the drug and subsequent binding of the conjugate to the highly soluble and ubiquitous protein, serum albumin. The cyclized form of the lipid, 3-pentadecylglutaric (PDG) anhydride, is reactive to a variety of nucleophiles including the 2'-OH on paclitaxel. It was discovered that the binding of the PDG derivative of paclitaxel to albumin resulted in the formation of 120 nm aggregates. This was also found when paclitaxel alone was bound to albumin. When injected intravenously to tumor bearing mice, the TAXOL formulation of paclitaxel was cleared rapidly, primarily to the liver, with a half-life of 7 hours. In the case of the PDG derivative of paclitaxel, the drug is quickly distributed uniformly giving rise to a 23 h half-life after equilibration. This is comparable to the half-life of human serum albumin in mice supporting strong albumin binding *in vivo*. The derivative is only moderately taken up by subcutaneously established tumors and is slowly hydrolyzed (<5% over 72 h) in serum, tumor cytosol and tumor tissue homogenate. The PDG derivative is less cytotoxic than the parent paclitaxel thus requiring hydrolysis for full potency. While superior to TAXOL in terms of serum pharmacokinetics, the PDG formulation should be comparable to the clinically approved paclitaxel-albumin product, ABRAXANE, another formulation that leads to aggregates of ~130 nm upon reconstitution.

2. Introduction

Paclitaxel (PTX) is a mitotic spindle inhibitor primarily indicated for ovarian cancer or in combination therapy for the treatment of non-small cell lung cancer and breast cancer. Notoriously insoluble, paclitaxel requires dissolution in ethanol and a surfactant Cremophor

EL in the commonly known product, TAXOL. The large quantities of Cremophor EL lead to neutropenia and hypersensitivity in patients thus requiring a prophylactic regimen of dexamethasone[1]. A second-generation formulation devoid of the surfactant uses the endogenous serum protein albumin as a vehicle. Abi-007, also known as ABRAXANE, utilizes the intrinsic binding of PTX to albumin to entrap the drug in submicron particles of approximately 130 nm after co-nebulization[1]. ABRAXANE showed itself superior to TAXOL in efficacy, half-life and toxicity and is currently indicated as a second line therapy for breast cancer[2,3].

At a vascular concentration of 40-50 mg/mL (0.6-0.75 mM) albumin is the most abundant serum protein[4]. The high vasculature concentrations of albumin are maintained due to recycling via a protective protein known as the Brambell receptor (FcRn) which grants albumin a 19-day half-life in humans[4]. This is an ideal characteristic sought by many synthetic vehicles for drug delivery in the literature today. The use of albumin as a drug carrier is not a novel concept, particularly for antineoplastics[5]. It has been hypothesized albumin is the major sustenance for growing tumors[6]. The high vascular concentrations beget high tumoral concentrations making albumin easily accessible as a nutritional source[7,8]. This tumoral accretion is believed to proceed via passive filtration and sequestration in the tumor microenvironment via leaky endothelia[5,9]. It has also been proposed albumin is actively transported into tumors via a selective overexpression of gp60 (albondin) and the secreted protein acidic and rich in cysteine (SPARC) at the vicinal tumor endothelium[10]. These proteins have been shown to facilitate transcytosis and paracellular transit of albumin across endothelia respectively. The net result is a large concentration of albumin localized in a highly proteolytic tissue[11,12]. Combined, these characteristics mold the paradigm of a desirable drug carrier.

The primary function of abumin is plasma expansion accomplished by maintaining an oncotic pressure across the vasculature with high (0.60-0.75 mM) intravasculature and lower (0.30 mM) extravasculature concentrations[13]. Ancillary to expansion, albumin acts as a sponge for various metals, hydrophobic xenobiotics and fatty acids[13]. Albumin is shown to have 6-7 binding sites for long chain fatty acids with K_d in the nanomolar range[14,15]. These highly specific binding sites are due to hydrophobic channels in the protein which cradle the fatty acid tails. The apex of these channels, at the protein/water interface, provides lysine or arginine cations which anchor the anionic carboxylate in place[16,17]. Drug-fatty acid conjugation is typically accomplished through amides or esters consequently removing the electrostatic interaction of conjugate and protein[18] such as in taxoprexin[19] and squalenoyl-paclitaxel[20]. This will decrease the affinity of the conjugate for the protein as demonstrated through the myristoylated insulin, LEVEMIR[21]. In the present study a new fatty acid, 3-pentadecylglutaric (PDG) acid, is described that can be conjugated to a variety of nucleophiles. The product of the reaction is a fatty acid conjugate that maintains an anionic carboxylate for the purpose of generating long-circulating albumin bound conjugates. The technology is demonstrated through PDG-paclitaxel (PP), but could potentially be applied to any nucleophilic therapeutic.

3. Experimental Procedures

3.1. Materials

All chemicals involved in the synthesis were purchased from Sigma-Aldrich at >98% purity and used without further purification. Delipidated human serum albumin was also purchased from Sigma-Aldrich at 96% purity. All solvents were purchased from BDH and were ACS grade or higher. Paclitaxel was purchased from AK Scientific (Union City, CA) and used without further purification. CT26 murine colon carcinoma cells were obtained from ATCC and grown at 37℃ at 5% CO_2 in RPMI-1640 media supplemented to 10% fetal

bovine serum, 1% penicillin and streptomycin. Cells were passaged twice before implantation to mice. Tritium labeled PP and PTX were synthesized by Moravek Biochemicals (Brea, CA) at a specific activity of 11 Ci/mmol and 36 Ci/mmol respectively with tritium substitutions at the *ortho* positions on the benzamide ring of paclitaxel. All animals were female BALB/c 6-8 week old, 18-20 g mice from NCI. Mice were allowed 1 week acclimation prior to beginning studies. All animal studies were performed under approval of the University of North Carolina Office of Animal Care and Use in accordance with the standards set forth by the Institutional Animal Care and Use Committee.

3.2. Spectroscopy

Mass spectra were obtained on an Agilent 1100-DAD-FLD Ion trap ESI mass spectrometer in MeOH or MeCN. ^{1}H NMR and ^{13}C NMR spectra were recorded on an Inova 400 MHz NMR at 30° C in $CDCl_3$ or CD_3OD; chemical shifts are referenced to TMS (δ 0.00 ppm) for ^{1}H NMR and $CDCl_3$ (δ 77.23 ppm) or CD_3OD (δ 49.15 ppm) for ^{13}C NMR. Spectral data for all intermediates are provided in the **Appendix** as **Figs. A-8**-**A-21**. UV/Vis spectrophotometry was carried out on a Shimadzu UV-2401PC. Scintillation counting was conducted on a Packard Tri-Carb 2900TL. Dynamic Light Scattering was conducted on a Malvern Zetasizer Nano ZS detecting 173° non-invasive backscatter.

3.3. Synthesis of Ethyl-(*E*)-octadec-2-enoate (1)

A suspension of pyridiniumchlorochromate (PCC), 7.98 g, (37 mmol, 1.5 eq) and NaOAc, 3.06 g, (37 mmol, 1.5 eq) was stirred in 250 mL anhydrous DCM in a two-neck flask equipped with an addition funnel and a condenser under nitrogen atmosphere. After 5 mins of stirring at room temperature, the solution became black. Hexadecanol, 6 g, (24.7 mmol, 1 eq) was dissolved in 125 mL anhydrous DCM and added to the reaction via the addition funnel at room temperature over 1 h. The mixture was stirred at room temperature for

another 2 h and (carboethoxymethylene)triphenylphosphorane, 12.10 g, (34.7 mmol, 1.4 eq) was added through the sidearm and the solution refluxed for 48 h. The reaction mixture was adsorbed on a plug of silica and eluted with EtOAc to remove the PCC and NaOAc. The eluent was concentrated and re-dissolved in 5% EtOAc in petroleum ether then eluted on silica gel with the same. The product was recovered as a colorless oil which solidifies upon cooling (6.54 g, 85% yield over two steps). This specific product has been synthesized and characterized before so only the ^{1}H NMR and MS is provided[22]. ^{1}H NMR (400 MHZ, $CDCl_3$) δ 6.96 (m, 1H, HC=C<u>H</u>-CH_2), 5.81 (d, 1H, <u>H</u>C=CH-CH_2), 4.18 (m, 2H, O-C<u>H</u>$_2$$CH_3$), 2.19 (q, 2H, γ$CH_2$), 1.54 (s, 1H, -$CH_2$-C<u>H</u>-$CH_2$), 1.45 (t, 2H, δ$CH_2$), 1.30-1.26 (m, 29H, -C<u>H</u>$_2$C<u>H</u>$_2$-,-OCH_2C<u>H</u>$_3$), 0.88 (t, 3H, C<u>H</u>$_3$). ESI-MS (pos, MeOH): 333.5 $[M+Na]^+$.

3.4. Synthesis of 3-Pentadecyldiethylglutarate (2)

Sodium metal, 111 mg, (4.83 mmol, 3 eq) was stirred in 10 mL dry EtOH at 0℃ until the solution became clear. To this was added diethylmalonate, 386 mg, (367 µL, 2.42 mmol, 1.5 eq) and **(1)**, 500 mg, (1.61 mmol, 1 eq) in 5 mL dry EtOH. The solution was refluxed for 3 h and cooled to ambient. The solution was concentrated, diluted with water and extracted with EtOAc. The EtOAc layer was dried over magnesium sulfate, filtered and concentrated to a colorless oil. The oil was dissolved in DMSO at a concentration of 6 mL/g and to it was added 1 equivalent of H_2O and 2 equivalents of NaCl and the solution refluxed for 5 h. Dilution with water and extraction into EtOAc yielded a colorless oil. The product was purified on silica gel eluting with 5% EtOAc in petroleum ether (603 mg, 94% over two steps). ^{1}H NMR (400 MHz, $CDCl_3$) δ 4.13 (q, 4H, -OC<u>H</u>$_2$$CH_3$), 2.34 (m, 5H, -C<u>H</u>$_2$-C<u>H</u>-C<u>H</u>$_2$-), 1.33-1.24 (m, 34H, -C<u>H</u>$_2$C<u>H</u>$_2$-,-OCH_2C<u>H</u>$_3$), 0.88 (t, 3H, C<u>H</u>$_3$). ^{13}C NMR (100 MHz, $CDCl_3$) δ 172.8, 60.4, 38.9, 34.2, 32.4, 32.1, 29.8, 26.8, 22.9, 14.4, 14.3. ESI-MS (pos, MeOH) m/z 399.7 $[M+H]^+$, 421.8 $[M+Na]^+$, 437.8 $[M+K]^+$.

3.5. Synthesis of 3-Pentadecylglutaric acid (3)

To a solution of **(2)**, 1.06 g, (2.66 mmol, 1 eq) in 15 mL MeOH was added 30 mL 2 N NaOH. The mixture was heated to a reflux with stirring for 6 h causing the suspension to become clear. The solution was cooled to ambient, acidified to pH 1 with concentrated HCl and extracted with methyl tert-butyl ether. The organic layer was dried with magnesium sulfate, filtered and concentrated. The product was collected as a white solid (900 mg, 99%). The compound was pure by TLC 10% Me_2CO in petroleum ether. ^1H NMR (400 MHz, CD_3OD) δ 2.33-2.27 (m, 5H, $C\underline{H}_2$-$C\underline{H}$-$C\underline{H}_2$), 1.37-1.29 (m, 28H, -$C\underline{H}_2C\underline{H}_2$-), 0.90 (t, 3H, -$C\underline{H}_3$). ^{13}C NMR (100 MHz, CD_3OD) δ 176.7, 39.6, 35.2, 33.5, 33.3, 30.9, 27.8, 23.9, 14.6. ESI-MS (neg, MeOH) m/z 341.7 $[M-H]^-$.

3.6. Synthesis of 3-Pentadecylglutaric anhydride (4)

The intermediate **(3)**, 900 mg, (2.63 mmol, 1 eq), was suspended in 3 mL EtOAc and heated gently until dissolved. To the solution was added trifluoroacetic anhydride (TFAA), 773 mg, (0.513 mL, 3.68 mmol, 1.4 eq) and the solution was capped and heated to 37℃ with shaking for 2 h. The solution was evaporated and the solid taken up in hot EtOAc and precipitated with cold petroleum ether followed by cooling the suspension to -18℃. Filtration of the solid and drying under vacuum produces the product as a fluffy white powder in quantitative yield (853 mg, 100%). ^1H NMR (400 MHz, $CDCl_3$) δ 2.89 (dd, 2H, $C\underline{H}_2$-CH-$C\underline{H}_2$), 2.43 (dd, 2H, $C\underline{H}_2$-CH-$C\underline{H}_2$), 2.19-2.12 (m, 1H, CH_2-$C\underline{H}$-CH_2), 1.40-1.26 (m, 28H, -$C\underline{H}_2C\underline{H}_2$-), 0.88 (t, 3H, -$C\underline{H}_3$). ^{13}C NMR (100 MHz, $CDCl_3$) δ 167.1, 36.3, 34.7, 32.1, 29.8, 28.9, 26.5, 22.9, 14.3. ESI-MS (pos, MeCN) m/z 325.4 $[M+H]^+$, 347.6 $[M+Na]^+$.

3.7. Synthesis of Paclitaxel-2'-O-3-pentadecylhemiglutarate (5)

Intermediate **(4)**, 21 mg, (64.5 µmol, 1.1 eq), PTX, 50 mg, (58.6 µmol, 1 eq) and 4-dimethylaminopyridine (DMAP), 0.7 mg,(5.86 µmol, 0.1 eq) were dissolved in 0.8 mL dry

pyridine and the reaction stirred overnight at room temperature. The reaction was concentrated by rotary evaporation and the solids taken up in DCM and washed with 0.1 N HCl. The DCM was dried with magnesium sulfate, filtered and concentrated. The solid was adsorbed onto silica and eluted with 1:1 EtOAc in petroleum ether supplemented with 1% AcOH. The product was recovered as a white solid. (58.4 mg, 85%). ^{1}H NMR (400 MHz, $CDCl_3$) δ 8.12 (d, 2H, ArH), 7.75 (d, 2H, ArH), 7.62-7.24 (m, 11H, ArH), 6.29 (s, 1H, C10), 6.24 (t, 1H, C-13), 5.99 (dd, 1H, C-3'), 5.68 (d, 1H, C-2), 5.50 (d, 1H, C-2'), 4.97 (d, 1H, C-5), 4.40 (dd, 1H, C-7), 4.29 (d, 1H, C-20), 4.20 (d, 1H, C-20), 3.80 (d, 1H, C-3), 2.56-2.50 (m, 1H, -CH_2-C$\underline{H}$-CH_2-), 2.45 (s, 3H, OAc), 2.40-2.28 (m, 3H, -C$\underline{H}_2$-CH-C$\underline{H}_2$-, C-6$_\alpha$), 2.24-2.13 (m, 7H, OAc, C-14, -C$\underline{H}_2$-CH-C$\underline{H}_2$-), 2.00-1.85 (m, 4H, C-18, C-6$_\beta$), 1.66 (s, 3H, C-19), 1.26-1.19 (m, 31H, -C$\underline{H}_2CH_3$, C-17), 1.13 (s, 3H, C-16), 0.88 (t, 3H, -CH_2C$\underline{H}_3$). ^{13}C NMR (100 MHz, $CDCl_3$) δ 204.0, 176.7, 171.9, 171.5, 170.2, 168.3, 167.7, 167.2, 142.9, 137.1, 133.8, 133.0, 132.2, 130.5, 129.0, 127.1, 84.7, 81.3, 79.2, 75.8, 75.3, 74.4, 72.2, 58.7, 53.1, 45.8, 43.4, 38.0, 35.7, 34.1, 32.2, 29.9, 29.7, 27.1, 22.9, 22.3, 21.0, 15.0, 14.3, 9.8. ESI-MS (pos, MeOH) m/z 1201.1 $[M+Na]^+$.

3.8. Cytotoxicity of PP

The cytotoxicity of PP and PTX were analyzed by the NCI as part of the NCI-60 DTP Human Tumor Cell Line Screen[23]. Various human cancer cell lines were plated at 5000-40000 cells/well and treated with five concentrations of PP or PTX from 10 nM to 100 µM. The effect on cell growth is compared to cell lines fixed at t=0 and the untreated control via the Sulforhodamine B test. Dose response curves were then generated across 60 cell lines and the 50% growth inhibition (GI50), total growth inhibition (TGI) and 50% lethal concentration (LC50) values were determined for each cell line.

3.9. Biochemical Stability of PP

CT26 cells were grown in a flask to confluency (~4 million cells) and the cells washed then scraped off the flask and suspended in 5 mL Hank's balanced salt solution (HBSS). The suspension was then centrifuged at 600 x g for 5 minutes at 4℃. The supernatant was removed and replaced with 0.5 mL fresh HBSS. The cells were homogenized on ice using a Potter-Elvehjem homogenizer attached to an Hitachi 12-Volt 3/8" cordless peak lithium ion micro driver drill at 1300 rpm while continuously plunging for 15 minutes. The suspension was centrifuged at 6000 x g to pellet the cell debris, the supernatant diluted to 1 mL and separated into 10 x 100 µL aliquots and stored at -18℃ until use. Prior to use, the aliquots had to be recombined and diluted twofold to attain the volume necessary to run an experiment in duplicate.

An 8-week old female BALB/c mouse was inoculated with 5 x 10^5 CT26 cells on the right flank and the tumor allowed to grow to ~1000 mm^3, as calculated using the volume of an ellipsoid (see **III.14**). At this point, the mouse was anesthetized with 0.1 mL 100 mg/mL ketamine administered intraperitoneally (*i.p.*) with subsequent cervical dislocation. The tumor mass was harvested, washed with PBS and blotted dry. The tumor was weighed and diluted with 2 volumes of PBS. The suspension was coarsely homogenized on ice using a PowerGen® 700 tissue homogenizer at speed 7 for 5 minutes until no lumps of tissue remained. The tissue homogenate was mixed thoroughly, separated into 1 mL aliquots and stored at -18℃ until use.

For serum preparation, 8 female 8-week old BALB/c mice were anesthetized with 0.1 mL 100 mg/mL ketamine *i.p.* until unresponsive to toe pinching. The mice were then exsanguinated by cardiac puncture with subsequent cervical dislocation. The whole blood was pooled and stored at 4℃ overnight. The fibrin clot was pelleted by centrifuging the

suspension at 6000 x g at 4℃ and the supernatant removed and separated into 500 µL aliquots.

Standard curves were generated by combining PP (160-1 µM) and PTX (1–160 µM) in EtOH with aliquots of the test matrix (serum, cell or tissue homogenate) at a 1:10 (v/v) ratio respectively. The matrices were then diluted with equal volumes of 1 N HCl and precipitated with 8 volumes of MeCN containing 500 nM docetaxel as internal standard. To examine the stability of the PP, the highest stock of PP in EtOH (160 µM) was diluted into each matrix in duplicate at a (v/v) ratio of 1:10. The matrices were warmed to 37℃ in a waterbath and shook vigorously. Each matrix was sampled at given times by taking 20 µL samples and adding 20 µL 1N HCl followed by 160 µL MeCN containing 500 nM docetaxel. The precipitate was pelleted at 800 x g for 2 minutes and the supernatant removed for analysis.

The supernatant was run on an Aquasil C18 reversed phase column (2.1 x 50 mm) with 5 µm particles and 80 Å pore size using 20 µL injections. The eluent was a binary gradient containing 0.1% formic acid in water (**A**) and 0.1% formic acid in MeOH (**B**). The gradient began with 1 minute of 30% B followed by a linear increase over 2 minutes to 95% B. The eluent was then held constant at 95% B for 15 sec followed by a 30 sec linear decrease down to 30% B and 30 sec re-equilibration at 30% B. The solvent pump used was a Shimadzu SCL-10Avp operating at a flow rate of 0.75 mL/min with an injection loop of 100 µL. Analysis was by an API 4000 Triple Quadrupole LC/MS/MS mass spec (AB Sciex Instruments) scanning for parent to daughter transitions of 854-525 m/z (PTX) and 854-525 m/z (PP) in negative mode. The 1178-854 transition for PP was inconsistent so the daughter paclitaxel and its subsequent daughter fragment were used for analysis for both standard curve and stability study.

Concentrations were determined by integrating the area under the curve for the various peaks and assigning a concentration per the standard curves. The extraction efficiencies of both PP and PTX were determined for the three matrices. This was done by spiking the individual matrices in duplicate with radiolabeled stock of either PP or PTX. Aliquots of the stock were weighed out and analyzed by liquid scintillation counting (LSC) to determine the concentration. Next the matrices were extracted with 1 volume of 1 N HCl and 4 volumes of MeCN. The samples were centrifuged at 16.1 x 1000g for 5 mins and the supernatants quantiated by LSC. Efficiencies were calculated as a ratio of concentration found from the extraction over the initial concentration in the matrix x 100.

3.10. Formulation of PP with Albumin

A 10x stock solution of PP in *t*-BuOH is made and confirmed via UV spectrophotometry after dilution in EtOH (ε_{228}=30,593 $M^{-1}cm^{-1}$, EtOH). The PP stock is then added to a 5% (w/v) stock of delipidated HSA in water (Sigma, A1887) at a 1:10 volume ratio of EtOH:HSA (ε_{278}=39,800 $M^{-1}cm^{-1}$, water)[24] which immediately causes turbidity due to precipitation of PP. The sample was shell-frozen and lyophilized over 24 h. The sample was then reconstituted in 0.1 M phosphate buffer at pH 7.4 and filtered through a 0.22 µm PVDF filter. (Millipore Billerica, MA) If the stock contains [^{3}H]-PP, it is quantified via LSC. If the stock is not radiolabeled, it is extracted by diluting with one volume of 1 N HCl and eight volumes of MeCN then added a quantity sufficient of EtOH to make the volume 5 mL in a volumetric flask and analyzed via UV-Vis. The loading efficiency of PP is inconsistent with a maximum loading of about 50% for higher doses.

3.11. Formulation of PTX as TAXOL

Paclitaxel solutions were prepared at either 6 mg/mL or 9.4 mg/mL in 1:1 (v/v) EtOH:Cremophor EL. The drug concentration was confirmed by diluting with EtOH and

analyzing by UV abosrobance (ε_{228}=29.800 $M^{-1}cm^{-1}$, EtOH). The organic stock was diluted 5-fold with PBS to produce a concentration of about 1.2 mg/mL or 1.9 mg/mL respectively immediately prior to injection.

3.12. Dialysis of PP-Human Serum Albumin (HSA) Complex

To determine whether the PP-HSA complex would dissociate over time, the complex was dialyzed against delipidated human serum albumin in phosphate buffer to create sink conditions. Dialysis was conducted across a Spectra Por 12-14 kDa MWCO regenerated cellulose dialysis membrane with 500 µL fiberglass compartments. A 0.1 M phosphate buffer pH 7.4 containing 0.01% NaN_3 was diluted 10:1 (v/v) with EtOH. This EtOH-containing buffer was saturated by shaking with solid PP for 24 h at 37℃ then cooled to ambient and filtered through a 0.22 µm PVDF filter. Albumin was dissolved in phosphate buffer without EtOH at concentrations of 40 mg/mL and 10 mg/mL as confirmed by UV. Finally a stock solution of [^{3}H]-PP in EtOH was made to a concentration of 15 mg/8.63 x 10^7 dpm/mL. The PP stock was added to the albumin stocks in a 1:10 (v/v) ratio and the stocks were filtered through a 0.22 µm PVDF filter. These stocks were analyzed by LSC for PP content and UV for HSA content.

The saturated solution of [^{3}H]-PP in 0.1 M phosphate buffer pH 7.4 was dialyzed against blank phosphate buffer for 5 h with sampling of both compartments every hour to determine how quickly free PP could establish equilibrium. The albumin solutions loaded with PP were sampled after shaking for 24 h at 37℃ a nd the compartment replenished with fresh aliquots of the initial contents. After another 24 h of shaking at 37℃, all contents were analyzed. Analysis involved weighing 200 µL aliquots of the sample into scintillation vials and adding 5 mL Ultima Gold scintillation cocktail followed by LSC (**Table III-1**).

Time (h)	A			B		
	[HSA] (μM)	[EtOH] %(v/v)	[PP] μM	[HSA] (μM)	[EtOH] %(v/v)	[PP] μM
0	0	10	2.8	0	10	0
1	0	10	2.1	0	10	0.7
2	0	10	1.8	0	10	1.0
3	0	10	1.7	0	10	1.1
4	0	10	1.5	0	10	1.3
5	0	10	1.5	0	10	1.3
0	0	10	2.8	131	10	0
24	0	10	1.2	131	10	1.6
0	722	0	467	609	0	0
24	722	0	455	609	0	12
48	722	0	454	609	0	14
0	179	0	127	146	0	0
24	179	0	123	146	0	4
48	179	0	115	146	0	4

Table III-1. Dynamic dialysis of [^{3}H]-PP-HSA against delipidated HSA. [^{3}H]-PP-HSA in compartment **A** was dialyzed against delipidated HSA in compartment **B** across a regenerated cellulose membrane with a MW cutoff of 12-14 kDa (Spectra Por). After 48 h, only 3% of PP bound in the form of PP-HSA had dialyzed across the membrane. As shown by the first 5 entries, free PP can diffuse freely across the membrane within hours suggesting dissociation of PP from the PP-HSA complex is very slow.

3.13. Pharmacokinetics/Biodistribution of [^{3}H]-PP-HSA and [^{3}H]-TAXOL

Female, 6-8 week old BALB/c mice were administered 5 x 10^5 CT26 murine colon carcinoma cells in 0.1 mL HBSS on the right flank. When the tumors were ~1000 mm^3, the mice received the radiolabeled dose as formulated in 4% HSA in 0.1 M phosphate buffer (0.08 mg PP equiv to 0.058 mg PTX/1.75 x 10^7 dpm/0.1 mL) or as TAXOL (0.147 mg PTX/2.22 x 10^6 dpm/0.1 mL) via the tail vein.

Approximately 5 minutes prior to the timepoint, the mice were injected *i.p.* with 0.1 mL 100 mg/mL ketamine. Once unresponsive to toe pinching, the mice were exsanguinated via cardiac puncture with subsequent cervical dislocation. The whole blood was quickly weighed as 200 µL aliquots in triplicate. The target organs were harvested, washed with PBS, blotted dry and small (~100 mg) pieces excised, weighed and stored in scintillation vials in duplicate. The target organs include the liver, lungs, heart, kidneys, spleen, tumor and injection site on the tail.

To the whole blood aliquots was added 1 mL of Solvable® tissue solubilizer. (Perkin Elmer, 6NE9100) The sample was incubated for 1 hour at 55℃ turning brownish-green. To this was added 100 µL of 0.1 M ethylenediaminetetraacetic acid disodium followed by 300 µL 30% H_2O_2 in 100 µL aliquots. The reaction can be quite vigorous and was allowed to continue at room temperature until the foaming subsided. The samples were then heated to 55℃ for an additional hour yielding clear to slightly yellow solutions. The samples were cooled to ambient and 15 mL Ultima Gold scintillation cocktail was added and mixed thoroughly. The samples were rested in the liquid scintillation counter for 1 h to adapt to light and temperature prior to counting.

To the organs was added 1 mL of Solvable® followed by heating to 55℃ for 2 h. Once dissolved (yellow to slightly yellow) the samples were cooled to ambient and 200 µL of

30% H_2O_2 was added in 100 µL aliquots. The samples were then heated to 55℃ again for 30 min. The samples were cooled to ambient and 15 mL Ultima Gold scintillation cocktail was added and thoroughly mixed. The samples were rested in the LSC for 1 h to adapt to light and temperature prior to counting.

Aliquots of PP stock were weighed in triplicate and analyzed via liquid scintillation counting. A tumor bearing mouse was then anesthetized with 0.1 mL 100 mg/mL ketamine *i.p.* and exsanguinated via cardiac puncture. The mouse was sacrificed and the target organs harvested. Aliquots of 175 µL, 200 µL and 225 µL of blood were weighed and spiked with a weighed amount of PP stock (~1 x 10^4 dpm). Additionally, ~75, 100 and 125 mg samples of organs were washed, blotted dry and weighed then spiked with a weighed amount of PP stock (~1 x 10^4 dpm). The samples were then processed in the same fashion as the unknown samples. The counting efficiency was calculated as the ratio of dpm in the organ sample / calculated PP stock dpm x 100. The efficiencies were plotted as a function of organ or blood mass and fitted with a linear regression. The calculated efficiency was then used to correct the counts for the unknown samples based on blood volume or organ mass.

3.14. Pharmacodynamics of PP-HSA and TAXOL

Female, 6-8 week old BALB/c mice were administered 5 x 10^5 CT26 murine colon carcinoma cells in 0.1 mL HBSS on the right flank. The mice were separated into groups; mice that developed tumors quickly and mice that developed tumors after a delay. When the quickly developed tumors were 600-700 mm^3 (n = 4 mice/group), the mice received their first dose. About 10 days later, the delayed tumors (n = 2 mice/group) were given their first injections with average tumor volumes of 400-700 mm^3. The dosing schedule for PP (7 mg/kg with respect to PTX) and PTX (10 mg/kg) was every 3 days for 15 days[25]. Efficacy was analyzed via tumor size measurements every three days. Tumors were measured

directly using digital calipers and the volume quantitated as an ellipsoid using the formula ($l \times w^2 \times \frac{\pi}{6}$) where width is the longest measured diameter. Both formulations were compared to a control group given injections of PBS on the same dosing schedule. Mice were sacrificed when the width of the tumor exceeded 2 cm. Results were compared using a one-way ANOVA for n=6 mice per group.

4. Results

4.1. Chemistry

The synthesis of 3-alkylglutaric anhydrides has already been demonstrated[26]. This synthetic scheme was shortened and modified (**Scheme III-1**). Hexadecanol was oxidized to palmitaldehyde using PCC and subsequently subjected to Wittig olefination using the ylide (carboethoxymethylene)triphenylphosphorane[22]. The α,β-unsaturated ethyl ester was then be used as a Michael acceptor for sodiomalonate under refluxing conditions[27]. The resultant triester is then decarboxylated and saponified to the 3-alkylglutaric acid[27]. Dehydration of the diacid can be affected with TFAA in EtOAc at 37℃[28]. PDG anhydride itself is reactive to amines and alcohols thus it could react with paclitaxel at three positions[29,30]. Paclitaxel is known to be reactive to glutaric anhydride at the 2'-OH position at room temperature. The 7-OH is only reactive under heated conditions and the 1-OH is unreactive[29,30]. Mixing PDG and PTX in pyridine with a catalytic amount of DMAP allows complete reaction at room temperature in 24 h (**Scheme III-2**).

4.2. Pharmaceutics

Paclitaxel is very poorly soluble (~10 ug/mL)[31] and adding a fatty acid to this molecule only exacerbates the issue. The solubility of PP was calculated using a radiolabel at about 0.36 µg/mL (0.26 µg/mL PTX) in 0.1 M phosphate buffer at pH 7.4, room temperature. In the presence of HSA, the solubility of PP should increase dramatically to a

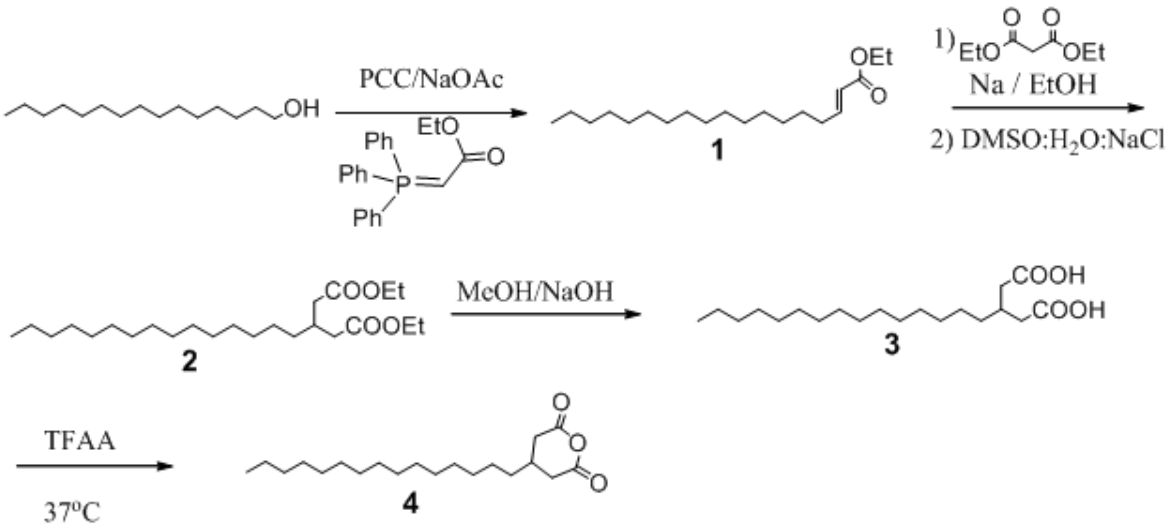

Scheme III-1. Synthesis of PDG anhydride from hexadecanol. PCC, pydridiniumchlorochromate; NaOAc, sodium acetate; TFAA, trifluoroacetic anhydride

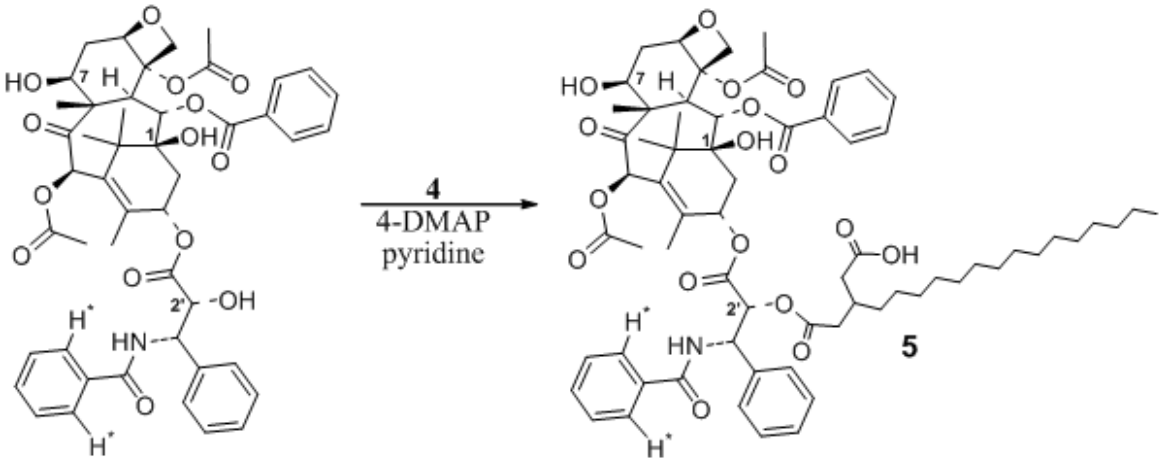

Scheme III-2. Synthesis of PP. The reaction is performed at room temperature as heating the solution will cause a mixture of isomers with the 7-ester. H^* corresponds to the sites replaced with [^{3}H] in the radiolabeled compounds synthesized by Moravek Biochemicals. (Brea, CA). DMAP, 4-dimethylaminopyridine.

theoretical maximum of the number of fatty acid binding sites multiplied by the concentration of HSA. This would be a solubility of about 3.6 mM (3.07 mg/mL with respect to PTX) conservatively assuming a 40 mg/mL physiological solution of albumin and 6 fatty acid binding sites. After two weeks of equilibration, the concentration of PP with respect to PTX (54 µg/mL) was substantially less than the theoretical maximum (**Fig. A-1**).

To improve solubility, PP was dissolved in a water miscible co-solvent, t-BuOH, and introduced to aqueous albumin at 10% (v/v). We found albumin to be structurally stable to *t*-BuOH at this concentration via circular dichroism analysis (**Fig. A-3**). This is unsurprising as other small alcohols at this concentration do not perturb its secondary or tertiary structure[32]. Distilled water was chosen as a solvent as electrolytes tend to create an unfavorable environment for PP leading to increased precipitation. After loading, the suspension was shell frozen and lyophilized to a cake which was reconstituted in an isotonic system. Filtration of the suspension yields a clear blue solution indicating particles due to Tyndall scattering. Analysis using Dynamic Light Scattering showed aggregates of 120 nm diameter.

The slow equilibration and poor solubility of PP precluded determination of the dissociation constant via conventional methods such as isothermal titration calorimetry or equilibrium dialysis. Instead, the PP-HSA complex was formed and the stability of the complex was examined. Dialysis of a PP solution over 5 h showed a rapid equilibrium could be attained within this time period. In contrast, dialysis of the PP-HSA complex against comparable concentrations of delipidated HSA, which should act as a sink for free PP, showed only about 3% of PP was released from the complex over two days at 37℃ for 5% and 1% concentrations of HSA (**Table III-1**).

4.3. Cytotoxicity

The IG_{50}, TGI and LC_{50} were determined for PP and PTX via the NCI-60 DTP Human Tumor Cell Line Screen. The results for all three values consistently showed a superior cytotoxicity of PTX to PP by at least an order of magnitude up to several orders. For simplicity, representative data on the TGI is presented (**Table III-2**). Due to the large number of cell lines, only two were selected from each cancer type which demonstrated the greatest toxicity for PTX and PP.

4.4. Biochemical Stability

Prior to the experiment, stock solutions of [^{3}H]-PP and [^{3}H]-PTX in EtOH were introduced to various milieu at a 1:10 (v/v) ratio. Subsequent to incubation for a given period of time, samples were taken and extracted with 1 volume of 1 N HCl and 8 volumes of MeCN, vortexed and pelleted. For undiluted murine serum, PP and PTX were quantitatively extracted. For CT26 cytosolic fraction, PP was extracted at 97% efficiency and PTX at 91%. For CT26 tissue homogenate, PP was extracted at 90% efficiency and PTX at 94% efficiency. Results of the stability study are presented as an average of duplicates and results from LC/MS were corrected for extraction efficiency. The stability study of PP in serum, tumor cytosol and tumor tissue homogenate is shown in **Fig. III-1**. The PP is stable in this particular concentration of cell homogenate attaining under 1% conversion to PTX after 36 h. The PP is similarly stable in serum attaining about 1.5% conversion to PTX within 72 h. Under the experimental conditions, the PP was also stable in the tumor tissue homogenate only attaining 5.5% conversion to PTX after 72 h.

4.5. Pharmacokinetics/Biodistribution

The PP formulation shows a rapid distribution (**Fig. III-2**) from the vasculature over 6 h accounting for a 10-fold dilution of concentration as is common for albumin based

TGI		µM	µM
Cancer Type	Cell Line	PTX	PP
Leukemia	HL-60(TB)	0.03	1.78
	RPMI-8226	0.32	2.75
NSCLC	NCI-H522	0.08	2.40
	NCI-H460	0.79	1.35
Colon	HC-2998	0.13	1.95
	KM12	0.16	1.26
CNS	SF-539	0.06	1.78
	SNB-75	0.08	1.20
Melanoma	MDA-MB-435	0.02	0.20
	LOX IMVI	1.00	1.78
Ovarian	OVCAR-3	0.16	0.60
	OVCAR-5	0.79	2.63
Renal	RXF 393	0.50	2.29
	SN12C	1.00	2.69
Prostate	DU-145	0.16	1.23
	PC-3	0.63	3.24
Breast	BT-549	0.79	2.24
	MDA-MB-468	1.00	0.27

Table III-2. Total Growth Inhibition of PP and PTX from the NCI-60 DTP Human Tumor Cell Line Screen. For simplicity, only the TGI data is presented for 2 cell lines representative of each type of cancer. The cell lines were selected as having the highest toxicity for PTX and PP. The results show PTX is consistently more cytotoxic than PP most likely due to the slow conversion of PP to PTX.

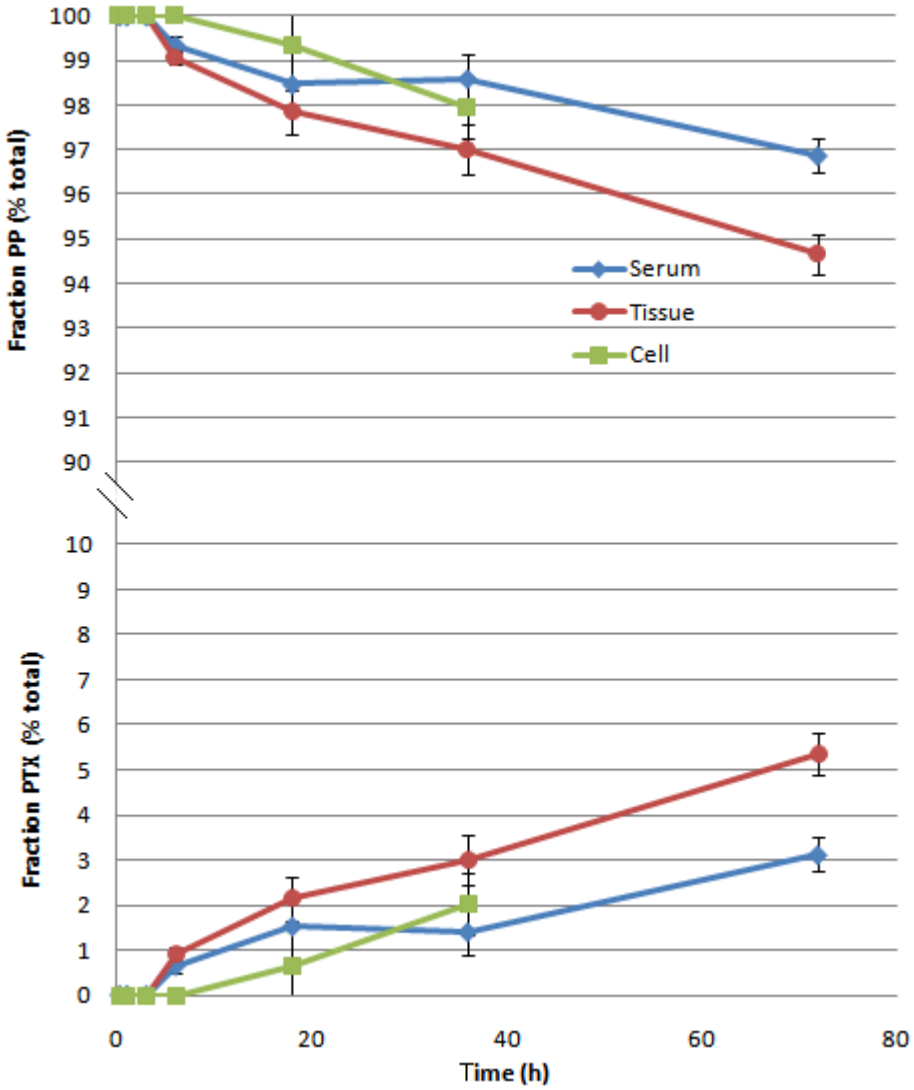

Figure III-1. Biochemical stability of PP in various biological milieus. The concentrations of PP and PTX were quantified by LC/MS over 36 or 72 h in duplicate in undiluted murine serum, CT26 murine tumor cell homogenate and CT26 tumor tissue homogenate. The PP formulation appears to be highly stable to all three matrices showing under 6% conversion to free PTX over the course of 72 h. The data is presented as a fraction of the total amount quantitated by LC/MS; extraction from the various tissues was shown to be greater than 90% for all matrices. Error bars represent the standard deviation of matrices performed in duplicate.

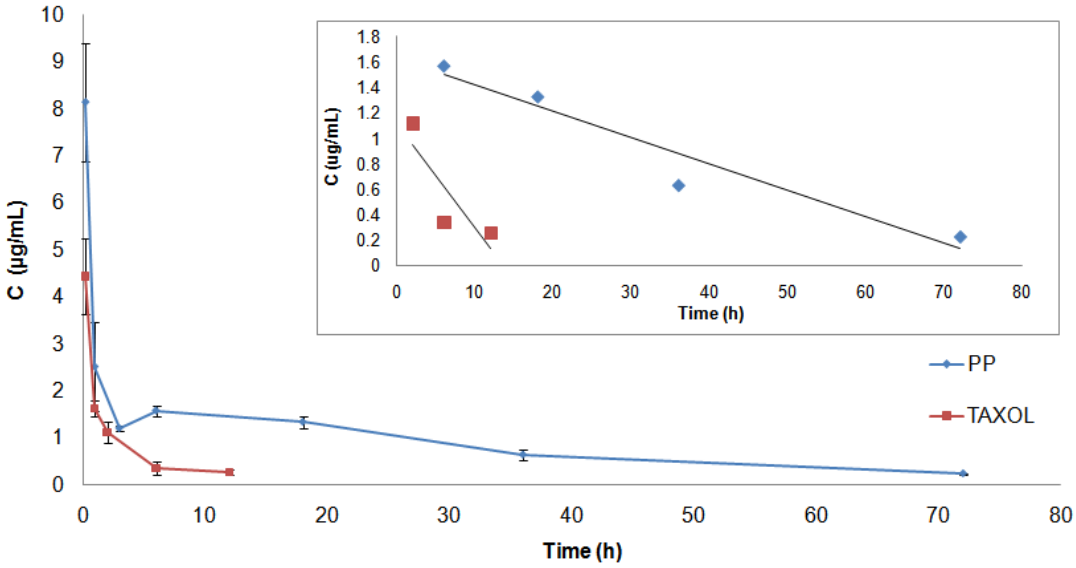

Figure III-2. Serum pharmacokinetics for [^{3}H]-PP-HSA and [^{3}H]-TAXOL in CT26 tumor bearing mice. as determined by liquid scintillation counting of serum samples in triplicate. The insert magnifies the terminal phase of each treatment which was used to calculate the half-life, $t_{1/2}$ in **Table III-2**, and shows the disparity of clearance rates between the two formulations. The reason for the rebound in PP concentration at 6 h is unknown but may be due to enterohepatic recycling. Error bars represent the standard deviation calculated from n = 3 mice in triplicate.

therapies[33]. The concentration then rebounds to about 20% of the initial concentration with a secondary peak that is within the quantified error. This concentration is then cleared very slowly with a half-life of 23 h. Biodistribution analysis shows accumulation primarily in the liver and spleen (**Fig. III-3**). The concentration in these organs is slowly diminished with quantifiable concentrations remaining at 72 h. The tumor rapidly accumulates 1-3% of the dose/g tissue which remains constant through 72 h. The rebound in concentration observed in the serum is mirrored in the various organ tissues. Paclitaxel from the TAXOL formulation shows a similarly rapid distribution (**Fig. III-2**). There is no rebound and the estimated terminal half-life of the formulation is 7 h. Biodistribution analysis shows accumulation primarily in the liver and kidneys (**Fig. III-4**), which eliminate PTX quickly from the system. The tumor shows a comparable uptake of about 3% of the dose/g tissue however concentrations approach the lower limit of detection by 6 h.

The serum pharmacokinetics were analyzed using non-compartmental analysis. The major pharmacokinetic parameters were extracted and presented in **Table III-3**. The PP formulation shows a 3.5-fold increased serum half-life due to a lower systemic clearance and volume of distribution. Consequently, while at only half the dose of TAXOL, PP shows a higher C_0, area under the curve (AUC) and mean residence time (MRT) in the system.

4.6. Pharmacodynamics

The albumin bound form of PP is expected to be significantly better tolerated than TAXOL due to the lack of required solvents and surfactants for dissolution as well as the slow release profile from the protein. This is in similar fashion to ABRAXANE. Due to the slowed clearance of PP compared to TAXOL, the bound PTX should have greater exposure to the tumor site albeit with only very moderate uptake. No mice died during the experiment

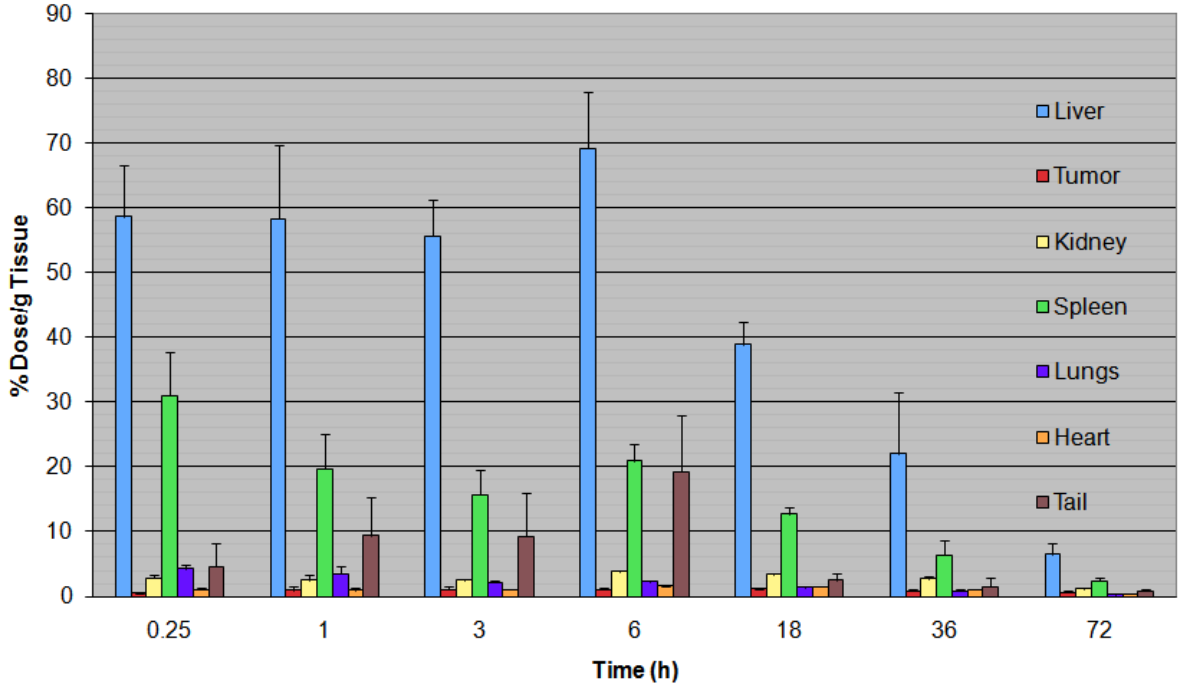

Figure III-3. Time resolved biodistribution of [^{3}H]-PP-HSA in CT26 tumor bearing mice. The liver and spleen are the major sinks for PP, however, the concentrations of PP in the respective tissues do not quickly drop but appear to mirror the serum concentrations. This could suggest the PP is intact in the various organs and is leeching back into the vasculature over time thus giving rise to the 23 h terminal half-life of the formulation. Error bars represent the standard deviation for n= 3 mice measured in duplicate.

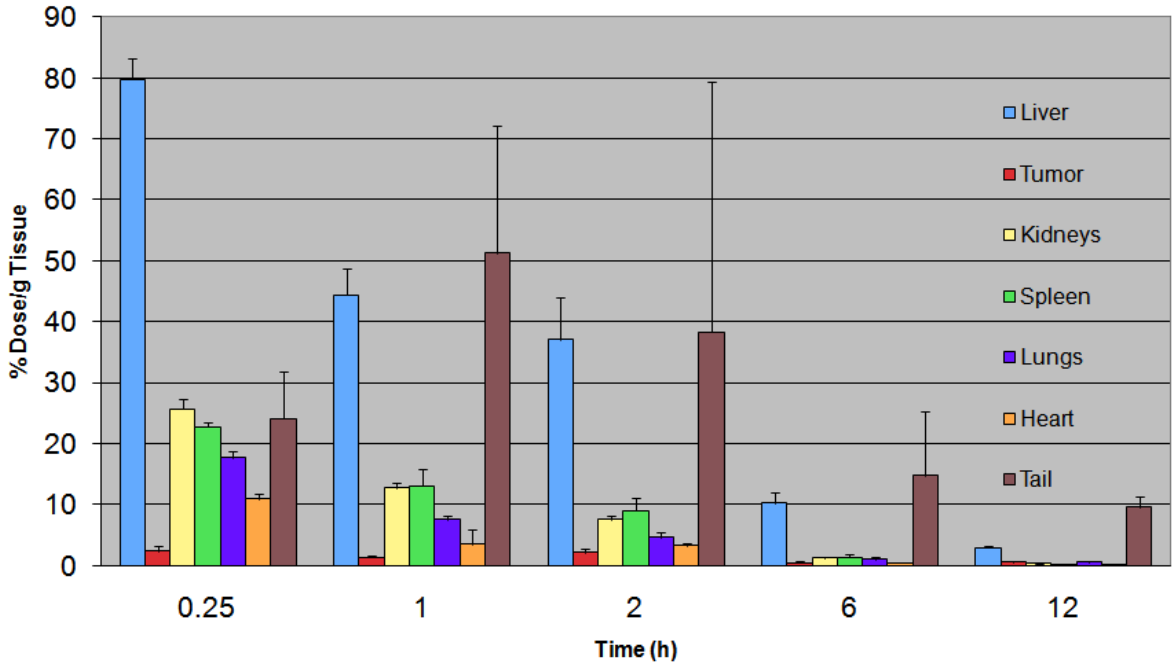

Figure III-4. Time resolved biodistribution of [^{3}H]-TAXOL in CT26 tumor bearing mice. The liver is the major uptake organ for TAXOL and the concentrations of PTX in the organ disappear very rapidly, mirroring the serum concentrations. This is clearance of PTX from the system and is the primary reason the TAXOL formulation has a short 7 h terminal half-life. Error bars represent the standard deviation for n = 3 mice in duplicate.

Treatment	Dose (μg)	C_0 (μg/mL)	V_d (mL)	$t_{1/2}$ (h)	Cl (mL/h)	AUC_∞ (h·μg/mL)	MRT_∞ (h)
PP	80	12.05	36.56	23.13	1.10	72.59	29.82
TAXOL	150	6.21	116.19	6.61	12.18	12.07	6.53
PP/TAXOL	0.53	1.94	0.31	3.50	0.09	6.01	4.57

Table III-3. Summary of important pharmacokinetic parameters for [^{3}H]-PP-HSA and [^{3}H]-TAXOL. The PP formulation shows a much greater retention in the vasculature, most likely due to tight albumin binding, which is manifest in a 23 h half-life. This also results in slower clearance from the system and consequently higher exposure to the tumor tissue even though the dose of PP is almost half the dose of TAXOL. A non-compartmental model was fitted to both formulations with a weighting of 1/Y using Winnonlin (Pharsight). $C_{0,}$ estimated initial serum concentration; V_d, volume of distribution; Cl, systemic clearance; AUC, area under the curve; MRT, mean residence time.

but all were sacrificed when the tumor burden exceeded allowable limits; this precluded continuation of the study after 9 days for most of the mice. Within this timeframe at a lower dose of 7 mg/kg with respect to PTX in the PP formulation compared to 10 mg/kg formulated as TAXOL, there was no statistical difference between any treatment group as analyzed by one-way ANOVA (**Fig. III-5**).

5. Discussion

The purpose of synthesizing the PP conjugate was to improve the solubility and pharmacokinetics of PTX by mimicking the endogenous serum protein, albumin. Loading of albumin with PP was exceedingly slow taking 2 weeks to reach only 54 µg/mL with respect to PTX. This is in contrast to the expected 3 mg/mL at saturation of 6 binding sites of 4% HSA. The slow binding could be a result of rate-limiting dissolution. To facilitate the kinetics of binding, PP was dissolved in *t*-BuOH prior to mixing with a solution of 4% HSA in water. Much of the PP precipitates but this process can result in much higher concentrations of PP; adding 12 eq of PP allowed full saturation of 6 binding sites of HSA.

The PP is stabilized in the form of 120 nm particles which remain after lyophilization and reconstitution in isotonic solutions. The structural details of the particles is not known, however it is hypothesized the paclitaxel moiety of the PP on the surface of albumin can interact with other paclitaxel moieties via van der Waals interactions or bind other molecules of albumin through PTX specific binding sites[34]. Formulation of PTX without the PDG moiety in this manner saturates at 0.5 eq PTX/HSA with formation of 120 nm particles as confirmed by DLS. This finding suggests particle formation is a PTX-specific phenomenon. This finding is similar to ABRAXANE but with notably lower saturable concentrations. ABRAXANE allows solubilization of 10 equivalents of PTX/HSA compared to a maximum of 0.5 by simple mixing.

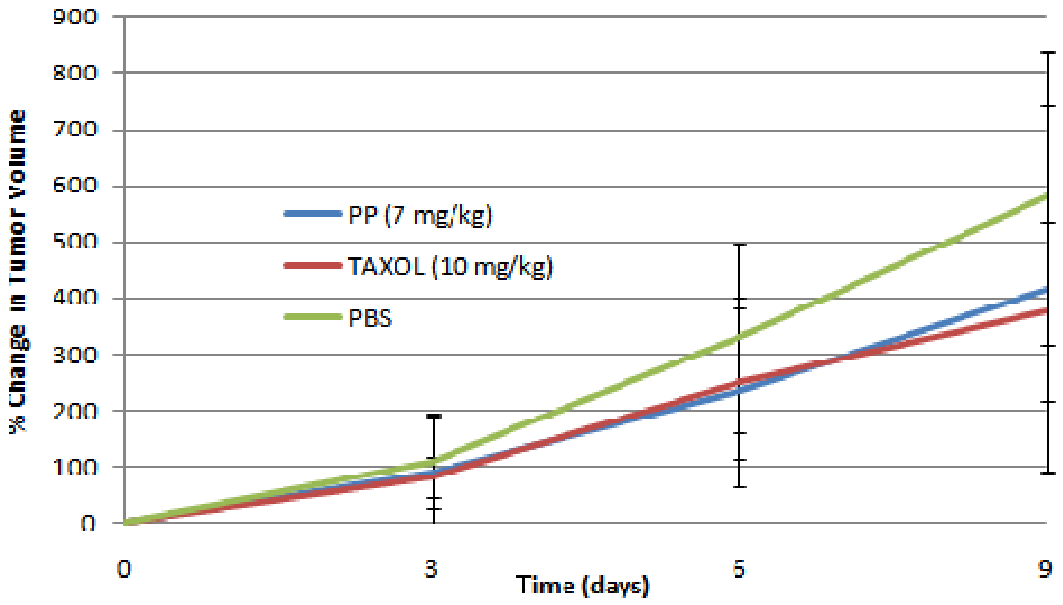

Figure III-5. Efficacy of PP-HSA and TAXOL on subcutaneous CT26 tumors. Tumors were measured with vernier calipers every 3 days with injections on day 0, 3 and 6. Mice were sacrificed when the tumor burden exceeded allowable limits forcing the study to conclude after 9 days. By one-way ANOVA, no statistical significance existed between the three treatments within this timeframe. Error bars represent the standard deviation of a population of n = 6 mice.

The PP conjugate is less cytotoxic than PTX towards a variety of human cancer cell lines when tested in vitro (**Table III-2)**. The mechanism of action of PTX is to bind and prevent microtubulin assembly, however various derivatives of paclitaxel have been shown to relinquish this binding capacity yet retain varying degrees of cytotoxicity[20,35]. This appears to be regiospecific as succinate esters on the 2'-OH or 7-OH also abolish microtubule binding[29] whereas the 1-OH succinate ester retains it[36]. Most likely the PP conjugate is also unable to bind microtubules explaining the decreased cytotoxicity. The PP conjugate was shown to be highly stable in a variety of milieu including undiluted murine serum, CT26 cellular cytosol and CT26 tissue homogenate over 72 h. The short time scale of 4 h for the in vitro cytotoxicity assay suggests the active PTX will not form which could explain why the PP conjugate itself is less toxic.

Ideally albumin-bound drugs will remain invisible to the liver, reticuloendothelial system (RES) as well as various esterases and peptidases encountered in the body. The release mechanism for bound drugs would then be concentration-driven dissociation or release due to digestion of the carrier albumin. A dialysis experiment aimed at assessing the off-rate of PP from albumin shows this too is very slow, even when sink conditions are created by dialyzing against similar concentrations of delipidated albumin. Thus, spontaneous dissociation from the intact protein may not be the major release mechanism for PP *in vivo*. Since the PP conjugate is utilizing albumin's natural utility as a fatty acid carrier but is not subject to rapid dissociation, albumin is expected to impart its physiological profile to the conjugate. Upon bolus intravenous injection, a 10-fold dilution of the complex should ensue[33]. This is not irreversible clearance from the body as the re-equilibration of the albumin back into the vasculature via the thoracic duct gives rise to the protracted half-life observed. After equilibration, the concentrations in the organs decreased slowly as the bulk of the complex was returning to the vasculature as opposed to being systemically cleared.

This observed serum half-life of 23 h is in agreement with another report on human serum albumin in mice. The truncated half-life is derived from human serum albumin lacking the ability to bind murine FcRn[37], the protein responsible for the protracted half-life.

The biodistribution analysis (**Fig. III-3**) suggests the majority of the conjugate is in the liver and the spleen which could be indicative of sequestration by the RES, however the concentrations in the liver and spleen appear to decrease at the same rate as the other organs which are not associated with RES. The higher uptake could then be simply a reflection of organ size and vasculature leakiness. Considering the PP formulation generated 120 nm aggregates, the PP-HSA particles could also be sequestered by the parenchymal cells of the spleen and liver.

The volume of distribution, V_d, is a ratio estimating the amount of drug in the tissues as compared to the amount of drug in the blood. Larger volumes of distribution are common for lipophilic drugs suggesting they tend to thoroughly permeate through the tissues of the body with little remaining in the blood. Lower volumes of distribution reflect hydrophilic drugs that do not readily permeate the endothelium or lipophilic drugs that are highly protein bound causing retention in the vasculature. The apparent V_d for PTX from the TAXOL formulation (120 mL) was much higher than from the PP formulation (36 mL) suggesting PTX from the former permeates the tissues more readily. While both species are highly lipophilic and bind albumin, the substantial decrease in V_d from TAXOL to PP is indicative of a stronger binding of PP with albumin than TAXOL. Thus, PTX is expected to dissociate from albumin more readily than PP in various tissues, particularly the liver and kidneys, allowing rapid clearance. The PP formulation shows a twofold higher initial concentration and greater AUC compared to the TAXOL formulation despite being half the dose; again most likely due to the large V_d for TAXOL. The longer retention within the vascular bed means more drug will be exposed to the tumor due to multiple passes through the tumor

vasculature with about a 4.5-fold increase in mean residence time (**Table III-3**). Because of this, PP may be equitoxic to TAXOL at lower doses. The tumor accumulation of PP is minimal, ~1% dose/g tissue. This is comparable to TAXOL, however the PTX is cleared from the tumor within 6 h when formulated as TAXOL. When formulated as PP, the radioactivity from PTX shows a sustained accumulation in the tumor even at 72 h. The comparable tumor uptake suggests PP-HSA may only be taken up passively by tumors. As such, it is unlikely that murine gp60, as in the case with murine FcRn, plays a role in the transcytosis of human serum albumin so no active accumulation of albumin is occurring.

The notable resurgence of PP at about 6 h is within the expected error. Secondary peaks in the circulation can occur for a variety of reasons, the most likely being enterohepatic recycling[38,39]. In this process, the PP is excreted into the biliary canalicula in the liver and passed into the jejunal portion of intestine. The PP can then be reabsorbed into the portal blood stream. This process is slow and can be modeled as if it happens a time τ after the bolus injection[40]. Unfortunately, the limited amount of data precluded successful modeling in this manner so a noncompartmental model was fit to the data as is common for this type of profile[41,42].

Submicron particles, including albumin, do not diffuse far into the high-pressure tumors[43]. In order for the PP-HSA complex to be cytotoxic, the albumin must be degraded in the tumor environment releasing PP; further hydrolysis to PTX would promote the greatest efficacy. Digestion in the tumor vicinity of albumin is expected to be rapid[12]. Conversely, as shown in **Fig. III-1**, the PP conjugate appears to be resistant to hydrolysis in both CT26 tumor cell cytosol as well as the tumor tissue homogenate. The decreased cytotoxicity will require greater doses of the PP conjugate in the tumor environment. A greater exposure is expected in the tumor environment due to the protracted half-life of the PP-HSA formulation, however only moderate tumor uptake is observed. Despite this, tumor accumulation is

observed for 72 h (**Fig. III-3**) for the aggregates whereas the PTX is cleared within 6 h for the TAXOL vehicle (**Fig. III-4**). The utter insolubility of PP mandates formulation in a solution containing albumin. This process entails PP precipitation and protein aggregation. As such a careful process control must be satisfied in scale-up. Apart from this, the PP-containing formulation is capable in providing: (1) a solution devoid of any undesirable detergents; (2) a cost-effective method for high affinity albumin binding via the simple reaction with PDG's one-step chemistry, (3) similar characteristics as ABRAXANE and (4) superior pharmacokinetics.

6. Acknowledgements

We would like to acknowledge Dr. Arlene Bridges of the UNC ADME Mass Spectrometry Center for preparing a protocol for separation and quantitation of our compounds by LC/MS. Funds were provided in part by the NCI R01 CA126825.

7. References

(1) Hawkins, M. J., Soon-Shiong, P., and Desai, N. (2008) Protein nanoparticles as drug carriers in clinical medicine. *Adv. Drug Delivery Rev. 60,* 876-885.

(2) Sparreboom, A., Scripture, C. D., Trieu, V., Williams, P. J., De, T., Yang, A., Beals, B., Figg, W. D., Hawkins, M., and Desai, N. (2005) Comparative preclinical and clinical pharmacokinetics of a cremophor-free, nanoparticle albumin-bound paclitaxel (ABI-007) and paclitaxel formulated in Cremophor (Taxol). *Clin. Cancer Res. 11,* 4136-4143.

(3) Gradishar, W. J., Tjulandin, S., Davidson, N., Shaw, H., Desai, N., Bhar, P., Hawkins, M., and O'Shaughnessy, J. (2005) Phase III trial of nanoparticle albumin-bound paclitaxel compared with polyethylated castor oil-based paclitaxel in women with breast cancer. *J. Clin. Oncol. 23,* 7794-7803.

(4) Andersen, J. T., and Sandlie, I. (2009) The versatile MHC class I-related FcRn protects IgG and albumin from degradation: implications for development of new diagnostics and therapeutics. *Drug Metab. Pharmacokinet. 24,* 318-332.

(5) Kratz, F. (2008) Albumin as a drug carrier: design of prodrugs, drug conjugates and nanoparticles. *J. Controlled Release 132,* 171-183.

(6) Stehle, G., Sinn, H., Wunder, A., Schrenk, H. H., Stewart, J. C., Hartung, G., Maier-Borst, W., and Heene, D. L. (1997) Plasma protein (albumin) catabolism by the tumor itself--implications for tumor metabolism and the genesis of cachexia. *Crit. Rev. Oncol. Hematol. 26,* 77-100.

(7) Sinn, H., Schrenk, H. H., Friedrich, E. A., Schilling, U., and Maier-Borst, W. (1990) Design of compounds having an enhanced tumour uptake, using serum albumin as a carrier. Part I. *Int J Rad Appl Instrum B. 17,* 819-827.

(8) Schilling, U., Friedrich, E. A., Sinn, H., Schrenk, H. H., Clorius, J. H., and Maier-Borst, W. (1992) Design of compounds having enhanced tumour uptake, using serum albumin as a carrier--Part II. In vivo studies. *Int J Rad Appl Instrum B. 19,* 685-695.

(9) Maeda, H. (2010) Tumor-selective delivery of macromolecular drugs via the EPR effect: background and future prospects. *Bioconjugate Chem. 21,* 797-802.

(10) Desai, N. P., Trieu, V., Hwang, L. Y., Wu, R., Soon-Shiong, P., and Gradishar, W. J. (2008) Improved effectiveness of nanoparticle albumin-bound (nab) paclitaxel versus polysorbate-based docetaxel in multiple xenografts as a function of HER2 and SPARC status. *Anti-Cancer Drugs 19,* 899-909.

(11) Søreide, J. A., Lea, O. A., and Kvinnsland, S. (1991) Cytosol protein content and prognosis in operable breast cancer. Correlations with steroid hormone receptors and other prognostic factors. *Breast Cancer Res. Treat. 20,* 25-32.

(*12*) Andersson, C., Iresjö, B. M., and Lundholm, K. (1991) Identification of tissue sites for increased albumin degradation in sarcoma-bearing mice, *J. Surg. Res. 50*, 156-162.

(13) van der Vusse, G. J. (2009) Albumin as fatty acid transporter. *Drug Metab. Pharmacokinet. 24,* 300-307.

(14) Simard, J. R., Zunszain, P. A., Hamilton, J. A., and Curry, S. (2006) Location of high and low affinity fatty acid binding sites on human serum albumin revealed by NMR drug-competition analysis. *J. Mol. Biol. 361,* 336-351.

(15) Spector, A. A. (1975) Fatty acid binding to plasma albumin. *J. Lipid Res. 16,* 165-179.

(16) Cistola, D. P., Small, D. M., and Hamilton, J. A. (1987) Carbon 13 NMR studies of saturated fatty acids bound to bovine serum albumin. II. Electrostatic interactions in individual fatty acid binding sites. *J. Biol. Chem. 262,* 10980 -10985.

(17) Simard, J. R., Zunszain, P. A., Ha, C., Yang, J. S., Bhagavan, N. V., Petitpas, I., Curry, S., and Hamilton, J. A. (2005) Locating high-affinity fatty acid-binding sites on albumin by x-ray crystallography and NMR spectroscopy. *Proc. Natl. Acad. Sci. U.S.A. 102,* 17958-17963.

(18) Lambert, D. M. (2000) Rationale and applications of lipids as prodrug carriers. *Eur. J. Pharm. Sci. 11 Suppl 2,* S15-27.

(19) Sparreboom, A., Wolff, A. C., Verweij, J., Zabelina, Y., van Zomeren, D. M., McIntire, G. L., Swindell, C. S., Donehower, R. C., and Baker, S. D. (2003) Disposition of docosahexaenoic acid-paclitaxel, a novel taxane, in blood: in vitro and clinical pharmacokinetic studies. *Clin. Cancer Res. 9,* 151-159.

(20) Dosio, F., Reddy, L. H., Ferrero, A., Stella, B., Cattel, L., and Couvreur, P. (2010) Novel nanoassemblies composed of squalenoyl-paclitaxel derivatives: synthesis, characterization, and biological evaluation. *Bioconjugate Chem. 21,* 1349-1361.

(21) Kurtzhals, P., Havelund, S., Jonassen, I., Kiehr, B., Larsen, U. D., Ribel, U., and Markussen, J. (1995) Albumin binding of insulins acylated with fatty acids: characterization of the ligand-protein interaction and correlation between binding affinity and timing of the insulin effect in vivo. *Biochem. J. 312 (Pt 3),* 725-731.

(22) Shet, J., Desai, V., and Tilve, S. (2004) Domino Primary Alcohol Oxidation-Wittig Reaction: Total Synthesis of ABT-418 and (E)-4-Oxonon-2-enoic Acid. *J. Cheminf. 35,* 1859-1863.

(23) Shoemaker, R. H. (2006) The NCI60 human tumour cell line anticancer drug screen. *Nat. Rev. Cancer 6,* 813-823.

(24) Fang, Y., Tong, G. C., and Means, G. E. (2006) Structural changes accompanying human serum albumin's binding of fatty acids are concerted. *Biochim. Biophys. Acta, Proteins Proteomics 1764,* 285-291.

(25) Oh, K. S., Song, J. Y., Cho, S. H., Lee, B. S., Kim, S. Y., Kim, K., Jeon, H., Kwon, I. C., and Yuk, S. H. (2010) Paclitaxel-loaded Pluronic nanoparticles formed by a temperature-induced phase transition for cancer therapy. *J. Controlled Release 148,* 344-350.

(26) Poldy, J., Peakall, R., and Barrow, R. A. (2008) Pheromones and analogs from Neozeleboria wasps and the orchids that seduce them: a versatile synthesis of 2,5-dialkylated 1,3-cyclohexanediones. *Tetrahedron Lett. 49,* 2446-2449.

(27) Alvarez, E., Cuvigny, T., du Penhoat, C., and Julia, M. (1988) Syntheses with sulfones XLIX : stereo- and enantioselective synthesis of (s)-(-)-3,9-dimethyl 6-(1-methylethyl) (e)-5,8-decadien 1-ol acetate, sexual pheromone of yellow scale. *Tetrahedron. 44,* 119-126.

(28) Buron, F., Deguest, G., Bischoff, L., Fruit, C., and Marsais, F. (2007) On the racemisation of aspartic anhydride during its preparation. *Tetrahedron: Asymmetry 18,* 1625-1627.

(29) Deutsch, H. M., Glinski, J. A., Hernandez, M., Haugwitz, R. D., Narayanan, V. L., Suffness, M., and Zalkow, L. H. (1989) Synthesis of congeners and prodrugs. 3. Water-soluble prodrugs of taxol with potent antitumor activity. *J. Med. Chem. 32,* 788-792.

(30) Lin, S., Fang, K., Hashimoto, M., Nakanishi, K., and Ojima, I. (2000) Design and synthesis of a novel photoaffinity taxoid as a potential probe for the study of paclitaxel-microtubules interactions. *Tetrahedron Lett. 41,* 4287-4290.

(31) Trissel, L. A. (1997) Pharmaceutical properties of paclitaxel and their effects on preparation and administration. *Pharmacotherapy 17,* 133S-139S.

(32) Kumar, Y., Muzammil, S., and Tayyab, S. (2005) Influence of fluoro, chloro and alkyl alcohols on the folding pathway of human serum albumin. J. Biochem. 138, 335-341.

(33) Xie, D., Yao, C., Wang, L., Min, W., Xu, J., Xiao, J., Huang, M., Chen, B., Liu, B., Li, X., and Jiang, H. (2010) An Albumin-Conjugated Peptide Exhibits Potent Anti-HIV Activity and Long In Vivo Half-Life. *Antimicrob. Agents Chemother. 54,* 191-196.

(34) Bertucci, C., Cimitan, S., Riva, A., and Morazzoni, P. (2006) Binding studies of taxanes to human serum albumin by bioaffinity chromatography and circular dichroism. *J. Pharm. Biomed. Anal. 42,* 81-87.

(35) Bradley, M. O., Webb, N. L., Anthony, F. H., Devanesan, P., Witman, P. A., Hemamalini, S., Chander, M. C., Baker, S. D., He, L., Horwitz, S. B., and Swindell, C. S. (2001) Tumor targeting by covalent conjugation of a natural fatty acid to paclitaxel. *Clin. Cancer Res. 7,* 3229-3238.

(36) Fu, Y., Li, S., Zu, Y., Yang, G., Yang, Z., Luo, M., Jiang, S., Wink, M., Efferth, T., (2009) Medicinal chemistry of paclitaxel and its analogues. *Curr. Med. Chem*. *16*, 3966-3985.

(37) Andersen, J. T., Daba, M. B., Berntzen, G., Michaelsen, T. E., and Sandlie, I. (2010) Cross-species binding analyses of mouse and human neonatal Fc receptor show dramatic differences in immunoglobulin G and albumin binding. *J. Biol. Chem. 285,* 4826-4836.

(38) Roberts, M. S., Magnusson, B. M., Burczynski, F. J., and Weiss, M. (2002) Enterohepatic circulation: physiological, pharmacokinetic and clinical implications. *Clin. Pharmacokinet. 41,* 751-790.

(39) Davies, N. M., Takemoto, J. K., Brocks, D. R., and Yáñez, J. A. (2010) Multiple peaking phenomena in pharmacokinetic disposition. *Clin. Pharmacokinet. 49,* 351-377.

(40) Steimer, J. L., Plusquellec, Y., Guillaume, A., and Boisvieux, J. F. (1982) A time-lag model for pharmacokinetics of drugs subject to enterohepatic circulation. *J. Pharm. Sci. 71,* 297-302.

(41) Okusanya, O., Forrest, A., DiFrancesco, R., Bilic, S., Rosenkranz, S., Para, M. F., Adams, E., Yarasheski, K. E., Reichman, R. C., Morse, G. D., and and the ACTG 5043 Protocol Team. (2007) Compartmental Pharmacokinetic Analysis of Oral Amprenavir with Secondary Peaks. *Antimicrob. Agents Chemother. 51,* 1822-1826.

(42) Naidoo, V., Mulders, M. S. G., and Swan, G. E. (2009) The intravenous pharmacokinetics of diminazene in healthy dogs. *J. S. Afr. Vet. Assoc. 80,* 215-219.

(43) Lichtenbeld, H. C., Yuan, F., Michel, C. C., and Jain, R. K. (1996) Perfusion of single tumor microvessels: application to vascular permeability measurement. *Microcirculation 3,* 349-357.

CHAPTER IV

CONCLUSIONS AND FUTURE EXPERIMENTS

1. Summary

The flagship therapeutic molecule selected for PDG modification was PTX. As a result of high affinity for albumin, it was expected the PP conjugate would have increased solubility, stability *in vivo*, a protracted circulation half-life and tumor accretion. Degradation of the albumin in the tumor periphery would release PP for diffusion into the tumor core. Experimentally, the PP conjugate was very slowly hydrolyzed in undiluted serum, CT26 tumor cell cytosol and CT26 tumor tissue homogenate over 72 h at 37℃. Like all other PTX conjugates at the 2'-OH, the cytotoxicity of the conjugate decreased most likely due to loss of microtubulin bundling (*1-3*). Dialysis of the PP-HSA complex against equimolar concentrations of delipidated HSA showed a great deal of stability. The aggregates should be very stable *in vivo* with little dissociation of PP over time. Pharmacokinetic and biodistribution analysis showed a large increase in circulatory half-life compared to TAXOL but only moderate tumor accumulation although uptake is sustained for 72 h. The fraction of dose that does reach the tumor will be inefficiently hydrolyzed to the more active PTX prior to clearance from the system. The result is a formulation comparable to TAXOL at lower doses very similar to ABRAXANE.

The PP conjugate is approximately 10-fold less soluble than PTX. This was marginally improved by the addition of albumin, however, solutions took two weeks to equilibrate and approached significantly lower concentrations than expected. This was thought to be dissolution rate limited, but PP became saturated in solution without HSA much more quickly than the albumin containing solutions. The kinetics of albumin loading should be second order with respect to the concentration of PP and the concentration of HSA. The slow rate could be due to the very low solubility of PP but this does not explain the very low equilibrium concentration of PP. Albumin is highly resistant to solvents (*4*). Thus to increase the solubility, PP was first dissolved in a water miscible alcohol; t-BuOH or

EtOH. The solution of PP in either alcohol was then introduced to an aqueous solution of albumin. The equilibrium concentration of PP obtained by this method was much higher than without the alcohol, even after lyophilization and reconstitution. This also resulted in the formation of aggregates. These aggregates also formed when PTX alone was dissolved in EtOH and added to albumin; there were no aggregates when stearic acid or PDG acid were dissolved in EtOH and added to albumin. Consequently PTX must be responsible for aggregation.

Albumin is believed to provide two binding sites for PTX with dissociation constants of 10^{-6} and 10^{-5} M by docking studies (*5*). Experimental values are lower, and showed EtOH may be required to create binding sites for PTX (*6*). How the PTX interacts with the albumin in these aggregates is unknown at this time. Adding multiple equivalents of PTX in EtOH to the albumin yielded a maximum concentration of 0.5 molar equivalents PTX/HSA. This value was surpassed by PP which dissolved six molar equivalents of PP when 12 were added. This suggests the PP conjugate interacting with the protein in a different manner than PTX alone. The fatty acid should be most stable within the binding pocket of the albumin with the PTX sitting on the surface. This can hypothetically allow the PTX to interact with other binding sites on albumin or other PTX molecules through van der Waals interactions yielding a heterogeneous matrix (**Fig. IV-1**).

2. Ancillary Data

The resulting particles are dependent on the electrolyte composition of the bulk solvent when mixing and after reconstitution. The loading efficiency is poorly reproducible and the aggregation exceedingly difficult to prevent without adding a large quantity of surfactant. When the PP was dissolved in a micellar solution of T80 or a Miglyol emulsion, it poorly transferred to bovine serum albumin immobilized on agarose as compared to dissolution of an alcoholic solution containing PP. This could be due to the high energy of

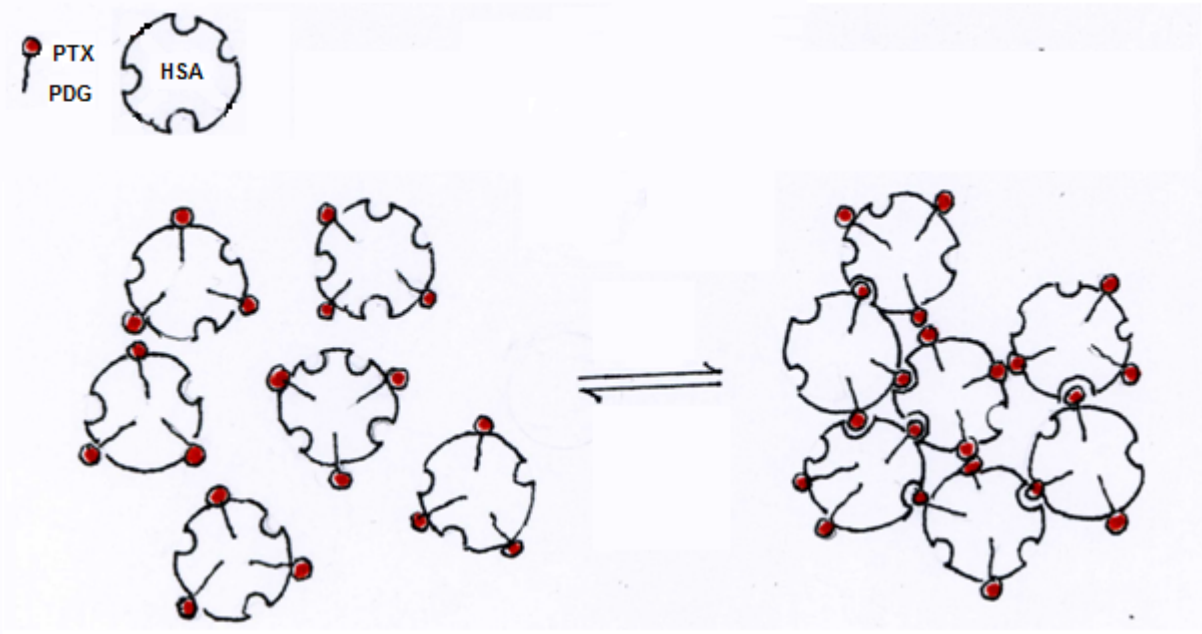

Figure IV-1. Hypothetical configuration of PP-HSA aggregates. The bound PP molecules orient the PTX into the bulk solvent causing PTX-HSA interactions as well as PTX-PTX interactions.

the albumin bound complex as a large portion of the PTX moiety will be exposed to the bulk aqueous phase. This high free energy could be dissipated by binding albumin or another PTX moiety to exclude bulk water. When micellar solutions of T80 containing PP with or without HSA were administered to CT26 tumor bearing mice, about 85% of the PP was distributed to various tissues within the first few hours (**Figs. A-6, A-7**). Subsequent to equilibration, the radioactivity was cleared slowly from the serum over 72 h with no rebound in concentration as observed for the PP-HSA particles (**Fig. A-5**). The very similar profile compared to the PP-HSA particles of **Chapter III** suggests the PP may be able to transfer from T80 micelles to albumin and mimic its half-life. From the immobilized BSA-agarose experiment, the T80 micellar solution does allow transfer of PP to albumin readily but less efficiently than from EtOH alone (**Table A-11**). Whether or not the murine albumin forms aggregates *in vivo* after binding PP is unknown, as is the stability of PP-HSA aggregates *in vivo*. This has not been shown directly as a monomeric solution of PP with HSA has not been found that provides high enough concentrations for PK analysis.

3. Future Experiments

The lower side-effects expected from a PP-containing formulation may allow a higher maximally tolerated dose compared to TAXOL. A dose escalation study could be conducted to determine a more efficacious dose for PP. Alternatively, improving the formulation begins with improving the PP-HSA interaction. The aforementioned *in vitro* data has demonstrated numerous difficulties for the PP molecule to bind albumin. The poor loading efficiency could be due to several issues. First, the very bulky PTX group in PP could sterically hinder the binding pocket such that the whole alkyl tail is not able to bind thus decreasing the affinity and minimizing binding. Secondly, the hypothesized convoluted network of binding through fatty acid binding sites, PTX binding sites and van der Waals interactions could effectively lead to non-covalent cross-linking thus inducing particle formation. Minimizing these

hydrophobic interactions could prevent the formation of 120 nm aggregates allowing elucidation of the benefits, if any, of binding native albumin *in vivo*.

To test these two hypotheses, the PP conjugate can be synthetically altered. It has been demonstrated succinylation at the hydroxyl on C-7 lowers the affinity of the molecule for albumin (*7*). Phosphorylation may also inhibit this interaction while also providing two negative charges at physiological pH for improving solubility and bulk water deposition around PTX in the binding pocket. This would also create a resistance to aggregation of other PTX molecules due to electrostatic repulsion thus removing the van der Waals interaction. With 2.5 anionic charges at physiological pH, this PP derivative may be able to form micelles and should not form aggregates when formulated with albumin. The resistance to proper seating in the binding pocket due to steric hindrance can be addressed by reacting a tetraethyleneglycol linker between the PTX and the PP molecule. This would improve solubility slightly but more importantly should decrease the steric hindrance of binding potentially caused by PTX. This would not preclude the binding of PTX to other PTX molecules or albumin molecules and thus might not eliminate aggregation. If both are unsuccessful, a combination of both modifications may be successful. Both syntheses can be accomplished (**Scheme IV-1**) with the more complex 7-phosphate being previously published (*8*).

Synthesis of the tetraethyleneglycol substituted PP can be synthesized by reacting a carbobenzyloxy (Cbz) protected propionyl(tetraethyleneglycol)ethylamine with paclitaxel and DCC with DMAP at room temperature (**Scheme IV-1**). The Cbz protecting group could then be removed by hydrogenolysis and the resulting free amine reacted with PDG anhydride in DCM at room temperature. Synthesis of the phosphorylated derivative is more difficult as the 7-position is more sterically hindered than the C-2' position. The 2'-OH can be protected with a trimethylsilyl ether and the 7-OH reacted with tetrabenzyl pyrophosphate in the

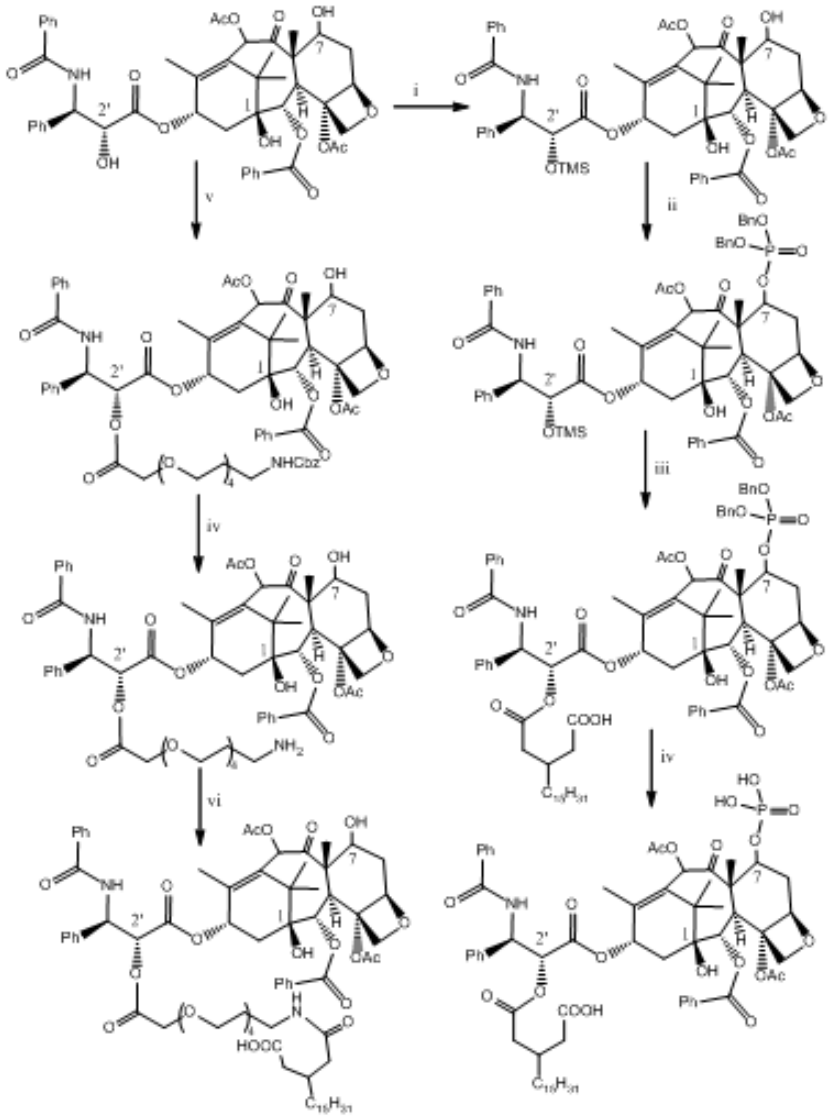

Scheme IV-1. Proposed Synthesis of two PDG-PTX derivatives. Reaction Conditions i: TMSCl, imidazole; ii: LDA/THF/-30℃, $O(PO(OCH_2Ph)_2)_2$; iii: EtOH/HCl(aq), PDG anhydride/DMAP room temperature; iv: EtOH/Pd/C(10%)/H_2; v: $DCC/HOOC(CH_2)_2(OCH2CH2)_4CH_2CH_2NHCbz/DMAP$; vi: PDG anhydride. TMSCl, trimethylsilyl chloride; LDA, lithium diisopropylamide; EtOH, ethanol; DMAP, 4-dimethylaminopyridine; DCC, dicyclohexylcarbodiimide; Cbz, carbobenzyloxy.

presence of freshly prepared lithium diisopropylamide (LDA). Deprotection of the trimethylsilyl ether with EtOH in HCl(aq) and reacting with PDG anhydride in the presence of DMAP at room temperature will esterify the PDG lipid moiety at the 2'-OH position. Hydrogenolysis to deprotect the dibenzylphosphate yields the desired compound. If neither of these drugs are as cytotoxic as PTX and hydrolytically resistant like PP then neither would be useful as a drug. Instead of disguising PTX as a water soluble drug, an intrinsically water soluble drug may offer insight into the formation of aggregates.

The opposite end of the spectrum is a high solubility drug which should demonstrate no albumin binding such as the nucleotide antagonist difluorodeoxycytidine or gemcitabine (dFdC). Modification can occur at the C4-exocyclic amine or the 5'-OH selectively (*9*, *10*) yielding a drug species that should be water soluble as micelles, bind albumin and not aggregate (**Scheme IV-2**). These molecules can be synthesized easily and may be more amenable to formulation. Once synthesized, binding affinity can be analyzed by isothermal titration calorimetry. If the molecules can successfully bind albumin, PK/BD studies can be conducted using a radiolabel or by LC/MS. Favorable pharmacokinetic outcomes would lead to cytotoxicity and PD studies.

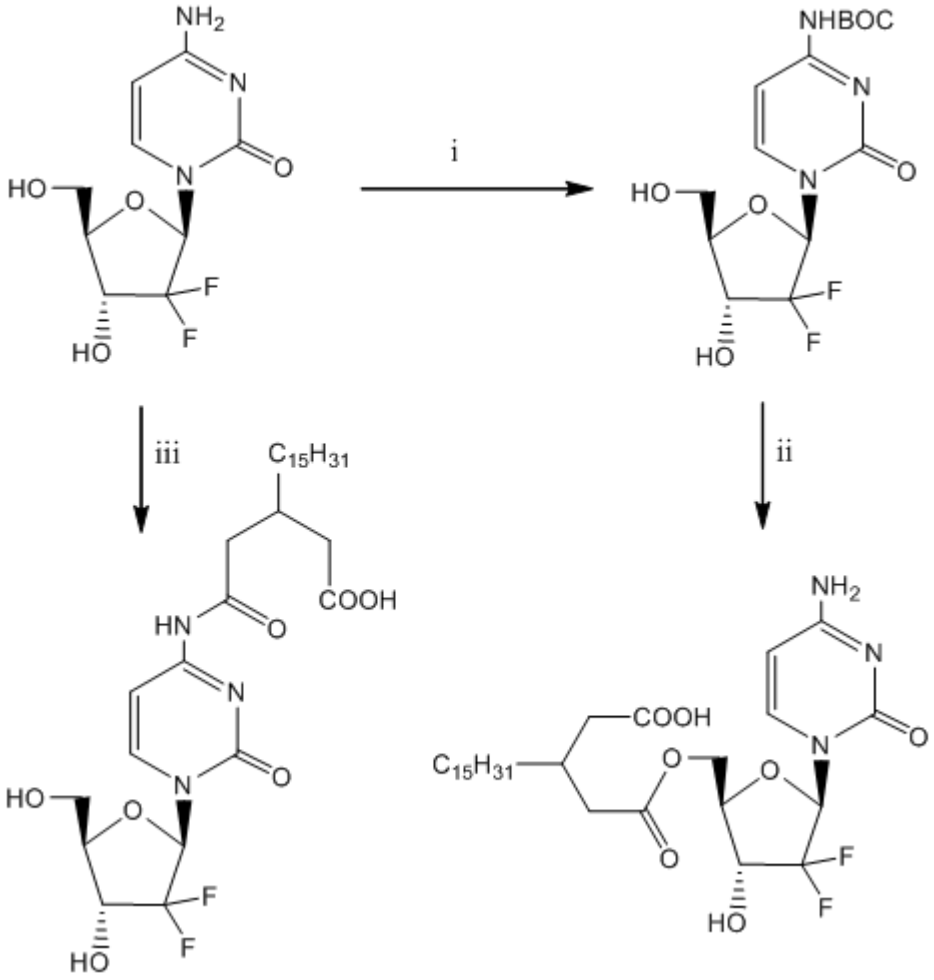

Scheme IV-2. Proposed synthesis of two PDG-dFdC derivatives. Reaction conditions i: $((CH_3)_3CCO)_2O$; ii: PDG anhydride/DMAP, TFAA/DCM; iii: PDG anhydride/DMAP DMAP, 4-dimethylaminopyridine; TFAA, trifluoroacetic anhydride.

4. References

1. Deutsch, H. M., Glinski, J. A., Hernandez, M., Haugwitz, R. D., Narayanan, V. L., Suffness, M., and Zalkow, L. H. (1989) Synthesis of congeners and prodrugs. 3. Water-soluble prodrugs of taxol with potent antitumor activity, *J. Med. Chem. 32*, 788-792.

2. Dosio, F., Reddy, L. H., Ferrero, A., Stella, B., Cattel, L., and Couvreur, P. (2010) Novel nanoassemblies composed of squalenoyl-paclitaxel derivatives: synthesis, characterization, and biological evaluation, *Bioconjug. Chem. 21*, 1349-1361.

3. Bradley, M. O., Swindell, C. S., Anthony, F. H., Witman, P. A., Devanesan, P., Webb, N. L., Baker, S. D., Wolff, A. C., and Donehower, R. C. (2001) Tumor targeting by conjugation of DHA to paclitaxel, *J. Cont. Rel. 74*, 233-236.

4. Kumar, Y., Muzammil, S., and Tayyab, S. (2005) Influence of fluoro, chloro and alkyl alcohols on the folding pathway of human serum albumin, *J. Biochem. 138*, 335-341.

5. Paal, K., Shkarupin, A., and Beckford, L. (2007) Paclitaxel binding to human serum albumin--automated docking studies, *Bioorg. Med. Chem. 15*, 1323-1329.

6. Bertucci, C., Cimitan, S., Riva, A., and Morazzoni, P. (2006) Binding studies of taxanes to human serum albumin by bioaffinity chromatography and circular dichroism, *J Pharm. Biomed. Anal. 42*, 81-87.

7. Battaglia, A., Bertucci, C., Bombardelli, E., Cimitan, S., Guerrini, A., Morazzoni, P., and Riva, A. (2003) Synthesis and HSA binding characterisation of the water soluble 7-succinylpaclitaxel, *Eur. J. Med. Chem. 38*, 383-389.

8. Vyas, D. M., Wong, H., Crosswell, A. R., Casazza, A. M., Knipe, J. O., Mamber, S. W., and Doyle, T. W. (1993) Synthesis and antitumor evaluation of water soluble taxol phosphates, *Bioorg. Medicinal Chem. Lett. 3*, 1357-1360.

9. Bender, D. M., Bao, J., Dantzig, A. H., Diseroad, W. D., Law, K. L., Magnus, N. A., Peterson, J. A., Perkins, E. J., Pu, Y. J., Reutzel-Edens, S. M., Remick, D. M., Starling, J. J., Stephenson, G. A., Vaid, R. K., Zhang, D., and McCarthy, J. R. (2009) Synthesis, Crystallization, and Biological Evaluation of an Orally Active Prodrug of Gemcitabine, *J. Med. Chem. 52*, 6958-6961.

10. Guo Zw, Z., and Gallo, J. M. (1999) Selective Protection of 2',2'-Difluorodeoxycytidine (Gemcitabine), *J. Org. Chem. 64*, 8319-8322.

APPENDIX

ANALYSIS OF PP-HSA AGGREGATES

1. Solubility of PP in the Presence of HSA

Stocks of 4%, 3%, 2%, 1% and 0% (w/v) HSA (Sigma A3782) were prepared in PBS. A stock (6.97 mg/8.21x10^5 dpm/mL) of tritiated PP was prepared and concentrated to a solid. The solid was then added to all HSA stock solutions. The suspensions were sealed and shook vigorously in a water bath at 25℃. The susp ensions were sampled at 1, 2, 3, 7, and 14 days followed by centrifugation at 12,000 x g for 5 min, filtration through a 0.1 µm inorganic membrane (Whatman Anotop 10, 6809-1012) and 40 µL aliquots of the supernatant were diluted in 5 mL Ultima Gold scintillation cocktail and analyzed by LSC (**Fig. A-1**). The concentrations of albumin were constant as confirmed by a BCA assay at each timepoint. (Pierce).

2. Solubility of PP as a Function of pH

Several buffers were prepared spanning pH 3.5-10 according to Gomori G., (1955) *Methods Enzymology*, **1**;138-146 as presented in (**Table A-1**). The pH 3.5 buffer contained 0.075 M formic acid/0.07 M sodium formate/0.03 M sodium chloride. The pH 4.0 buffer contained 0.024 M formic acid/0.07 M sodium formate/0.03 M sodium chloride. The pH 5.0 buffer contained 0.034 M acetic acid/0.1 M sodium acetate. The pH 6.0 buffer contained 0.006 M sodium succinate/0.031 disodium succinate. The pH 7.0 buffer contained 0.016 M potassium dihydrogenphosphate/0.028 M disodium hydogenphosphate. The pH 8.0 buffer contained 0.16 M tris(hydroxyaminomethane) (Tris) and 0.1 M Tris·hydrochloride. The pH 8.5 buffer contained 0.20 M Tris and 0.06 M Tris·hydrochloride. The pH 9.0 buffer contained 0.045 M sodium bicarbonate/0.019 sodium carbonate. The pH 10.0 buffer contained 0.02 M sodium bicarbonate/0.027 sodium carbonate. The pH of the buffers was determined using a pH meter (**Table A-1**) (Accumet Basic AB15, Fisher Scientific). A stock solution of PP was prepared in EtOH at 5.55 mg/1.11x10^6 dpm/mL. Aliquots of the stock were added to eppendorf tubes and the EtOH evaporated with nitrogen; 2 mg for pH 8.0 and above, 1 mg

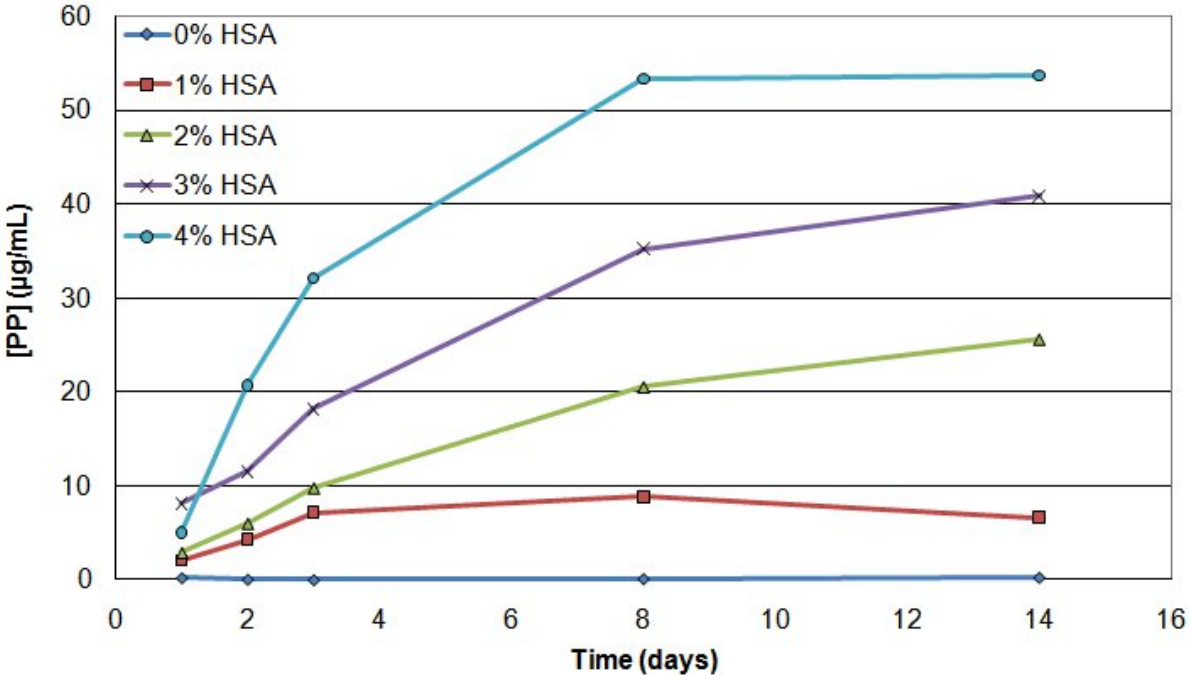

Figure A-1. Time resolved solubility diagram of PP in the presence of HSA in phosphate buffer pH 7.4. The concentration of PP is given with respect to PTX. The maximum concentration of ~54 µg/mL is well below the expected 3 mg/mL for saturation of 6 binding sites of 4% HSA. The 0% HSA formulation represents the rate at which PP can saturate the buffer. This occurs within 24 h.

Expected pH	Actual pH before adding PP	Actual pH after adding PP
3.5	3.61	3.59
4.0	4.21	4.18
5.0	5.35	5.32
6.0	6.57	6.49
7.0	7.09	7.17
8.0	8.08	7.93
8.5	8.56	8.40
9.5	9.64	9.47
10	10.15	9.82

Table A-1. Summary of buffers used in pH dependent solubility of [^{3}H]-PP. All buffers were prepared according to (Gomori, G. (1955) "Preparation of Buffers for Use in Enzyme Studies". Method Enzymol 1:138-146. The addition of the acidic PP molecule was not enough to substantially change the pH of any stock.

for pH 7 and pH 6, 0.1 mg for pH 5.0 and below. The samples were capped, sealed sonicated for 30 minutes and shook at 37℃ for 48 h. The samples were removed and allowed to cool to 25℃ in a water bath then centrifuged at 16.1 x 1000g for 30 minutes. Aliquots of the supernatant were filtered through a 0.22 µm PVDF filter and weighed in 100 µL triplicates, dissolved in 5 mL Ultima Gold scintillation cocktail and analyzed by LSC (**Fig. A-2**). The remaining samples were resealed, sonicated for 30 minutes and shook at 37℃ for another 5 days. The samples were again cooled to 25℃ in a water bath and centrifuged at 16.1 x 1000g for 30 minutes. The bottom of the pH 3.5 and pH 10 tubes was scratched with a pipet tube to disturb the cakes. Large flakes were found at pH 10 and small particles found in the pH 3.5 tube suggesting the solutions were saturated. The samples were centrifuged again at 16.1 x 1000g for 30 minutes and the supernatants filtered through a 0.22 µm PVDF filter and 100 µL aliquots weighed in triplicate, dissolved in 5 mL Ultima Gold scintillation cocktail and the samples analyzed by LSC (**Fig. A-2**).

3. Circular Dichroism of HSA in the Presence of t-BuOH

A stock solution of 26 µM of delipidated HSA (Sigma A1887) in 0.1 M phosphate buffer was prepared and aliquoted into 5 samples. To two of the samples was added t-BuOH to make a 10% (v/v) solution and to two other samples was added enough t-BuOH to make a 20% (v/v) solution. Of the t-BuOH containing solutions, 1 of each concentration was lyophilized overnight to a cake and reconstituted in distilled water to regenerate the 26 µM solution. The 5 samples were then analyzed via CD against a blank of phosphate buffer, phosphate buffer with 10% (v/v) t-BuOH or phosphate buffer with 20% (v/v) t-BuOH (**Fig. A-3**). The minor differences observed the spectrum were assumed to be due to minor concentration differences. This was confirmed by plotting the absorbance as a function of wavelength (**Fig. A-4**). Taking a ratio of all mdeg (λ) of the highest (yellow, 26 µM HSA 20% t-BuOH) and lowest (navy, 26 µM HSA) datasets revealed a constant. The same was true

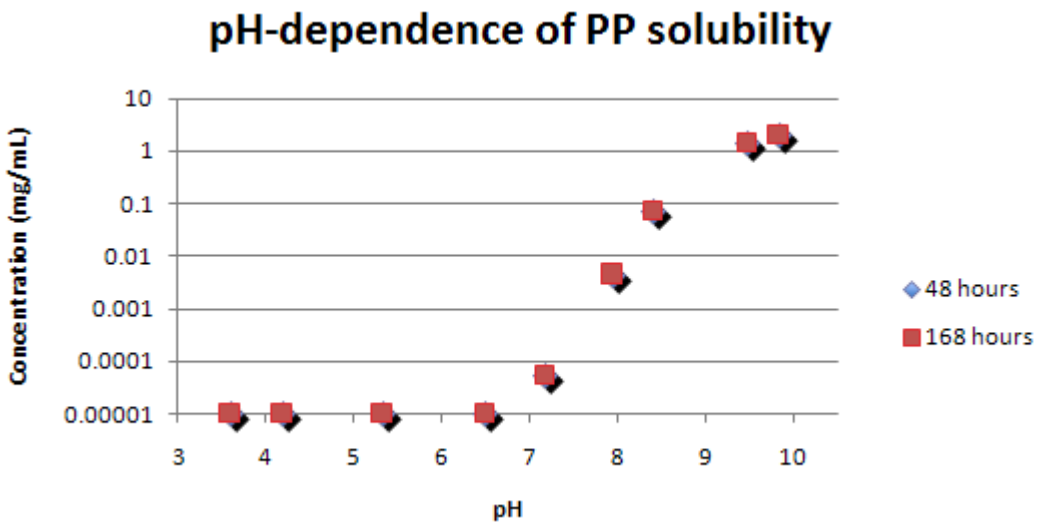

Figure A-2. pH dependent solubility of [^{3}H]-PP. Concentrations at pH 6.5 and below were not quantifiable. TLC on the quantifiable fractions showed only intact conjugate.

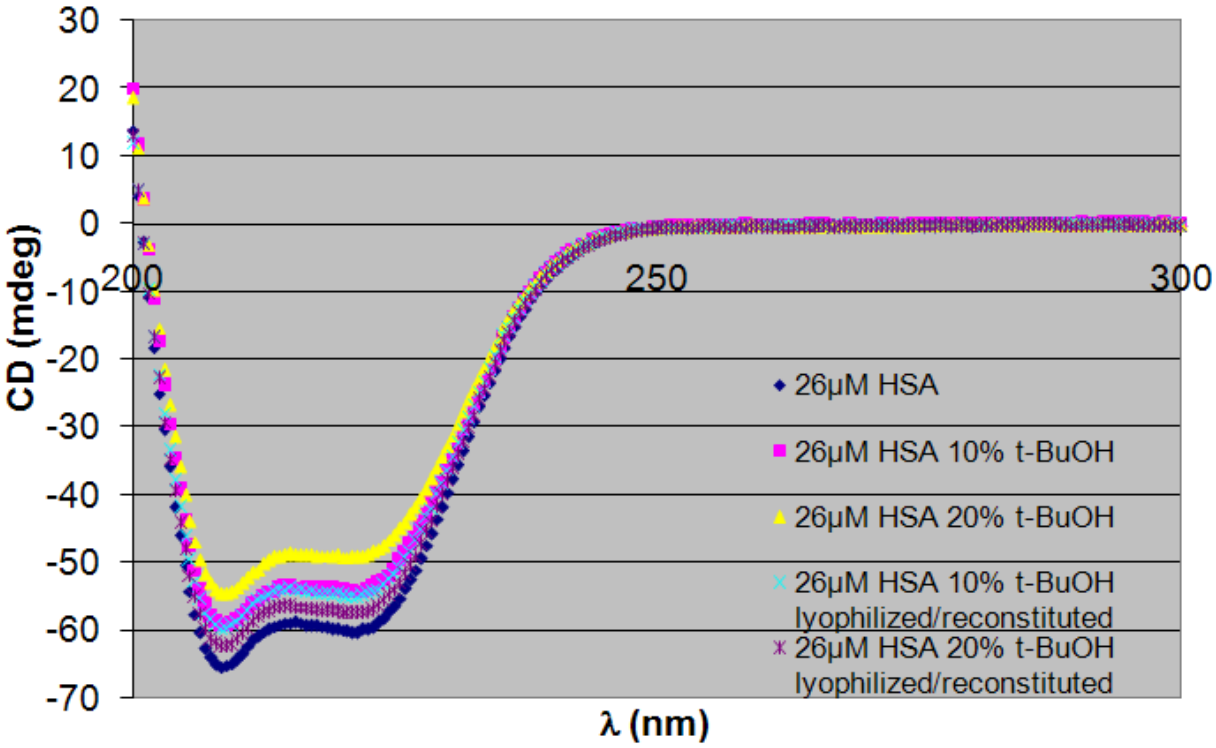

Figure A-3. Circular Dichroism analysis of HSA in the presence of t-BuOH. Data was collected using an Applied Photophysics Pistar-180 CD/Fluorescence spectrometer.

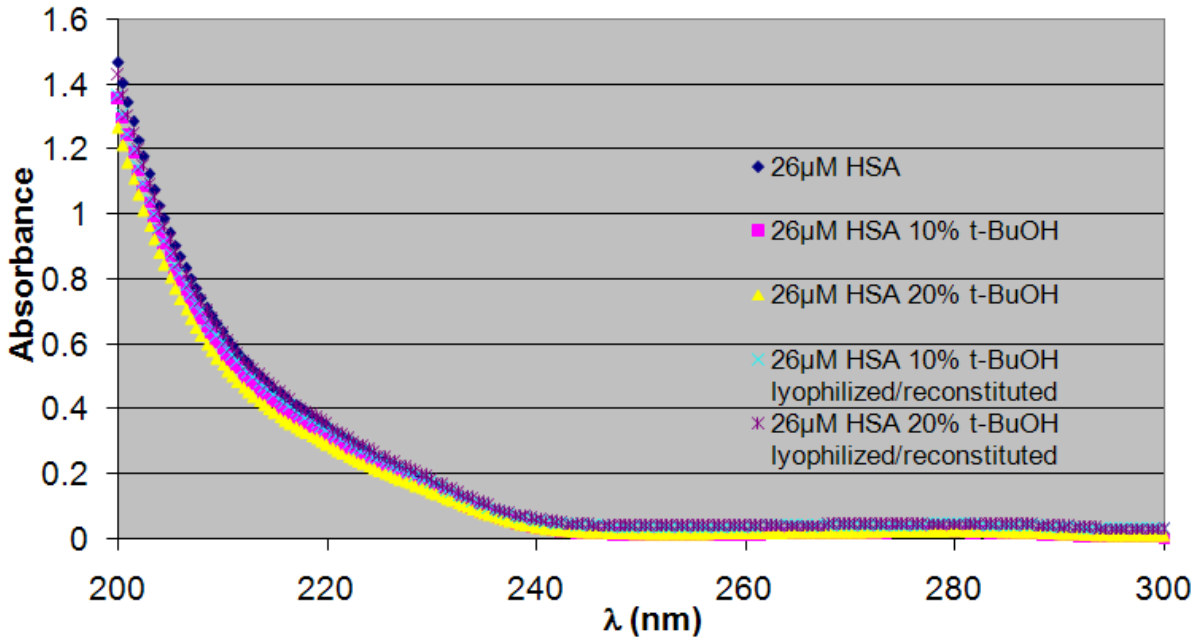

Figure A-4. Absorbance spectrum of HSA in the presence of t-BuOH. The minor differences in absorbance are most likely due to dilution with t-BuOH and imprecise quantities of water added during reconstitution after lyophilization.

when applied to absorbance (λ). This suggests the dilution of HSA as a result of the t-BuOH is the cause of the change in CD spectrum, not any change in structure. In other words, from the absorbance (λ) spectrum, it is clear the concentrations are different between 26 µM HSA and 26 µM HSA containing 20% t-BuOH. If each absorbance is normalized to the same absorbance, the CD spectra would superimpose.

4. Effect of PTX on Aggregation of HSA

A stock solution of tritiated PTX (AK Scientific, Union City, CA 65648, Moravek Biochemicals, Brea, CA MT 1646) in t-BuOH was prepared at 6.41 mg/1.64x10^6 dpm/mL. Stocks of HSA were also prepared as 4 samples of 40 mg/mL HSA (Sigma A1887) in D5W. To the albumin stocks was added 1, 2, 3 or 6.5 eq PTX/HSA at a concentration of 1:10 (v/v) t-BuOH:D5W. Increasing turbidity was observed for increasing equivalents of PTX. The samples were gently heated and shook for 5 min then shell frozen at -78℃ and lyophilized overnight. Samples were reconstituted with distilled water to 40 mg/mL HSA and subsequently centrifuged at 16.1 x 1000g for 10 min. The supernatants were removed and analyzed by DLS then aliquots dissolved in 5 mL Ultima Gold scintillation cocktail and analyzed by LSC. The pellets were also dissolved in MeOH and 5 mL Ultima Gold scintillation cocktail and analyzed by LSC for mass balance (**Table A-2**).

5. Effect of Loading HSA in Water and Stability of Resultant Particles

A 50 mg/mL solution of delipidated HSA (Sigma A1887) in water and a stock of PP in t-BuOH (24.7 mg/8.04x10^5 dpm/mL) were prepared. To the HSA solution was added 2 eq PP in t-BuOH to a final volume of 1:10 (v/v) t-BuOH in water. The suspension was lyophilized to a cake and reconstituted in phosphate buffer. The suspension was filtered through a 0.22 µm PVDF filter yielding a colloidal suspension. Two aliquots were removed, weighed and dissolved in 5 mL Ultima Gold scintillation cocktail for LSC analysis confirming

eq PTX	Z ± σ nm (PDI)	Intensity nm (%)	Volume nm (%)	Number nm (%)	eq loaded	%PTX recovered
1	70 ± 60 (0.717)	165 (90%) 3 (10%)	25 (.3%) 3 (99.7%)	2 (100%)	0.41 / 1	75%
2	105 ± 75 (0.525)	182 (94%) 3 (6%)	3 (100%)	3 (100%)	0.41 / 2	76%
3	80 ± 60 (0.556)	150 (93%) 3 (7%)	110 (0.1%) 3 (99.9%)	3 (100%)	0.51 / 3	81%
6.5	100 ± 70 (0.484)	160 (80%) 30 (12%) 3 (8%)	25 (0.3%) 3 (99.7%)	3 (100%)	0.47 / 6.5	67%

Table A-2. Particle size and solubility of PTX in PTX-HSA aggregates. PTX only weakly binds HSA and appears to form aggregates with HSA. Saturation of the protein with PTX appears to occur at a 1:2 molar ratio.

1.9 eq PP loaded. The suspension was added to a cuvette, sealed and analyzed by DLS over 48 h (**Table A-3**).

After 48 h the sample was subject to ultracentrifugation at 14 x 1000g through a 100 kDa MWCO regenerated cellulose membrane (microcon ultracel YM-100, 42412, lot R7PN22647) for 40 min yielding the first filtrate. The cake was resuspended in 0.1 M phosphate buffer and ultracentrifuged at 14 x 1000g through a 100 kDa MWCO regenerated cellulose membrane for 40 min yielding the second filtrate. The cake was then resuspended in phosphate buffer yielding the retentate. All three samples were monitored by DLS over several days to determine the stability of the individual species (**Table A-4**).

From the retentate, 0.6 mL was aliquoted into six samples of 0.1 mL which were then diluted fivefold to 1% HSA with 0.1 M phosphate buffer. To these samples were added 2% (w/v) PEG 3350, 2% (w/v) PEG 8000, 20% (v/v) glycerol, L-Arg at a concentration of 0.5 M and 0.1% (v/v) Triton X-100. The remaining sample was saved as an untreated control. All the samples were mixed gently and analyzed by DLS (**Table A-5**).

6. Stability of PP-HSA Particles to Various Additives

Stock solutions of500 µL containing 10 mg/mL delipidated HSA (Sigma A1887) were prepared in water and additives of various concentrations were dissolved to potentially preclude aggregation. To the final samples was added 2 eq PP in t-BuOH at a final volume ratio of 1:10 t-BuOH:water. The samples were then analyzed using DLS (**Table A-6**). The samples are compared to reference solutions in which 2 eq PP was added to 10 mg/mL delipidated HSA (Sigma A1887) in water at 1:10 (v/v) t-BuOH. Additionally 50 mg/mL delipidated HSA (Sigma A1887) in D5W and a fivefold dilution of the previous sample in water were prepared with no t-BuOH or PP. After DLS analysis (**Table A-6**) all samples (excluding the D5W and D1W solutions) were shell frozen at -78℃ and lyophilized over 3

	0 days	1 day	2 days
Z±σ (PDI)	120 ± 60 nm (0.246)	120 ± 60 nm (0.250)	120 ± 60 nm (0.259)
Intensity	150 nm (100%)	160 nm (100%)	160 nm (100%)
Volume	130 nm (100%)	130 nm (100%)	130 nm (100%)
Number	85 nm (100%)	70 nm (100%)	75 nm (100%)

Table A-3. Stability of PP-HSA aggregates by DLS over 48 h. The PP-HSA aggregates appear stable over 48 h at room temperature.

First Filtrate

	0 days	1 day	2 days	3 days
Z±σ (PDI)	8 ± 2 nm (0.073)	12 ± 6 nm (0.236)	9 ± 4 nm (0.182)	8 ± 3 nm (0.101)
Intensity	9 nm (100%)	13 nm (95%) 4000 nm (4%) 3 nm (1%)	9nm (97%) 4000 nm(3%)	9 nm (100%)
Volume	7 nm (100%)	8 nm (71%) 3 nm (29%)	7 nm (100%)	7 nm (100%)
Number	6 nm (100%)	3 nm (100%)	5 nm (100%)	5 nm (100%)

Second Filtrate

	0 days	1 day	2 days	3 days
Z±σ (PDI)	13 ± 8 nm (0.450)	9 ± 5 nm (0.311)	12 ± 7 nm (0.417)	150 ± 90 nm (0.318)
Intensity	9 nm (68%) 275 nm (32%)	8 nm (89%) 175 nm (10%) 5000 nm(1%)	9 nm (72%) 325 nm (28%)	8 nm (59%) 450 nm (38%) 80 nm (3%)
Volume	7 nm (100%)	6 nm (100%)	7 nm (100%)	7 nm (100%)
Number	6 nm (100%)	5 nm (100%)	6 nm (100%)	6 nm (100%)

Retentate

	0 days	1 days	2 days	3 days
Z±σ (PDI)	100 ± 50 nm (0.292)	100 ± 50 nm (0.281)	100 ± 50 nm (0.264)	100 ± 50 nm (0.272)
Intensity	140 nm (100%)	140 nm (95%) 10 nm (5%)	125 nm (100%)	145 nm (100%)
Volume	110 nm (100%)	100 nm (98%) 7 nm (2%)	110 nm (100%)	105 nm (100%)
Number	65 nm (100%)	5 nm (100%)	80 nm (100%)	60 nm (100%)

Table A-4. Equilibrium of PP-HSA monomers and aggregates over 48 h after ultrafiltration. Neither the monomers nor aggregates appear to re-equilibrate over 72 h. This may not be a concentration driven phenomenon. The concentrations of the various samples are unknown; it is possible very little albumin was ultrafiltered.

	Phosphate Buffer	2% PEG 3350	2% PEG 8000	20% Glycerol	0.5 M L-Arg	0.1% Triton X-100
Z±σ (PDI)	80 ± 45 nm (0.292)	95 ± 50 nm (0.297)	115 ± 60 nm (0.281)	80 ± 45 nm (0.292)	30 ± 28 nm (0.902)	15 ± 8 nm (0.351)
Intensity	110 nm (94%) 10 nm (6%)	135 nm (100%)	160 nm (100%)	115 nm (94%) 10 nm (6%)	275 nm (59%) 15 nm (41%)	12 nm (75%) 100 nm (25%)
Volume	8 nm (98%) 80 nm (2%)	95 nm (100%)	140 nm (100%)	9 nm (97%) 85 nm (3%)	10 nm (99.7%) 334 nm (0.3%)	8 nm (99.9%) 75 nm (0.1%)
Number	6 nm (100%)	60 nm (100%)	90 nm (100%)	6 nm (100%)	9 nm (100%)	6 nm (100%)

Table A-5. Stability of PP-HSA aggregates to PEG, glycerol, L-Arg and Triton X-100. L-Arg and Triton X-100 appear to facilitate disaggregation of the particles. Dilution of the particles without additive also appears to break the particles indicating it could be a concentration driven interaction. This is in contrast to data observed after ultrafiltering the particles.

Additive	Z±PDI width nm (PDI)	Intensity	Volume	Number
L-arginine·HCl (500mM)	165 ± 85 nm (0.274)	195 nm (100%)	195 nm (100%)	130 nm (100%)
L-arginine (OMe)·2HCl (500mM)	190 ± 100 nm (0.263)	245 nm (100%)	265 nm (100%)	145 nm (100%)
L-arginine (500mM)	850 ± 735 nm (0.749)	3100 nm (71%) 320 nm (29%)	2600 nm (94%) 350 nm (6%)	270 nm (96%) 2000 nm (4%)
PEG 8000 (2%)	165 ± 120 nm (0.529)	280 nm (91%) 5 nm (6%) 45 nm (3%)	5 nm (99.7%) 320 nm (0.2%) 40 nm (0.1%)	4 nm (100%)
CHAPS (5mM)	195 ± 115 nm (0.340)	200 nm (100%)	200 nm (100%)	145 nm (100%)
Pluronic L35 (3mM)	155 ± 105 nm (0.450)	205 nm (97%) 5000 nm (3%)	205 nm (93%) 5000 nm (7%)	110 nm (100%)
OGP (10mM)	130 ± 75 nm (0.322)	185 (100%)	160 nm (57%) 35 nm (43%)	30 nm (100%)
L-arginine (OEt)·2HCl (500mM)	205 ± 95 nm (0.201)	255 nm (100%)	270 nm (100%)	185 nm (100%)
5% HSA 5% dextrose	30 ± 30 nm (1.000)	175 nm (72%) 3 nm (19%) 15 nm (9%)	2 nm (99.5%) 10 nm (0.5%)	2 nm (100%)
1% HSA 1% dextrose	22.8 ± 22.7 nm (0.987)	120 nm (69%) 2 nm (22%) 15 nm (9%)	2 nm (99.8%) 15 nm (0.2%)	2 nm (100%)
1% HSA 10% t-BuOH	105 ± 90 nm (0.708)	240 nm (84%) 3 nm (11%) 25 nm (5%)	3 nm (99.9%) 20 nm (0.1%)	2 nm (100%)
Additive	Z±PDI width (PDI)	Intensity	Volume	Number
L-arginine·HCl (500mM)	110 ± 60 nm (0.283)	150 nm (100%)	125 nm (100%)	80 nm (100%)
L-arginine (OMe)·2HCl (500mM)	120 ± 60 nm (0.256)	155 nm (100%)	140 nm (100%)	100 nm (100%)
L-arginine (500mM)	20 ± 15 nm (0.472)	15 nm (57%) 150 nm (43%)	8 nm (99.9%) 105 nm (0.1%)	6 nm (100%)
PEG 8000 (2%)	50 ± 40 nm (0.660)	160 nm (76%) 15 nm (24%)	9 nm (100%)	7 nm (100%)
CHAPS (5mM)	25 ± 20 nm (0.704)	165 nm (60%) 10 nm (38%) 4000 nm (2%)	8 nm (100%)	7 nm (100%)
Pluronic L35 (3mM)	50 ± 35 nm (0.606)	135 nm (79%) 15 nm (21%)	9 nm (100%)	6 nm (100%)
OGP (10mM)	Insoluble	Insoluble	Insoluble	Insoluble
L-arginine (OEt)·2HCl (500mM)	135 ± 65 nm (0.240)	170 nm (100%)	165 nm (100%)	115 nm (100%)
1% HSA 10% t-BuOH	17.67±12.64nm (0.512)	13.09 (61%) 150 (39%)	8.284 (100%)	6.461 (100%)

Table A-6. Effect of various additives on aggregate formation. Most additives have no effect until reconstituted in buffer and only CHAPS, PEG 8000, Pluronic L35 and L-Arg appear to be effective. OGP = octylglucopyranoside, CHAPS = 3-[(3-Cholamidopropyl)dimethylammonio]-1-propanesulfonate.

days then reconstituted in 0.1 M phosphate buffer. The samples were filtered through a 0.22 µm PVDF filter and again analyzed via DLS (**Table A-6**).

7. Effect of Albumin Batch on Aggregate Formation

Stock solutions of 50 mg/mL of two different albumin batches in 0.1 M phosphate buffer were prepared; lyophilized powder, fatty acid free, Globulin free, ~99% (agarose gel electrophoresis) (Sigma A3782) and lyophilized powder, essentially fatty acid free ~96% (Sigma A1887). Aliquots of 500 µL were ultracentrifuged through a 100 kDa MWCO regenerated cellulose membrane (microcon ultracel YM-100, 42412, lot R7PN22647) at 14 x 1000g for 40 minutes. The filtrates should have contained monomeric albumin while the retentate should contain any aggregates. The retentates were resuspended in 500 µL 0.1 M phosphate buffer and examined using DLS (**Table A-7**). The samples were then incubated at room temperature for 48 h and DLS was run again on the filtrates (**Table A-7**).

Another batch of 50 mg/mL (Sigma A3782) delipidated HSA in distilled water was treated with 3 or 6 eq of PP in t-BuOH (26.4 mg/8.48x10^5 dpm/mL) at a ratio of 1:10 or 1:5 (v/v) t-BuOH:water respectively. Both suspensions were turbid and centrifuged at 16.1 x 1000g for 10 min and the supernatant filtered through a 0.22 µm PVDF filter for DLS analysis then dissolved in 5 mL Ultima Gold scintillation cocktail for LSC analysis (**Table A-7**).

8. Solvent effect on Aggregate Formation

Phosphate buffer appears to help reduce particle size, but also leads to turbidity and poor retention of the conjugate via LSC. Thus it is interesting to determine whether PBS or D5W would be better suited for reconstitution. Solutions of 10 mg/mL HSA (Sigma A1887) and 5 mM CHAPS in D5W or water were prepared and 2 eq [^{3}H]-PP (24.7 mg/1.08x10^6 dpm/mL) was added in t-BuOH at a 1:10 v/v ratio. All samples were shell frozen at -78℃

24 h

	5% A3782	5% A3782 (10% t-BuOH)	5% A3782 (10% t-BuOH 3EQ)	5% A3782 (20% t-BuOH 6EQ)
Z±σ (PDI)	5±3 nm (0.302)	18 ± 17nm (0.897)	145 ± 50nm (0.125)	335±105nm (0.096)
Intensity	3 nm (71%) 900 nm (19%) 26 nm (10%)	290 nm (60%) 4 nm (35%) 40 nm (5%)	163.6 (100%)	365.4 (100%)
Volume	2 nm (100%)	4 nm (100%)	155 nm (100%)	400 nm (100%)
Number	2 nm (100%)	3.034 (100%)	115 nm (100%)	320 nm (100%)

48 h

	A3782 Filtrate (48h)	A1887 Filtrate (48h)
Z±σ (PDI)	125 ± 125 nm (1.000)	80 ± 55 nm (0.477)
Intensity	950 nm (63%) 6 nm (33%) 5000 (4%)	5 nm (60%) 790 nm (36%) 5000 (4%)
Volume	5 nm (99.9%)	5 nm (100%)
Number	5 nm (100%)	4 nm (100%)

LSC

Sample	Mass (g)	Volume (µL)	P (g/mL)	dpm	dpm/mL	mg/mL
Stock 6µL (1)	0.0036	4.61	0.781	4064	8.82×10^5	26.4
Stock 6µL (2)	0.0045	5.76	0.781	4684	8.13×10^5	26.4
3EQ 200µL (1)	0.1956	195.6	1	6809	34811	0.80
3EQ 200µL (2)	0.1996	199.6	1	7053	35336	0.81
6EQ 200µL (1)	0.1928	192.8	1	2602	13496	0.31
6EQ 200µL (2)	0.1974	197.4	1	2729	13825	0.32

Table A-7. Effect of albumin purification state on formation of PP-HSA aggregates. A3782 tends to aggregate equally as poorly as A1887 and has poor loadability. From LSC: 1 eq = 0.88 mg/mL. 3 eq: 0.91 eq/HSA loaded (33%) 6 eq:0.35 eq/HSA (16% loaded). This suggests the interaction is not due to albumin after purification by a specific method.

and lyophilized overnight. The resultant cakes were resuspended in water, D5W, phosphate bufferor PBS and filtered through a 0.22 µm PVDF filter for DLS analysis (**Table A-8**). The filtrates were also weighed out, dissolved in 5 mL Ultima Gold scintillation cocktail and analyzed by LSC (**Table A-8**).

9. Effect of Diluents and Reconstitution Solvent on PP Loading and Aggregate Formation

The best formulation involves injecting PP in t-BuOH into HSA dissolved in water followed by lyophilization and reconstitution in D5W. Instead of CHAPS, biologically compatible surfactants were examined including T20, T80 and TPGS. The concentrations used were 3 molar eq, 3 molar eq and the CMC of 0.02 mM respectively. Samples of 500 µL 10 mg/mL delipidated HSA (Biocell, Rancho Dominguez, CA 3101-00, Albumin, Human, Cohn Fraction V) in water were prepared and the surfactant was added. To the mixtures was added 2 eq [^{3}H]-PP (24.7 mg/1.08x10^{6} dpm/mL) in t-BuOH in a 1:10 v/v ratio. All samples were lyophilized overnight. The samples were reconstituted with 500 µL of either D5W or PBS. The samples were filtered through a 0.22 µm PVDF filter and analyzed via DLS then dissolved in 5 mL Ultima Gold scintillation cocktail and analyzed by LSC (**Table A-9**).

10. Effect of Fatty Acids on HSA Aggregate Formation

Stock solutions of 10 mg/mL HSA (Biocell, Rancho Dominguez, CA 3101-00, Sigma A3782) were prepared in water. To the HSA solutions was added 2 eq of stearic acid or PDG acid both ~1 mg/mL in t-BuOH at a ratio of 1:10 (v/v) t-BuOH:water. The samples were compared to 10 mg/mL standards of both albumin stocks in water and in 10% t-BuOH in water. No turbidity was observed in any sample, nor did any sample appear colloidal which was confirmed by DLS (**Table A-10**). All samples were shell frozen at -78℃ and

	D5W/water	Water/D5W	Water/0.1M PB	Water/PBS
Z±σ (PDI)	115 ± 60 nm (0.264)	20 ± 15 nm (0.554)	150 ± 70 nm (0.200)	150 ± 150 nm (1.000)
Intensity	150 nm (100%)	115 nm (52%) 10 nm (48%)	190 nm (100%)	1700 nm (73%) 9 nm (14%) 70 nm (13%)
Volume	125 nm (100%)	7 nm (100%)	180 nm (100%)	1900 nm (1%) 6.5 nm (99%)
Number	80 nm (100%)	5.5 nm (100%)	100 nm (100%)	5.5 nm (100%)
# EQ / HSA	0.68	1.1	0.08	0.35

Table A-8. Effect of diluent and reconstitution solvent on aggregate formation. Ionic systems are unfavorable for HSA loading and water is more favorable for loading than D5W. The effect on the secondary structures of albumin after dissolution in water was not examined.

	T20 PBS	T20 D5W	T80 PBS	T80 D5W	TPGS PBS	TPGS D5W
Z±σ (PDI)	85±75 nm (0.753)	110±81 nm (0.520)	125±93 nm (0.552)	130±78 nm (0.349)	115±60 nm (0.261)	100±50 nm (0.251)
Intensity	225 nm (87%) 8nm (13%)	180 nm (93%) 9 nm (7%)	240 nm (92%) 9 nm (8%)	200 nm (94%) 9 nm (6%)	155 nm (100%)	125 nm (100%)
Volume	230 nm (0.2%) 7 nm (99.8%)	170 nm (1%) 8 nm (99%)	8 nm (99.3%) 90 nm (0.3%) 315 nm (0.4%)	8 nm (99%) 105 nm (0.5%) 275 nm (0.5%)	120 nm (100%)	100 nm (100%)
Number	6 nm (100%)	7nm (100%)	7 nm (100%)	7 nm (100%)	65 nm (100%)	65 nm (100%)
EQ / HSA	0.31	0.52	0.88	1.03	1.05	1.41

Table A-9. Effect of T20, T80 and TPGS surfactants on PP-HSA aggregate formation. Both Tweens appear to minimize aggregate formation but T80 offers a higher loading capability. Only 50% of the added 2 eq bound HSA.

	Z (PDI)	Intensity	Volume	Number
A3782 (Aq)	130±125 nm (0.897)	1000 nm (42%) 115 nm (31%) 3 nm (14.6%)	2 nm (99.9%) 15 nm (0.1%)	2 nm (100%)
A3782 10% t-BuOH	125±125 nm (1.000)	950 nm (63%) 6 nm (33%) 5000 nm (4%)	5 nm (99.9%) 1100 nm (0.1%)	5 nm (100%)
A3782 10% t-BuOH 2EQSA	70±70nm (1.000)	320 nm (84%) 4 nm (15%) 5000 nm (1%)	3 nm (100%)	3 nm (100%)
A3782 10% t-BuOH 2EQPDG	100±100nm (1.000)	265 nm (81%) 4 nm (15%) 5000 nm (4%)	4 nm (100%)	3 nm (100%)
Biocell (Aq)	15±10nm (0.445)	9 nm (60%) 70 nm (30%) 3500 nm (10%)	7 nm (99.9%) 50 nm (0.1%)	5 nm (100%)
Biocell 10% t-BuOH	14±8nm (0.364)	12 nm (74%) 115 nm (26%)	8 nm (99.9%) 85 nm (0.1%)	7 nm (100%)
Biocell 10% t-BuOH 2EQSA	55±50nm (0.792)	550 nm (50%) 10 nm (30%) 50 nm (13%)	8 nm (99%) 40 nm (1%)	7 nm (100%)
Biocell 10% t-BuOH 2EQPDG	110±80nm (0.499)	440 nm (49%) 10 nm (37%) 40 nm (11%)	500 nm (0.1%) 9 nm (99.3%) 35 nm (0.5%)	8 nm (100%)
	A3782 PDG	**A3782 SA**	**Biocell PDG**	**Biocell SA**
Z (PDI)	12±7nm (0.389)	11±7nm (0.368)	17±13nm (0.579)	27±21nm (0.628)
Intensity	9 nm (70%) 115 nm (30%)	9 nm (74%) 140 nm (26%)	120 nm (51%) 9 nm (49%)	105 nm (66%) 9 nm (33%) 4500 nm (1%)
Volume	7 nm (100%)	7 nm (100%)	7 nm (99.9%) 75 nm (0.1%)	8 nm (99.7%) 75 nm (0.3%)
Number	6 nm (100%)	6 nm (100%)	6 nm (100%)	7 nm (100%)

Table A-10. Formation of HSA aggregates using stearic or PDG acid**.** Both stearic and PDG-acid appear to completely solubilize in the presence of albumin but do not form aggregates at 2 eq/HSA. Addition of the lipids without HSA causes turbidity. This suggests the PP-HSA aggregation is a PTX specific phenomenon.

lyophilized overnight. The cakes were reconstituted in 0.1 M phosphate buffer and analyzed by DLS again (**Table A-10**).

11. Formulation of PP as a Tween 80/Miglyol Emulsion

A 5% (o/w) emulsion was desired so the amount of surfactant to stabilize the emulsion was estimated accordingly.

T80 FW = 1310 g/mol Miglyol 812 ρ = 0.95 g/mL

Assume: 200 nm particles (r = 100 nm), 5% oil/water emulsion, T80 molecular surface area = 50 $Å^2$/molecule T80

Total volume:

5 g Miglyol / 100 g emulsion

5 g Miglyol * 0.95 g/mL = 4.75 mL Miglyol (*Total Volume of Miglyol*)

Drop volume:

100 nm = 0.1 μm = 0.0001 mm = 0.00001 cm

$V = 4/3\pi r^3 = 4/3 * 3.14 * (0.00001cm)^3 = 4.19 \times 10^{-15}$ mL / drop Miglyol

Drop surface area:

100 nm = 1000 Å

$SA = 4\pi r^2 = 4 * 3.14 * (1000 Å)^2 = 1.26 \times 10^7 Å^2$ / drop Miglyol

T80/drop Miglyol:

$(1.26 \times 10^7 Å^2$ / drop Miglyol) / (50 $Å^2$/molecule T80) = 2.52×10^5 molecules T80 / drop Miglyol

Drops Miglyol:

Total volume / drop volume = 4.75 mL Miglyol / 4.19 x 10^{-15} mL Miglyol / drop = 1.13 x 10^{15} drops Miglyol

Total T80:

2.52 x 10^{5} molecules T80 / drop Miglyol * 1.13 x 10^{15} drops Miglyol = 2.85 x 10^{20} molecules T80

2.85 x 10^{20} molecules T80 / 6.022 x 10^{23} molecules T80 / mol T80 = 4.73 x 10^{-4} mol T80

473 µmol T80 * 1.31 mg T80 / µmol T80 = 620 mg T80

620 mg T80 / 5 g Miglyol / 94.4 g H_2O (0.6 : 5 : 94.4)

~ 1 g T80 / 5 g Miglyol 812 should be able produce ~200 nm particles.

Formulation:

Aqueous: 5% dextrose in water, 1% T80

Oil: 5% Miglyol

Added 5% (w/v) Miglyol 812 to a 1% (v/v) EtOH and 1% (v/v) T80 solution in D5W or PBS containing 0.08 mg/8.22x10^{4} dpm/mL [^{3}H]-PP stock. The sample was vortexed for 5 minutes then emulsified using a tissue Powergen700 tissue homogenizer (Fisher Scientific) on speed 7 for 5 minutes.

12. Albumin-Agarose Extraction of PP from a Tween 80/Miglyol Emulsion

BSA-Agarose from Sigma Aldrich (10.1 mg/mL, A3790) was aliquoted as 0.5 mL samples which were centrifuged at 3,000 x g for 3 min and the supernatant discarded. The samples were washed twice with D5W, PBS, 1% (v/v) T80 in D5W, 1% (v/v) T80 in PBS, 1%

(v/v) EtOH in D5W or 1% (v/v) EtOH in PBS. The suspensions were centrifuged at 3,000 x g for 3 min and the supernatants discarded. The BSA-Agarose was then resuspended in 0.4 mL of the test solution. To the BSA-Agarose samples was added 40 µL of t-BuOH stock (**Table A-11**) or 0.4 mL of the Miglyol emulsion which already contained the radiolabeled PP. The samples were rocked at room temperature for 1 h. The samples were then centrifuged at 3,000 x g for 3 min and an aliquot of the supernatant filtered through a 0.22 µm polycarbonate membrane, (Poretics, Cat: 11013, Material: 1220693, Batch: 215896) dissolved in 5 mL Ultima Gold scintillation cocktail and analyzed by LSC to determine the percent of the dose that precipitated (**Table A-11**). The remaining supernatant, along with 2 washes of the resin with D5W or PBS, were dissolved in 5 mL Ultima Gold scintillation cocktail and analyzed by LSC to determine the filtrate concentration (**Table A-11**).

13. Formulation of PP as Pluronic F-68/Miglyol Emulsion

The Miglyol 812 samples were prepared by adding 40 µL of PP stock (0.334 mg/ 6.18x106 dpm/mL) to 50 µL of Miglyol 812. The EtOH was removed via a stream of nitrogen. To this was added 200 µL of 2% (w/v) Pluronic F-68 (poloxamer 188) in D5W. The two layers were vortexed heavily for 20 minutes then passed through a 0.22 µm polycarbonate membrane. (Poretics, Cat: 11013, Material: 1220693, Batch: 215896) This was done using an extruder under pressure with nitrogen for 5 extrusions. The amount of material yielded was little ~60 µL. Because of this, 25 µL of the emulsion was used in duplicate.

14. Albumin-Agarose Extraction of PP from a Pluronic F-68/Miglyol Emulsion

BSA-agarose (10.1 mg/mL, Sigma A3790) was aliquoted as 1 mL fractions into 4 different 1.5 mL eppendorf tubes. The tubes were centrifuged at 3,000 x g for 3 min to pellet the agarose and the supernatant decanted. Two samples were washed twice with D5W alone. Washing involved mixing the thoroughly suspending the resin in solvent then

t-BuOH stock		0.8 mg/mL	
mass	volume	dpm	dpm/mL
0.0191	0.024455826	20167	824630
0.0199	0.025480154	21066	826761
0.0199	0.025480154	21027	825231
0.0384	0.049167734	40480	823304
0.0396	0.050704225	41227	813088
0.038	0.04865557	39882	819680
AVERAGE			822116

D5W	**super dpm**	**filtrate dpm**	**% bound**	**% supernatant**	**% precipitated**
Miglyol	14235	5701	31	69	15
w/ T80	13119	6954	37	63	7
w/o T80	3994	187	81	19	11
PBS	**super dpm**	**filtrate dpm**	**% bound**	**% supernatant**	**% precipitated**
Miglyol	9375	4071	55	45	9
w/ T80	5717	2524	72	28	4
w/o T80	3453	795	83	17	6

Table A-11. Transfer of PP from t-BuOH, a Miglyol 812 emulsion or T80 micelles to BSA immobilized on agarose. All dpms unaccounted for were assumed to be bound. All values reported are % added dose. PBS appears more conducive to PP transfer than D5W.

centrifuging at 3,000 x g for 3 min and decanting the supernatant. To these solutions was then added 300 µL D5W and the suspension was warmed to 37°C in the incubator. The remaining two samples were were washed thrice via the same procedure but with 5 mM CHAPS (~3 mg/mL) in D5W. To these agarose pellets were added 400 µL D5W/5 mM CHAPS and the suspensions warmed to 37°C in the incubator. To the 1 mL samples of BSA-agarose was added 100 µL (0.0334 mg/6.18x10^5 dpm/mL) of the [^{3}H]-PP stock or 25 µL Miglyol emulsion. The samples were heated to 37°C and shook for 2 h.

Standards were run for each formulation (assumed ρ = 1.02 g/mL for Miglyol formulation, ρ = 0.789 for EtOH). For the various formulations, aliquots of the stock solution were weighed out, dissolved in 5 mL Ultima Gold scintillation cocktail and analyzed for LSC (**Table A-12**). The samples were analyzed by centrifuging the agarose at 3,000 x g for 3 mins then removing the supernatant and adding it to a scintillation vial. The agarose was then washed twice with 400 µL D5W, mixed thoroughly and centrifuged again. All washes were pooled with the initial supernatant. The pellets were then diluted with 100 µL 1N HCl and 400 µL MeCN, vortexed heavily and centrifuged at 3,000 x g for 3 min. The supernatant (bound fraction) was removed and added to a scintillation vial. The resin was washed with 2 x 400 µL MeCN, vortexed, centrifuged and the supernatant removed and pooled in the bound fraction. Finally the whole resin was washed into a scintillation vial with acetone (resin fraction). To all samples was added 10 mL Ultima Gold XR scintillation cocktail and the samples analyzed via LSC (**Table A-12**).

15. TAXOTERE-like Formulation of PP

Prepared a solution of 50 mg/mL delipidated HSA (Sigma A1887) in D5W and a stock of [^{3}H]-PP (18.73 mg/1.58x10^6 dpm/mL) in EtOH. An aliquot of 40 µL of the stock was evaporated and resuspended in 8 µL of 1:1 (v/v) T80:EtOH to which was added 400 µL of

Miglyol/Pluronic emulsion						
mass (g)	volume (mL)	dpm	dpm/mL			25uL samples
0.0052	0.0051	4056	795600	outlier not averaged		
0.0044	0.0043	13024	3019200			
0.0085	0.0083	27899	3347880			dpm added
AVERAGE			3183540			79589
PP stock in EtOH						10uL samples
mass (g)	volume (mL)	dpm	dpm/mL			
0.009	0.011406844	22030	1931297	outlier not averaged		
0.0038	0.004816223	87042	18072668			
0.0041	0.005196451	92989	17894712			dpm added
AVERAGE			17983690			179837
Miglyol 1						
super dpm	bound dpm	resin dpm	% super	%bound	%resin	%recovered
8472	10445	3159	38	47	14	28
Miglyol 2						
super dpm	bound dpm	resin dpm	% super	%bound	%resin	%recovered
9491	6310	1614	55	36	9	22
CHAPS 1						
super dpm	bound dpm	resin dpm	% super	%bound	%resin	%recovered
29090	111281	18147	18	70	11	88
CHAPS 2						
super dpm	bound dpm	resin dpm	% super	%bound	%resin	%recovered
30156	103271	22798	19	66	15	87

Table A-12. Transfer of PP from a Miglyol emulsion and CHAPS solution to BSA immobilized on agarose. Miglyol 812 again appears to poorly transfer PP to BSA. The very poor recovery of PP from the emulsion could be due to overestimating the specific activity of the emulsion due to only a modicum being available for stock characterization.

the HSA stock making a final concentration of 1% (v/v) EtOH, 1% (v/v) T80 containing 2 eq PP/HSA. No turbidity was observed in the solution. The solution was filtered through a 0.22 µm PVDF filter and the filtrate analyzed by DLS (**Table A-13**). Aliquots of the filtrate were weighed out, dissolved in 5 mL Ultima Gold scintillation cocktail and analyzed by LSC as well (**Table A-13**).

16. Analysis of TAXOTERE-like Formulations for Pharmacokinetics

To prepare the stock solutions for pharmacokinetic analysis, 6 mg [^{3}H]-PP was weighed out and dissolved in a weighed aliquot of 58.5 µL 1:1 (v/v) EtOH:T80 yielding a concentration of 97.5 mg/mL. Half of this stock (30 µL) was diluted to 3 mL with D5W and the remaining 30 µL was diluted with 3 mL 50 mg/mL delipidated HSA (Sigma A1887) in D5W. The individual stocks were mixed gently at room temperature, filtered through a 0.22 µm PVDF filter and the formulation without HSA was diluted 40x from 50 µL (0.0534 g) to 2 mL (actual dilution 38.2 x) in EtOH using a volumetric flask. The diluted formulation was analyzed by UV to quantify PP (ε_{228}=30,593 $M^{-1}cm^{-1}$, EtOH). Aliquots of 250, 100, 50 and 20 µL of the diluted formulation were then weighed out in triplicate, dissolved in 5 mL Ultima Gold XR scintillation cocktail and analyzed by LSC (**Table A-14**). Additionally, both undiluted stocks were weighed out in aliquots of 20, 50 and 100 µL triplicates, dissolved in 5 mL Ultima Gold XR scintillation cocktail and analyzed by LSC (**Table A-14**).

17. Pharmacokinetics/Biodistribution of TAXOTERE-like Formulations

Female 6-8 week old BALB/c mice were inoculated with $5x10^{5}$ CT26 murine colon carcinoma cells on the right flank. The tumors were allowed to grow for 14 days and the mice were randomly sorted into 14 sets of triplicates. The average tumor size for both groups (7 triplicates) was 12.7x8.5 mm for the HSA containing formulation and 12.4x8.3 mm for the non HSA formulation (**Table A-15**). The mice were injected with 0.104 mg/$9.40x10^{6}$ dpm/0.1 mL for the HSA containing formulation and 0.105 mg/$9.47x10^{6}$ dpm/0.1 mL for the

	Z±σ (PDI)	Intensity	Volume	Number
TAXOTERE-like	21±20 nm (0.911)	205 nm (56%) 4 nm (26%) 30 nm (18%)	3 nm (99.8%) 25 nm (0.2%)	3 nm (100%)

sample	mass (g)	Volume (µL)	dpm	dpm/mL	mg/mL	eq/HSA
1	0.0262	25.6	3845	150195	1.78	1.93
2	0.0275	26.8	3917	146157	1.73	1.88
3	0.0278	27.1	4046	149299	1.77	1.92

Table A-13. Particle size analysis of a TAXOTERE-like formulation of PP. The TAXOTERE-like formulation allows nearly complete solubilization of PP while precluding aggregates from forming and only requires 10% of the T80/EtOH used by TAXOTERE.

Without HSA diluted			
weight (g)	volume (mL)	dpm	dpm/mL
0.2575	0.252451	5160	20440
0.2582	0.2531373	5155	20364
0.2582	0.2531373	5106	20171
0.1029	0.1008824	12100	119942
0.1025	0.1004902	12152	120927
0.1019	0.099902	12233	122450
0.0506	0.0496078	24466	493188
0.0515	0.0504902	24307	481420
0.0516	0.0505882	24256	479479
0.0217	0.0212745	61667	2898633
0.0215	0.0210784	61860	2934753
0.0214	0.0209804	61893	2950040
AVERAGE			888484

Undiluted stock (g)	Undiluted stock (mL)	dilution ratio at 2 mL
0.0534	0.052353	38.20225

A278	ε278 (1/M*cm)	undiluted [PP] mM	**undiluted [PP] mg/mL**
0.711	30593	0.888	**1.05**

With HSA			
weight (g)	volume (mL)	dpm	dpm/mL
0.0218	0.021268	200045	9405786
0.0219	0.021366	202865	9494823
0.0228	0.022244	208858	9389450
0.0525	0.05122	481657	9403780
0.0531	0.051805	488684	9433166
0.0526	0.051317	482077	9394086
0.1033	0.10078	943303	9359977
0.1052	0.102634	959020	9344064
0.1048	0.102244	956865	9358651
AVERAGE			**9398198**

dpm/ug
9022.367

dpm/mg	**dpm/mL**	**undiluted [PP] mg/mL**
9022367	**9398198**	**1.041655**

With HSA			
weight (g)	volume (mL)	dpm	dpm/mL
0.0218	0.021268	200045	9405786
0.0219	0.021366	202865	9494823
0.0228	0.022244	208858	9389450
0.0525	0.05122	481657	9403780
0.0531	0.051805	488684	9433166
0.0526	0.051317	482077	9394086
0.1033	0.10078	943303	9359977
0.1052	0.102634	959020	9344064
0.1048	0.102244	956865	9358651
AVERAGE			**9398198**

dpm/ug
9022.367

dpm/mg	**dpm/mL**	**undiluted [PP] mg/mL**
9022367	**9398198**	**1.041655**

Table A-14. Characterization of stock solutions of TAXOTERE-like formulations of PP for pharmacokinetic analysis. Since both formulations are derived from the same mother stock, the dpm/mg should be constant in both formulations, even if the concentrations are different so the HSA containing formulation can be completely quantified from just LSC. The concentrations are nearly identical; 1.04 and 1.05 mg/mL.

	With HSA			Without HSA		
	width	length	volume	width	length	volume
	12.34	6.37	970	10.42	8.12	882
	13.39	6.19	1110	14.04	8.25	1626
	16.29	12.17	3229	19.24	8.96	3317
	11.97	8.91	1277	15.47	8.2	1962
	10.82	8.58	1004	10.87	7.8	922
	11.55	9.4	1254	13.42	8.01	1443
	12.53	9.24	1451	12.31	5.93	899
	10.24	7.61	798	13.47	7.8	1415
	11.2	8.22	1031	10.36	9.83	1055
	10.17	9.15	946	12.42	10.67	1646
	13.42	6.53	1176	11.89	6.07	858
	14.65	8.1	1738	13.93	6.69	1298
	19.1	9.33	3404	15.49	12.71	3050
	10.85	8.87	1044	12.64	10.25	1638
	9.85	8.41	816	11.99	8.43	1212
	15.28	5.77	1347	8.43	6.36	452
	10.94	10.67	1277	10.7	6.99	800
	10	8.69	869	13.73	10.09	1902
	14.38	7.72	1596	9.8	9.34	897
	14.7	7.59	1640	8.3	7.51	517
	12.26	10.19	1532	11.5	6.6	873
Average	12.66	8.46	1405	12.40	8.31	1365

Table A-15. Tumor sizes of the two treatment groups for the TAXOTERE-like PK study. The volume is calculated as (lxw^2) where w is the longest diameter.

non-HSA containing formulation. For both experiments, animals were sacrificed at 0.25, 1, 3, 6, 18, 36 and 72 h. Prior to sacrifice the mice were anesthetized with 0.1 mL 100 mg/mL ketamine hydrochloride intraperitoneally. Once the mice were unresponsive to toe pinching, the mice were exsanguinated by cardiac puncture followed by cervical dislocation. The whole blood was aliquoted as ~200 µL into scintillation vials in triplicate and weighed. Target organs were then harvested from the mice, washed thoroughly with PBS, blotted dry and small ~100 mg pieces of the organ were weighed in scintillation vials in duplicate.

Target organs include the liver, tumor, kidneys, spleen, lungs, heart and injection site. The whole blood was processed by adding 1 mL Solvable® tissue homogenizer (Perkin Elmer) and heating to 55℃ for 1 h. The brownish-green solution was then treated with 0.1 mL 0.1 M ethylendiaminetetraacetic acid disodium and 0.3 mL 30% hydrogen peroxide. When the foaming settled, the samples were heated to 55℃ for an additional hour then cooled to ambient and dissolved in 15 mL Ultima Gold XR scintillation cocktail. The samples were equilibrated in the liquid scintillation counter for 1 h prior to counting to adapt to temperature and light. The results of the serum concentrations for both formulations are shown in **Fig. A-5**. The organs were processed by adding 1 mL Solvable® tissue homogenizer (Perkin Elmer) and heating to 55℃ for 2 h. Once dissolved, the yellow solutions were treated with 0.3 mL 30% hydrogen peroxide and once the foaming subsided, heated to 55℃ for an additional hour. The samples were cooled to ambient and dissolved in 15 mL Ultima Gold XR scintillation cocktail. The samples were all mixed thoroughly to ensure complete dissolution then the samples were placed in the scintillation counter for 1 h prior to counting to adapt to temperature and light. The uncorrected biodistribution data is provided for the HSA containing (**Fig. A-6**) and non-HSA containing formulations (**Fig. A-7**). The LSC data (**Table A-16**) was analyzed by noncompartmental analysis using Winnonlin (Pharsight) and the major pharmacokinetic parameters extracted (**Table A-17**).

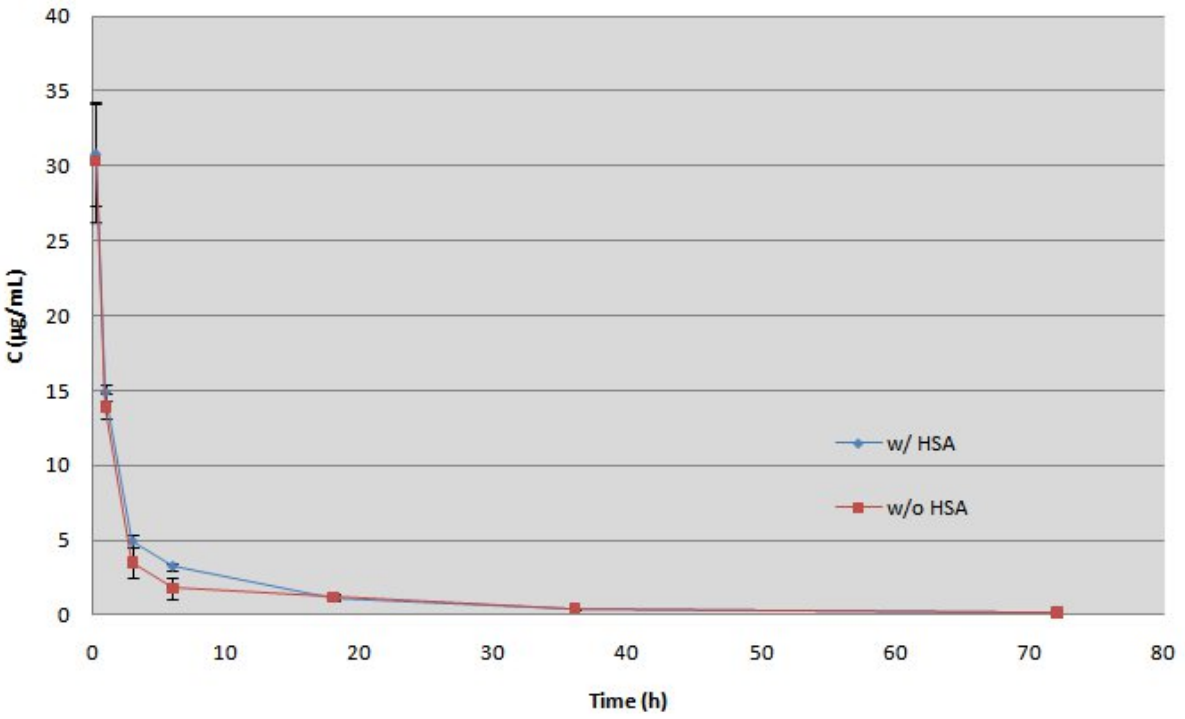

Figure A-5. Serum pharmacokinetics of [^{3}H]-PP in a TAXOTERE-like formulation with or without HSA. Both formulations are nearly superimposable showing the same rapid distribution observed with the PP-HSA particles followed by a nearly 24 h terminal half-life. Concentrations were calculated by LSC in triplicate without correction by a standard curve. Error bars are calculated as the standard deviation from n=3 mice.

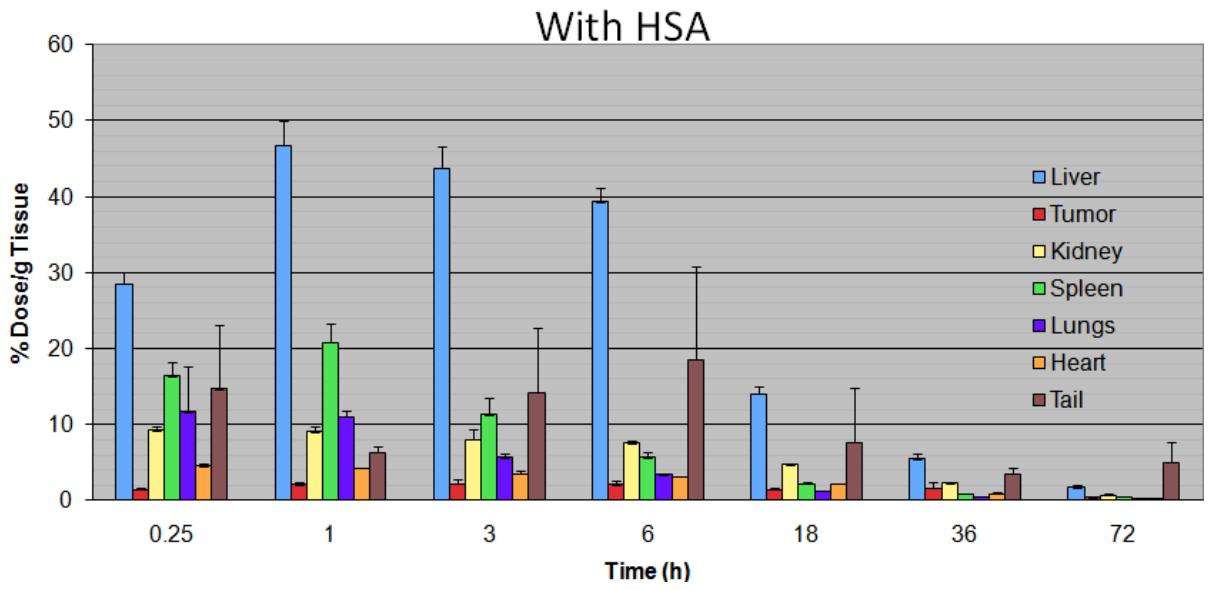

Figure A-6. Time resolved biodistribution of the [^{3}H]-PP in a TAXOTERE-like formulation containing HSA. Like the PP-HSA particles, there is a rapid accumulation in the liver and spleen although clearance from the organs is a slow process. Tumor accumulation is constant but no different from the previous formulation. Concentrations were quantitated in duplicate by LSC without correction by a standard curve. Error bars are calculated as the standard deviation of n=3 mice.

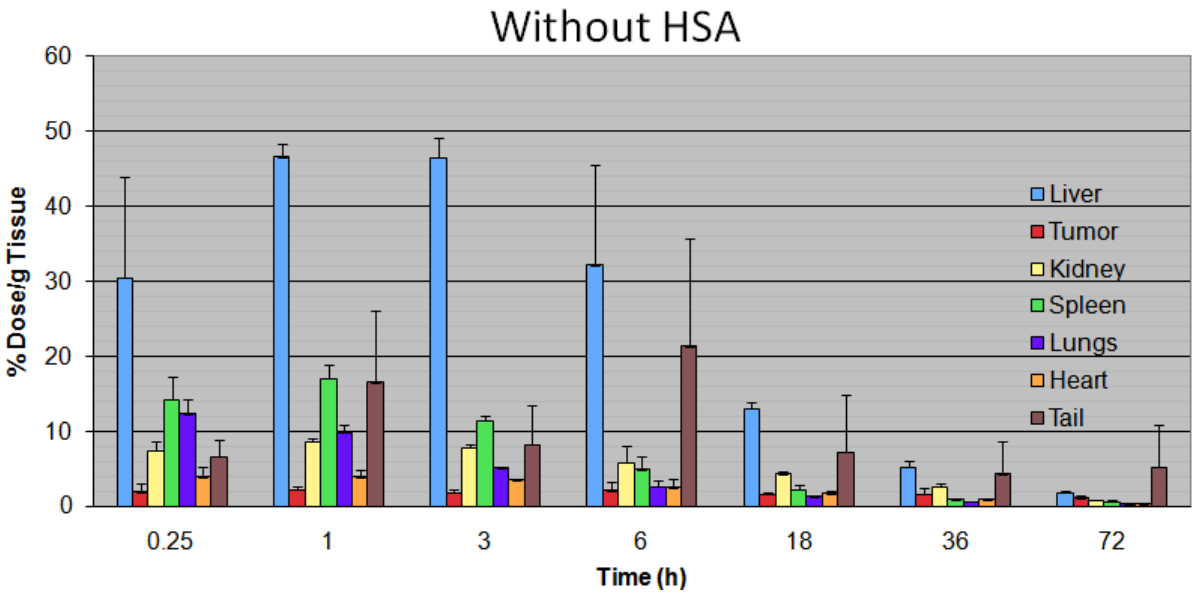

Figure A-7. Time resolved biodistribution of [^{3}H]-PP in a TAXOTERE-like formulation without HSA. Concentrations were quantitated in duplicate by LSC without correction by a standard curve. Error bars are calculated as the standard deviation of n=3 mice. The BD data is also nearly superimposable with the other TAXOTERE-like formulation.

With HSA

C_{blood} (µg/mL)	σ_{blood} (µg/mL)	C_{Liver} (µg/g)	σ_{Liver} (µg/g)	C_{Tumor} (µg/g)	σ_{Tumor} (µg/g)	C_{Kidney} (µg/g)	σ_{Kidney} (µg/g)	C_{Spleen} (µg/g)	σ_{Spleen} (µg/g)	C_{Lungs} (µg/g)	σ_{Lungs} (µg/g)	C_{Heart} (µg/g)	σ_{Heart} (µg/g)	C_{Tail} (µg/g)	σ_{Tail} (µg/g)
30.74	3.37	28.56	1.53	1.49	0.23	9.20	0.64	16.41	1.87	11.73	5.97	4.53	0.31	14.66	8.37
14.86	0.52	46.72	3.27	2.06	0.30	9.03	0.70	20.83	2.43	10.99	0.90	4.22	0.17	6.31	0.80
4.91	0.43	43.77	2.91	2.16	0.56	8.05	1.41	11.32	2.13	5.69	0.60	3.51	0.51	14.23	8.59
3.25	0.22	39.34	1.83	2.14	0.44	7.52	0.31	5.69	0.65	3.42	0.20	3.18	0.03	18.59	12.17
1.16	0.23	14.01	0.97	1.45	0.17	4.69	0.08	2.18	0.26	1.25	0.07	2.15	0.06	7.61	7.31
0.43	0.07	5.47	0.63	1.66	0.79	2.30	0.23	0.86	0.16	0.47	0.05	0.91	0.17	3.51	0.73
0.23	0.04	1.71	0.31	0.39	0.08	0.73	0.16	0.48	0.14	0.21	0.06	0.23	0.04	5.05	2.59

Without HSA

C_{blood} (µg/mL)	σ_{blood} (µg/mL)	C_{Liver} (µg/g)	σ_{Liver} (µg/g)	C_{Tumor} (µg/g)	σ_{Tumor} (µg/g)	C_{Kidney} (µg/g)	σ_{Kidney} (µg/g)	C_{Spleen} (µg/g)	σ_{Spleen} (µg/g)	C_{Lungs} (µg/g)	σ_{Lungs} (µg/g)	C_{Heart} (µg/g)	σ_{Heart} (µg/g)	C_{Tail} (µg/g)	σ_{Tail} (µg/g)
30.33	4.00	30.38	13.56	1.83	1.18	7.36	1.28	14.19	3.00	12.25	2.06	3.85	1.34	6.56	2.26
13.92	0.82	46.57	1.74	2.15	0.56	8.61	0.49	16.94	1.99	9.80	1.01	3.88	0.98	16.47	9.63
3.50	0.99	46.40	2.58	1.81	0.32	7.77	0.44	11.37	0.58	5.08	0.25	3.51	0.06	8.16	5.26
1.79	0.69	32.14	13.25	2.04	1.19	5.76	2.22	4.84	1.88	2.58	0.83	2.51	1.10	21.28	14.35
1.20	0.12	12.96	0.95	1.54	0.38	4.29	0.38	2.17	0.57	1.24	0.03	1.72	0.30	7.21	7.63
0.46	0.07	5.19	0.84	1.62	0.84	2.55	0.39	0.88	0.06	0.56	0.09	0.92	0.11	4.29	4.26
0.17	0.02	1.73	0.21	1.02	0.41	0.82	0.09	0.56	0.18	0.24	0.03	0.26	0.03	5.19	5.74

Table A-16. Raw data from the TAXOTERE-like PK/BD experiment used in the PK and BD analysis. C, concentration; σ, standard deviation from n=3 mice.

Formulation	Dose (μg)	C_0 (μg/mL)	V_d (mL)	$t_{1/2}$ (h)	Cl (mL/min)	AUC_∞ (μg*h/mL)	MRT_∞ (h)
w/ HSA	104	39.2	31.3	25	0.9	119	18
w/o HSA	105	39.3	31.4	21	1.1	100	16

Table A-17. Summary of important pharmacokinetic parameters obtained from TAXOTERE-like PP formulations. A non-compartmental model was fitted to the data with a weighting of 1/Y using Winnonlin (Pharsight). As with the serum pharmacokinetics and biodistribution, these results are very similar to the PP-HSA formulation from Chapter III.

18. Spectral Data

Raw spectral data for all intermediates synthesized in **Chapter III** are provided including mass spectrometry, ^{1}H NMR and ^{13}C NMR.

18.1. Ethyl-(*E*)-octadec-2-enoate (1)

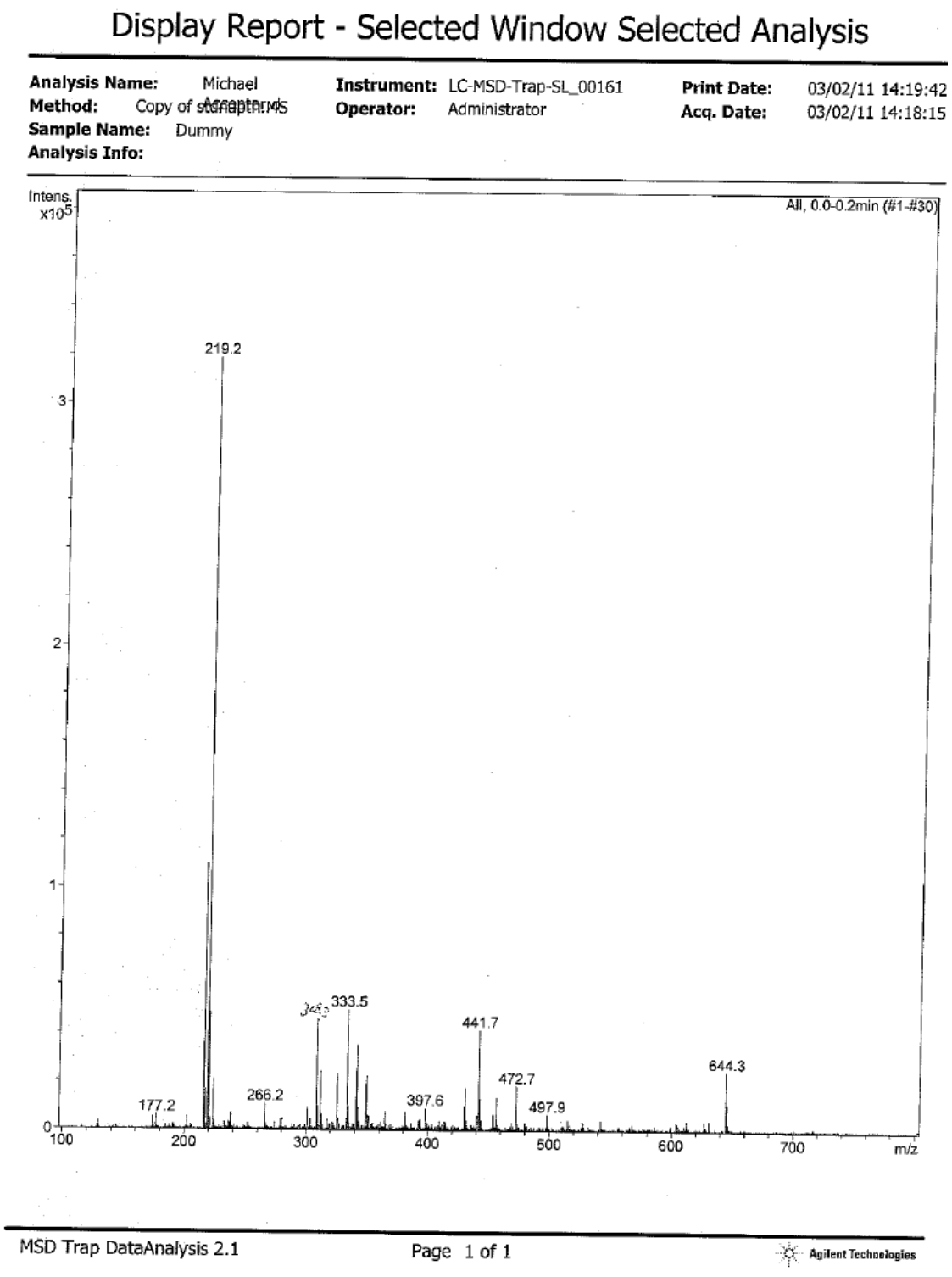

Figure A-8. Mass spectrum of **ethyl-(*E*)-octadec-2-enoate (1)**.

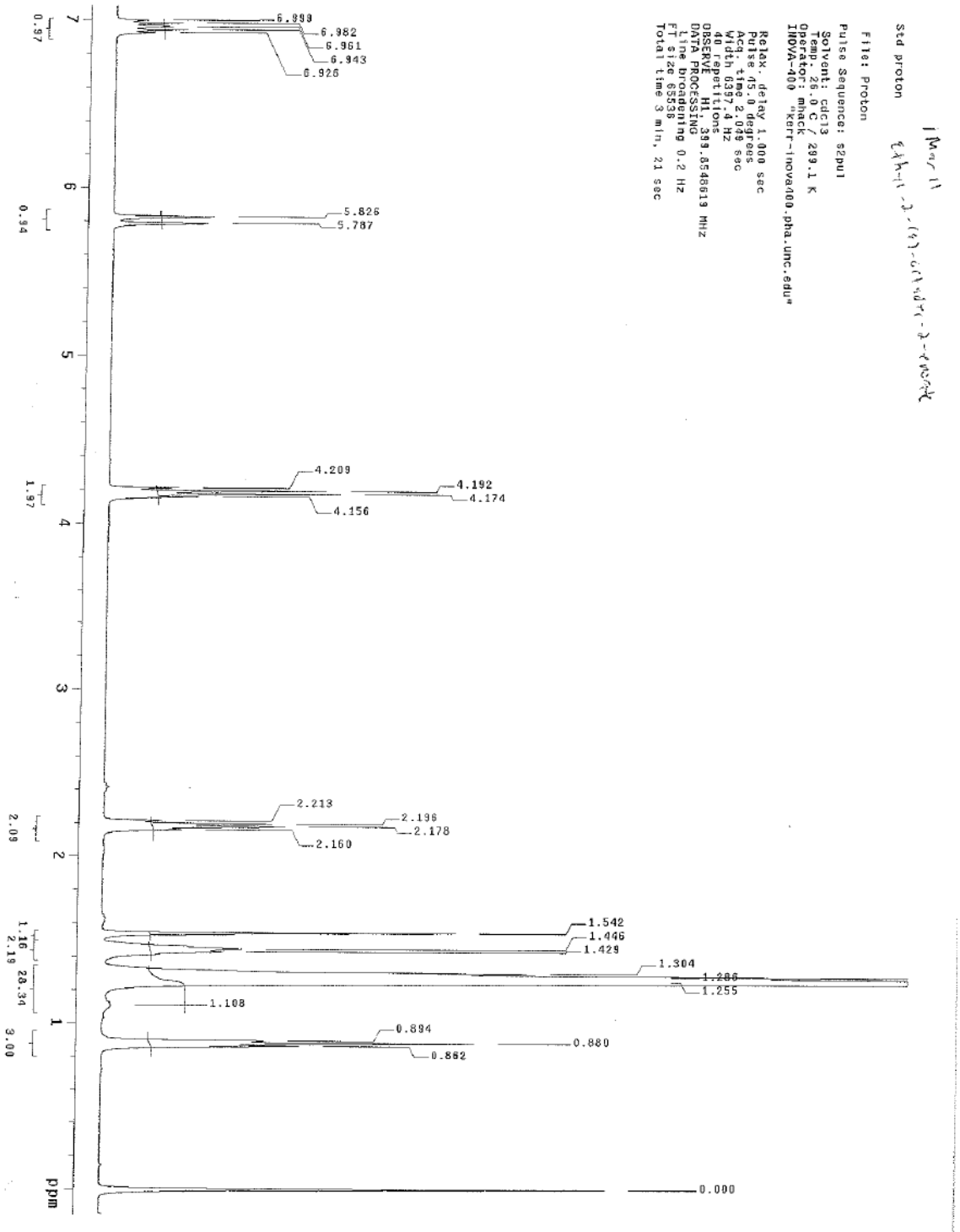

Figure A-9. ^{1}H NMR spectrum of **ethyl-(*E*)-octadec-2-enoate (1)**.

18.2. 3-Pentadecyldiethylglutarate (2)

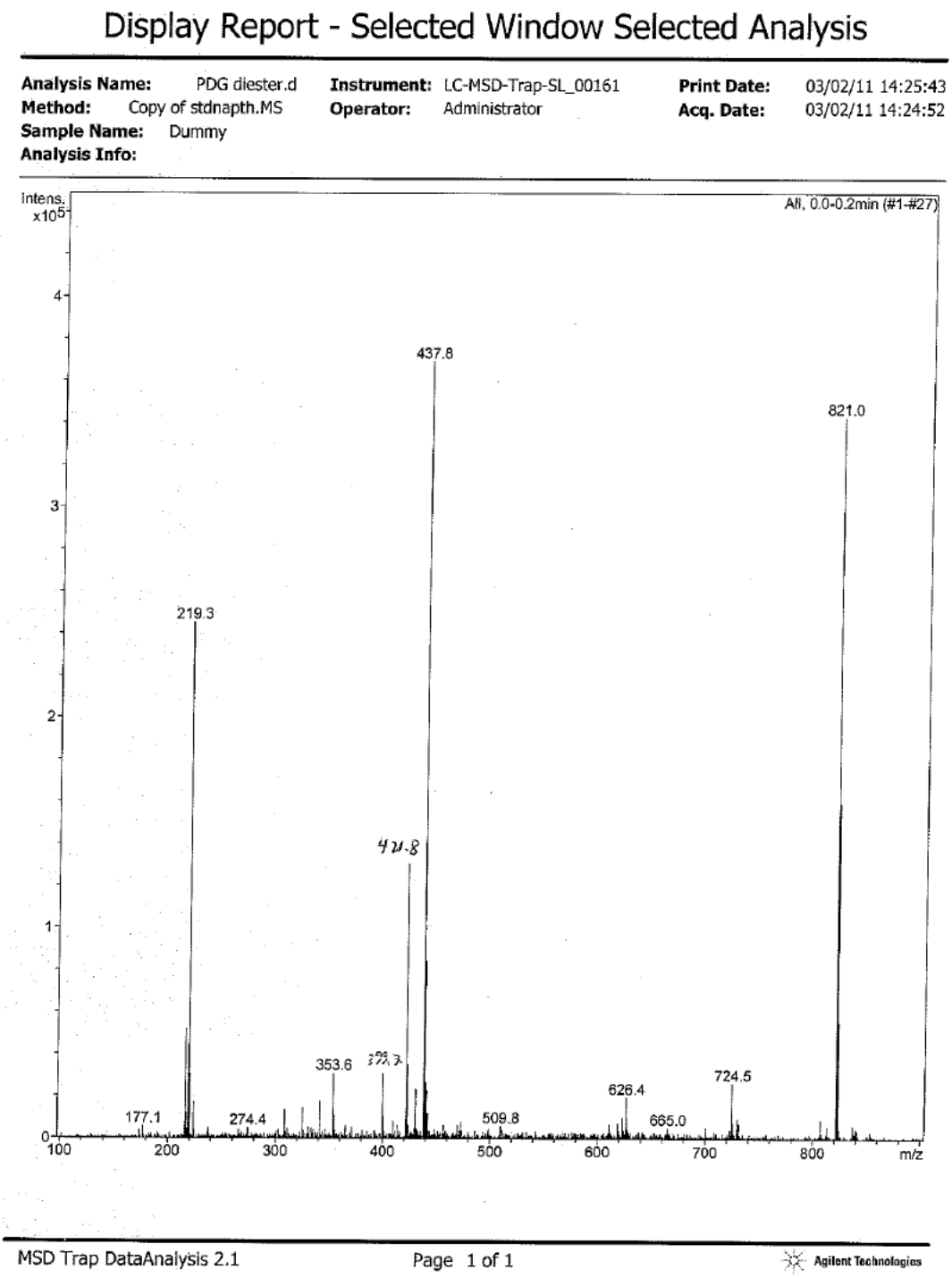

Figure A-10. Mass spectrum of **3-pentadecyldiethylglutarate (2)**.

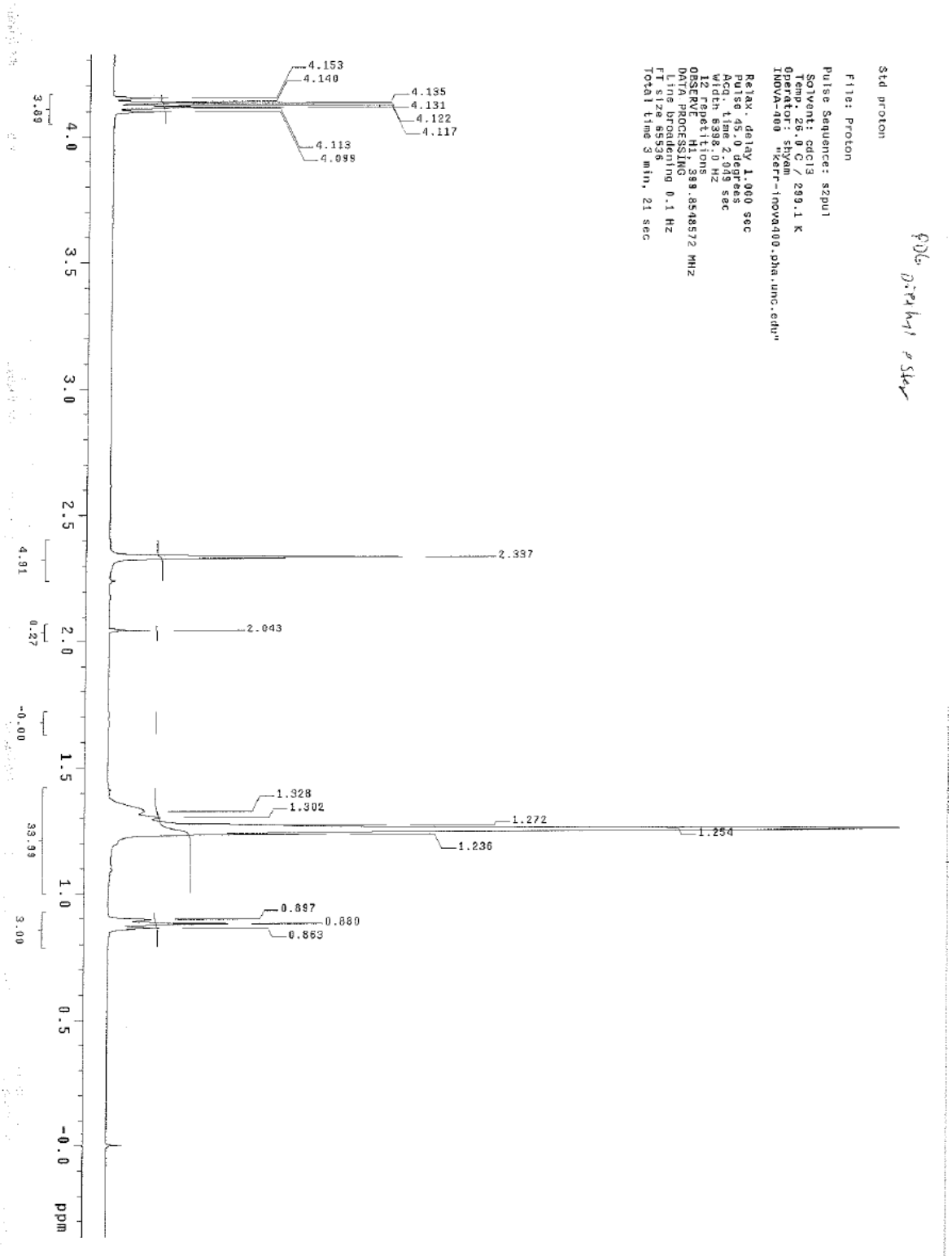

Figure A-11. ^{1}H NMR spectrum of **3-pentadecyldiethylglutarate (2)**.

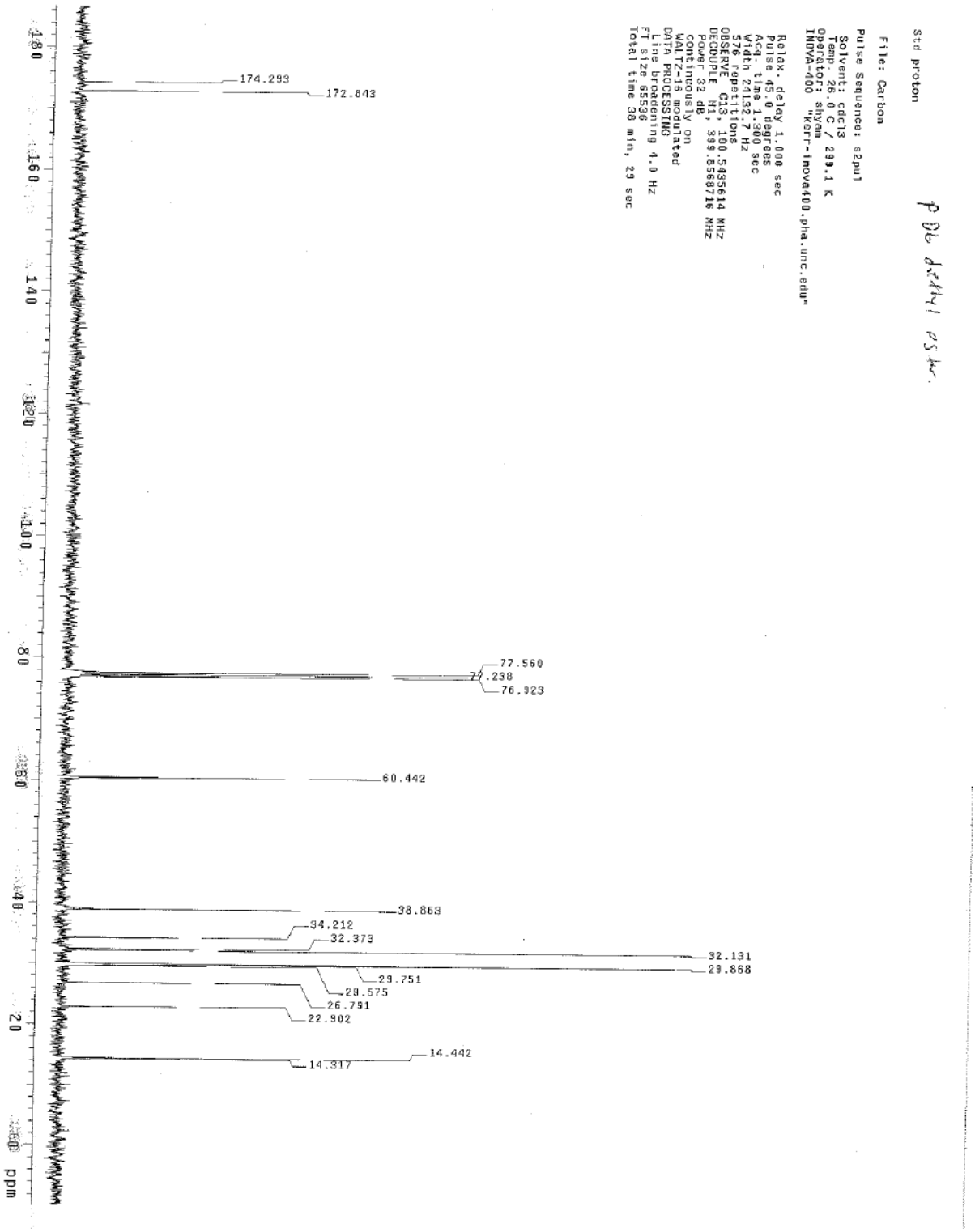

Figure A-12. ^{13}C NMR spectrum of **3-pentadecyldiethylglutarate (2)**.

18.3. 3-Pentadecylglutaric acid (3)

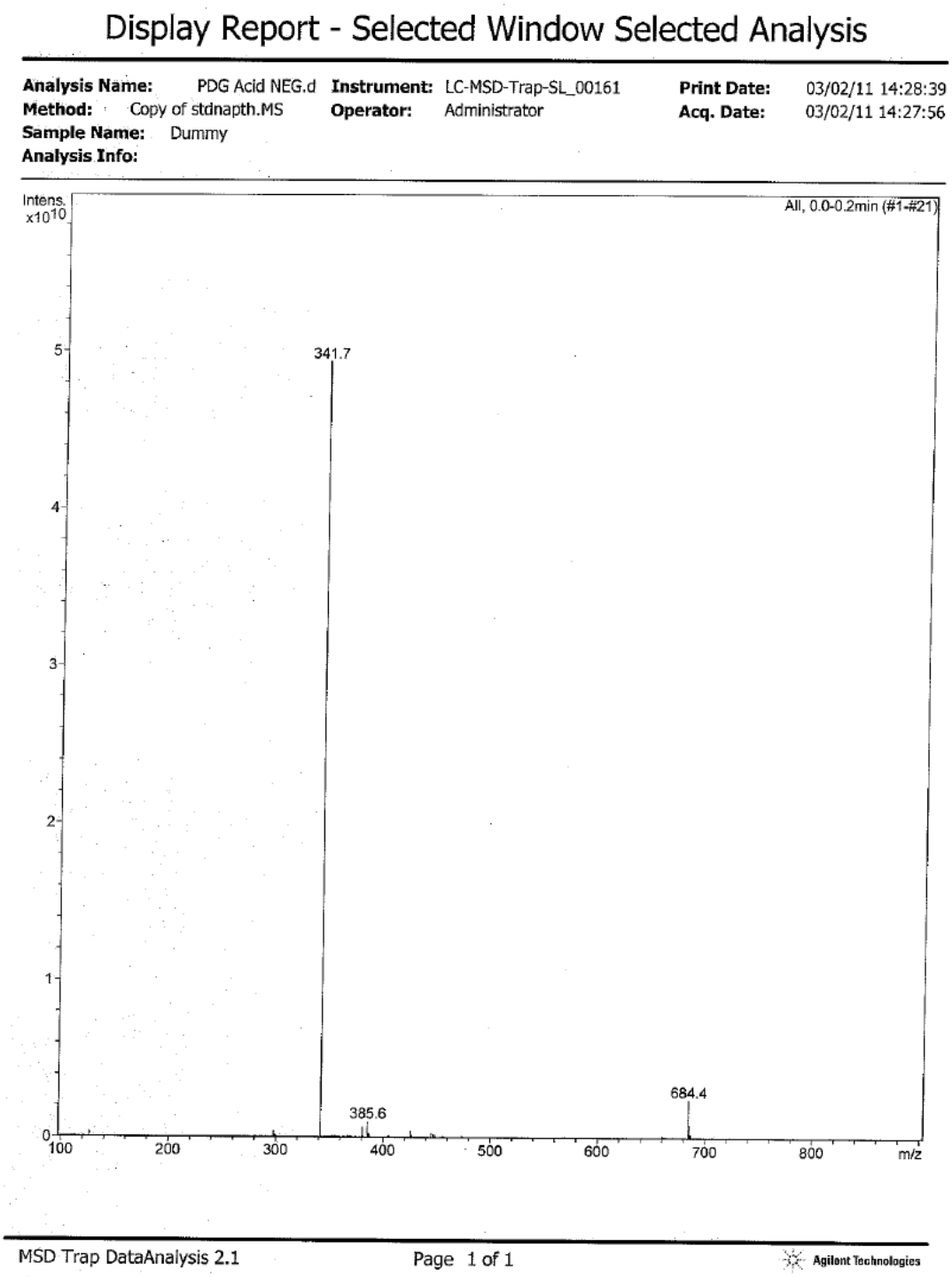

Figure A-13. Mass spectrum of **3-pentadecylglutaric acid (3)**.

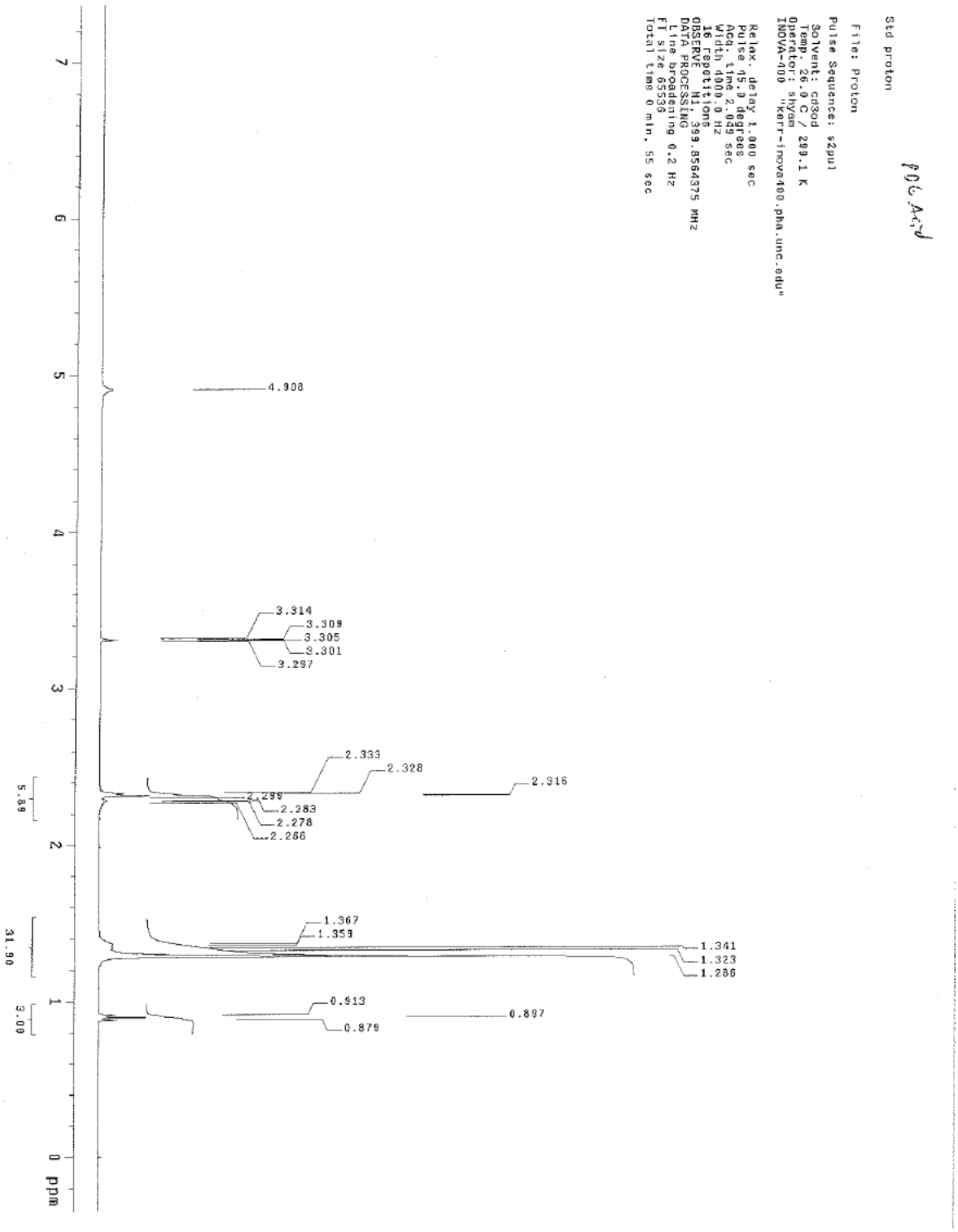

Figure A-14. ^{1}H NMR spectrum of **3-pentadecylglutaric acid (3)**.

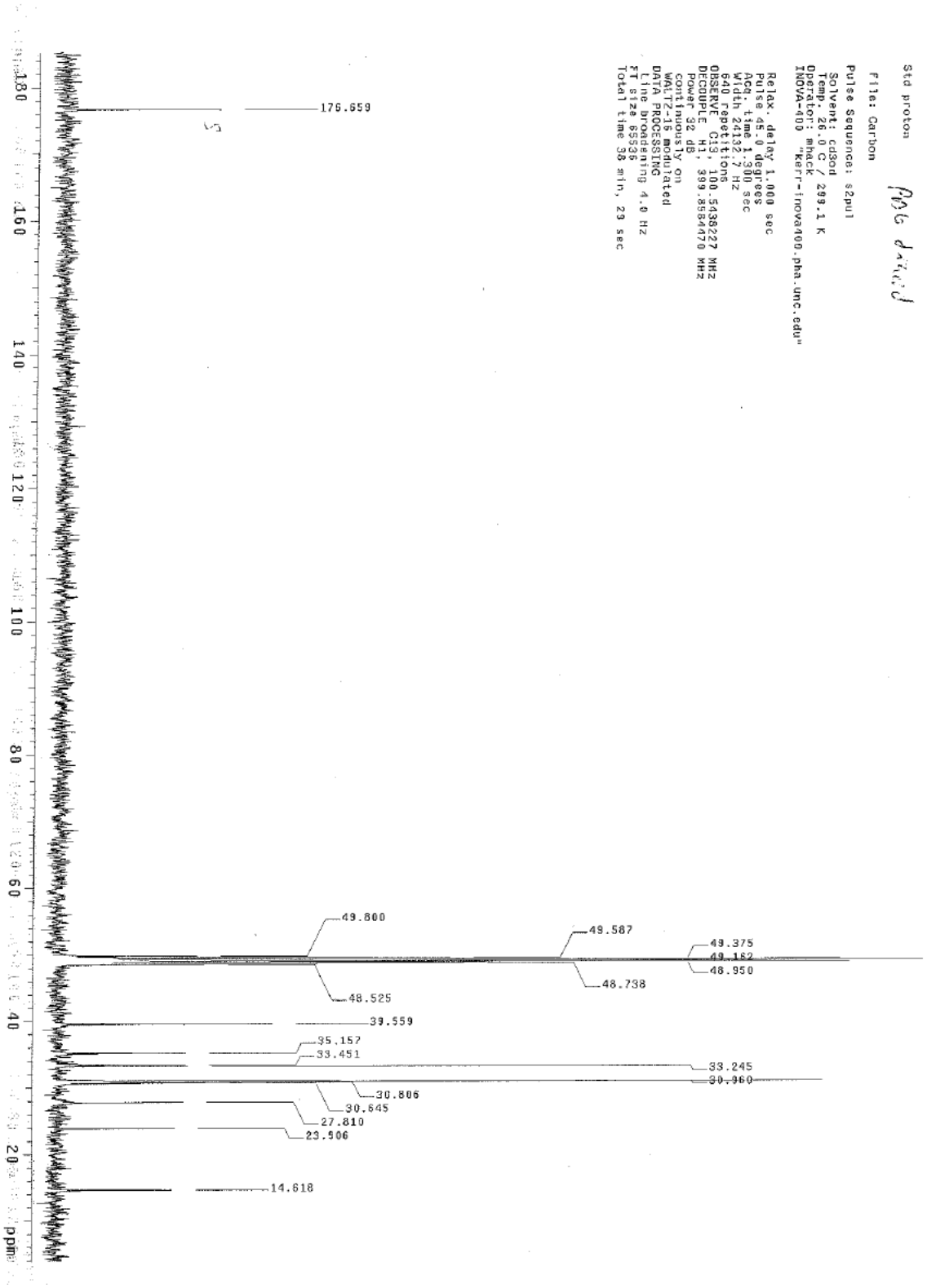

Figure A-15. ^{13}C NMR spectrum of **3-pentadecylglutaric acid (3)**.

18.4. 3-Pentadecylglutaric anhydride (4)

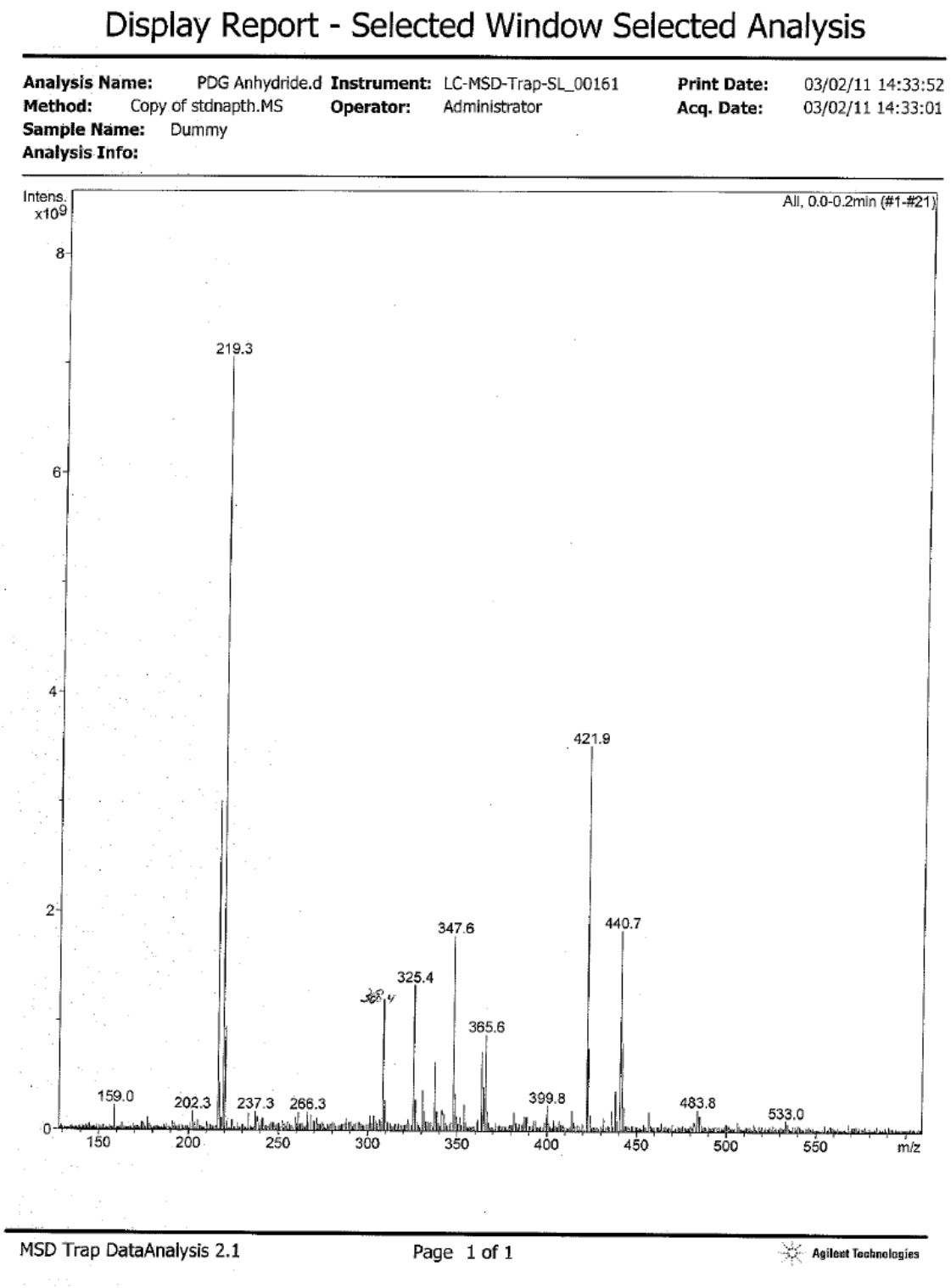

Figure A-16. Mass spectrum of **3-pentadecylglutaric anhydride (4)**.

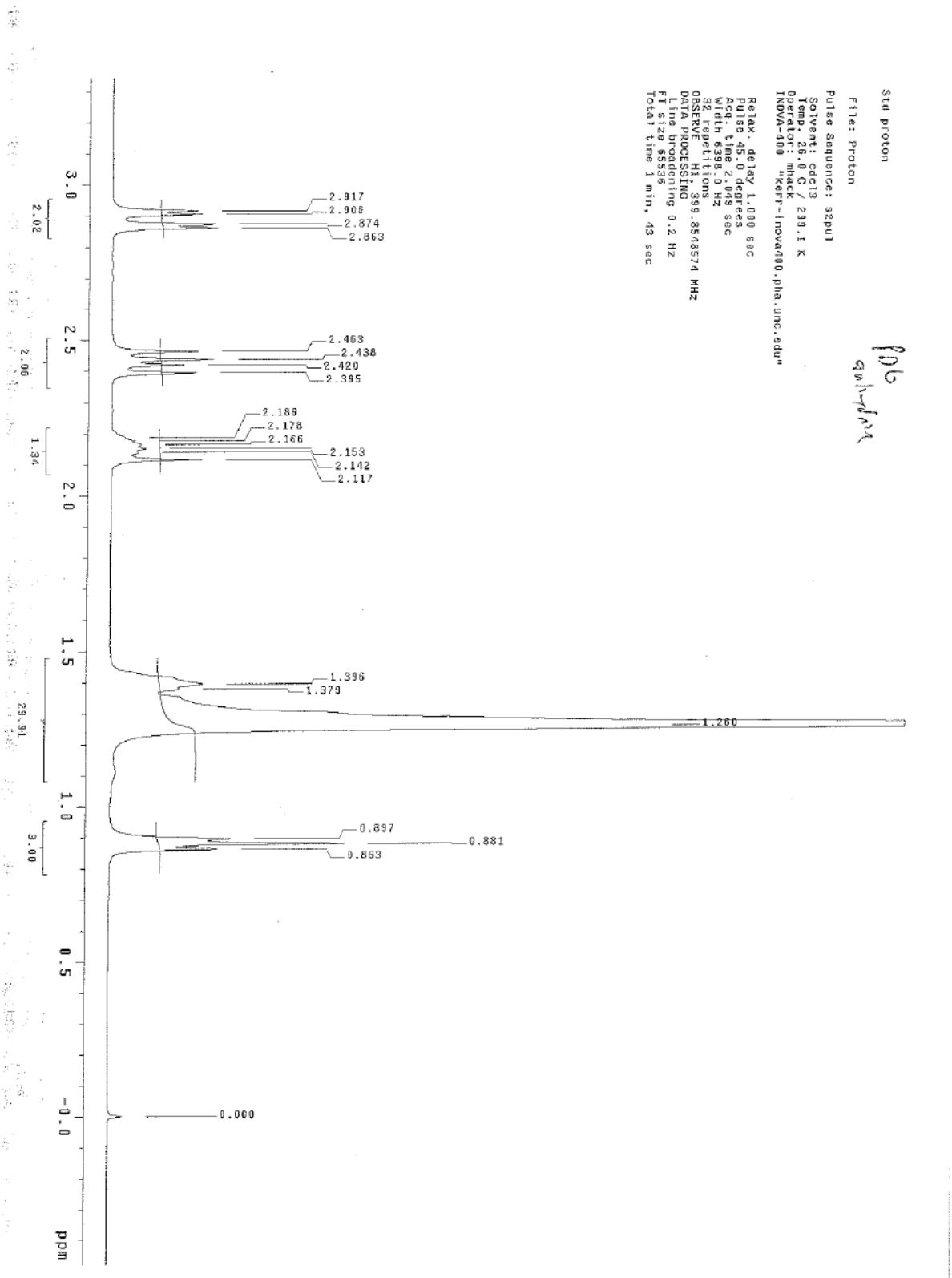

Figure A-17. ^{1}H NMR spectrum of **3-pentadecylglutaric anhydride (4)**.

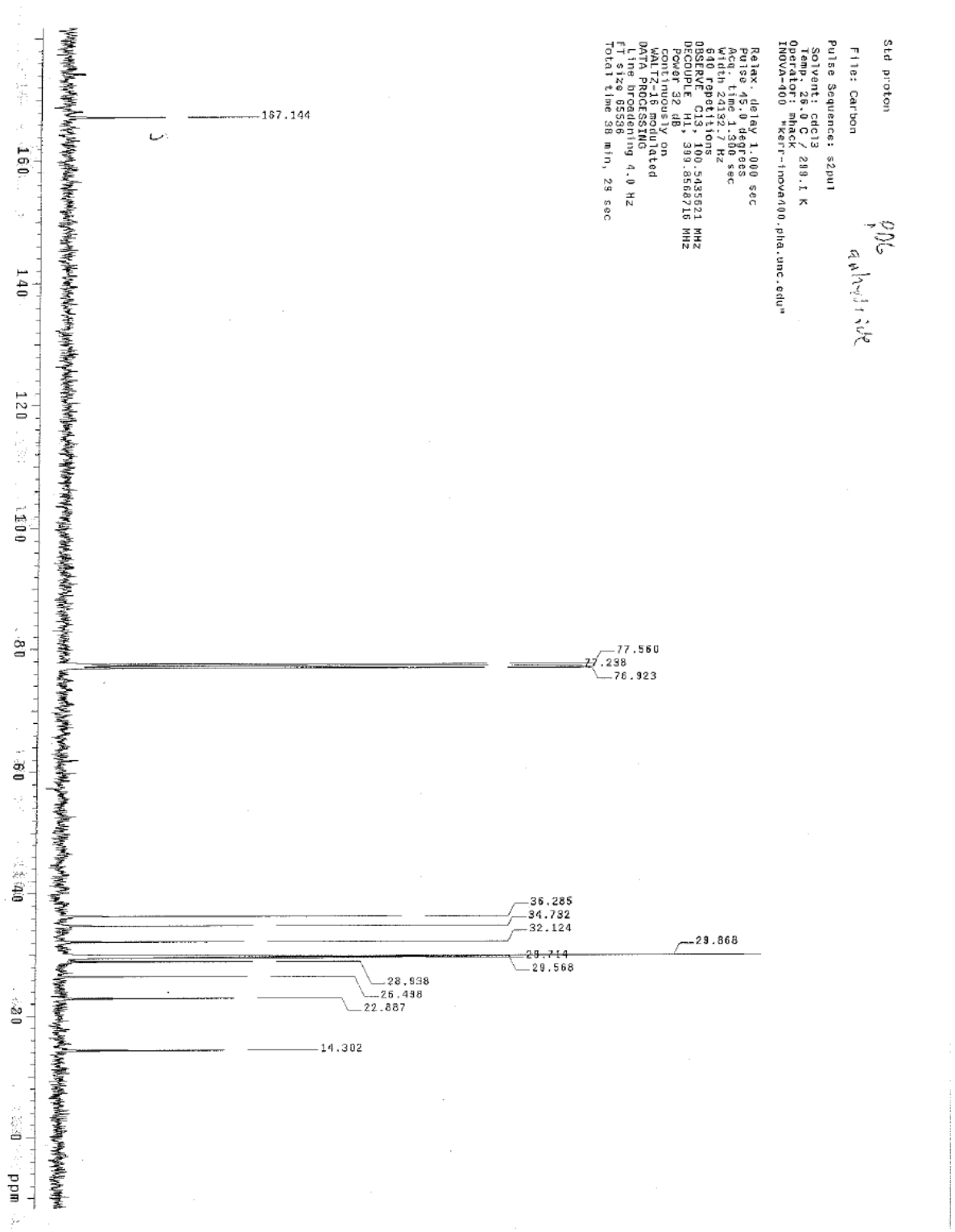

Figure A-18. ^{13}C NMR spectrum of **3-pentadecylglutaric anhydride (4)**.

18.5. Paclitaxel-2'-*O*-3-pentadecylhemiglutarate (5)

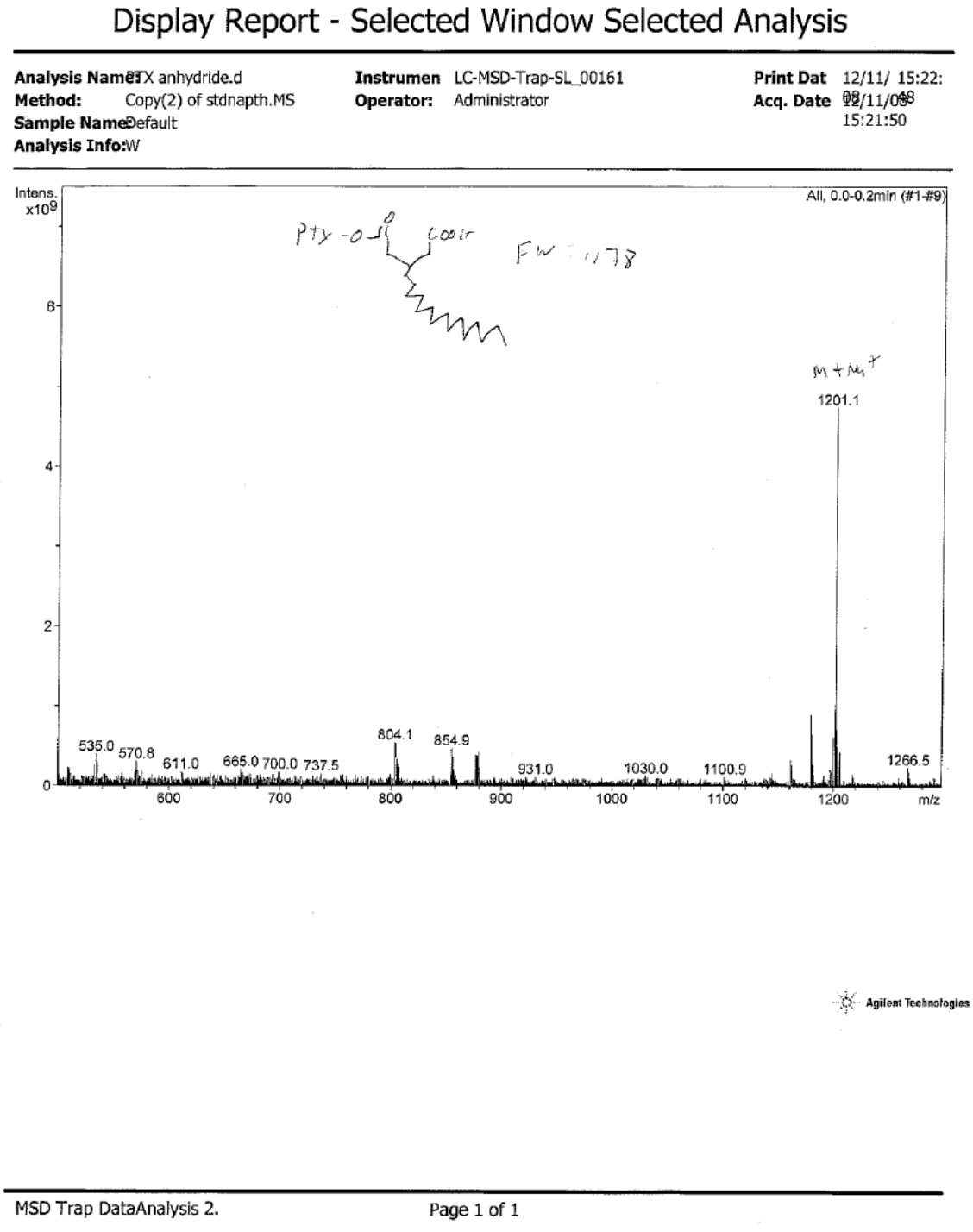

Figure A-19. Mass spectrum of **paclitaxel-2'-*O*-3-pentadecylhemiglutarate (5)**.

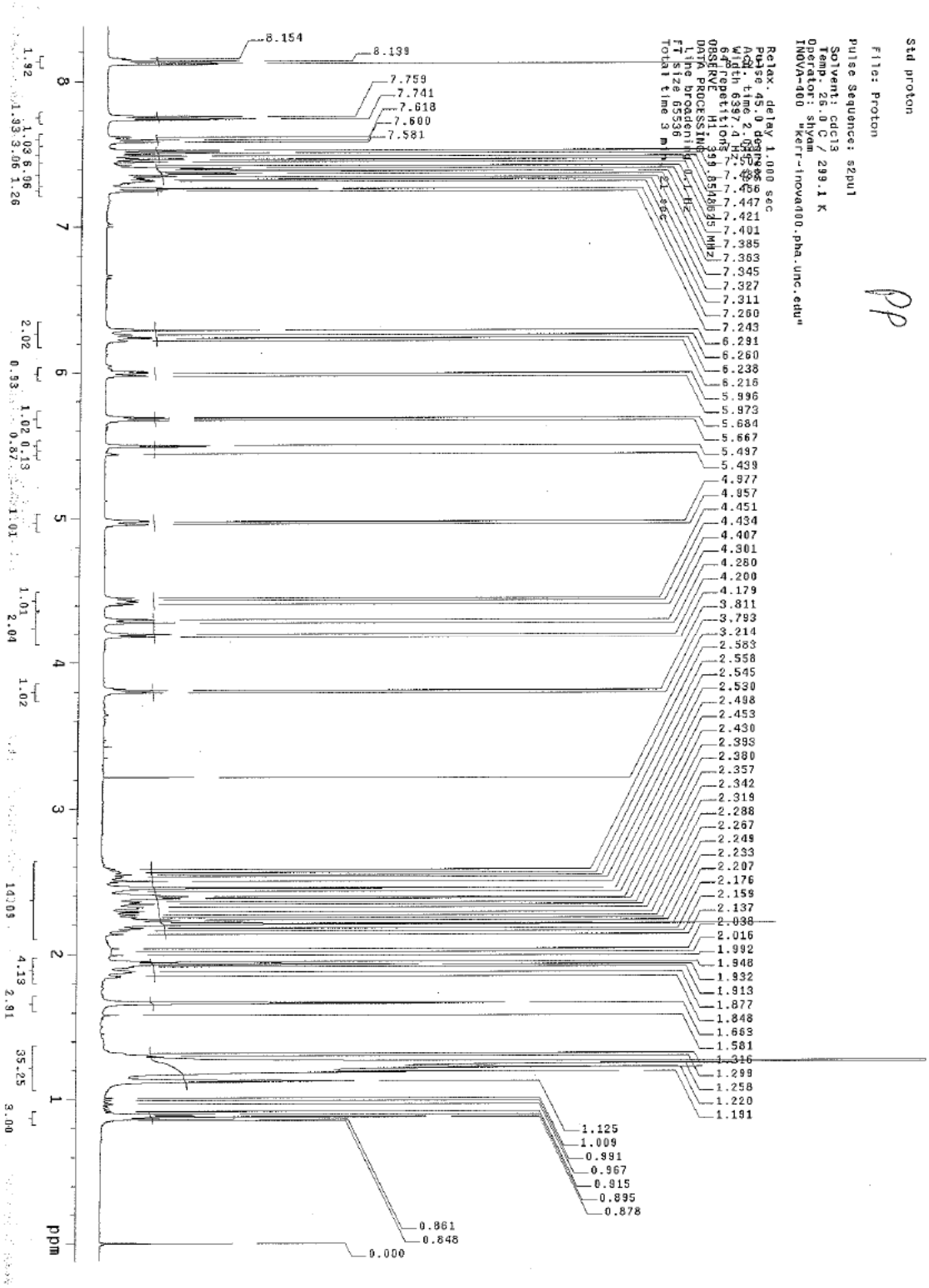

Figure A-20. ^{1}H NMR spectrum of **paclitaxel-2'-*O*-3-pentadecylhemiglutarate (5)**.

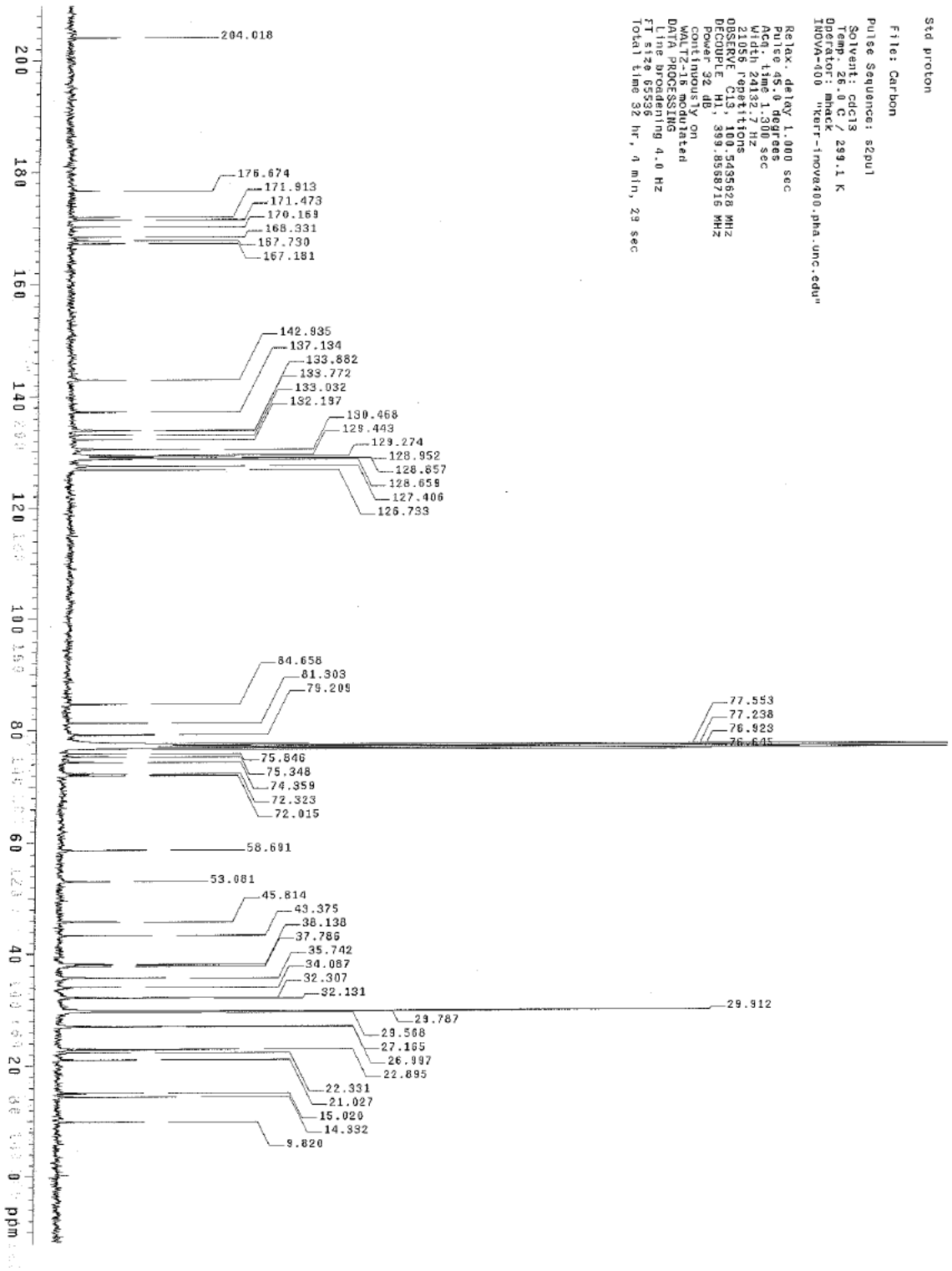

Figure A-21. ^{13}C NMR spectrum of **paclitaxel-2'-*O*-3-pentadecylhemiglutarate (5)**.